Integrating Cortical Sensorimotor Representations Across Spatial Scales and Task Contexts

by

Dylan Albert Royston

BS in Engineering Science (BME)/Neuroscience, University of Virginia, 2013

Submitted to the Graduate Faculty of

Swanson School of Engineering in partial fulfillment

of the requirements for the degree of

Doctor of Philosophy

University of Pittsburgh

2019

UNIVERSITY OF PITTSBURGH

SWANSON SCHOOL OF ENGINEERING

This dissertation was presented

by

Dylan Albert Royston

It was defended on

November 15, 2019

and approved by

Aaron P. Batista, Ph.D., Associate Professor, Department of Bioengineering

Robert A. Gaunt, Ph.D., Assistant Professor, Department of Physical Medicine and Rehabilitation

Timothy D. Verstynen, Ph.D., Associate Professor, Department of Psychology, Carnegie Mellon University

Dissertation Director: Jennifer L. Collinger, Ph.D., Assistant Professor, Department of Physical Medicine and Rehabilitation

Integrating Cortical Sensorimotor Representations Across Spatial Scales and Task Contexts

Dylan Albert Royston, PhD

University of Pittsburgh, 2019

Our understanding of how brains function is stratified between two very different scales: mesoscale (what function a given cortical area performs), measured with tools like fMRI; and microscale (what a given neuron does), measured with implanted microelectrodes. While extensive research has been done to characterize brain activity at both of these spatial scales, describing relationships between these two domains has proven difficult. Identifying ways to integrate findings between these scales is valuable for both research and clinical applications, but is particularly important for intracortical brain-computer interfaces (BCIs), which aim to restore motor function after paralysis or amputation. In humans, the brain is much larger than the available microelectrode arrays, so determining where to place the arrays is a critical aspect of ensuring optimal performance. BCIs preferentially target primary motor and somatosensory cortices, due to their direct relationship to motor control and critical role in skilled and dexterous movements. However, despite these areas displaying a relatively ordered spatial organization, it is difficult to accurately predict the behavior of neurons recorded from a given area for several reasons. Mesoscale activity is overlapping, with activity relating to multiple different movements observed in a single area. Additionally, neurons have flexible behavior, displaying different "tuning" to similar behavior under different contexts.

Here I present my research integrating neuroimaging-based cortical mapping with directly-recorded neural activity in human sensorimotor cortex. First, I examine how the large-

scale organization of sensorimotor representations measured with fMRI is affected by contextual sensory information. I then examine how spatially separate neural populations recorded with intracortical microelectrode arrays encode different types of movement. Finally, I examine whether how population encoding changes to reflect contextual sensory information using the same task as in the fMRI study. Together, these results provide a foundation for reconciling neural activity across spatial scales and task contexts, and will inform the design and placement of more capable BCI systems.

Table of Contents

List of Tables

List of Figures

Preface

The time I have spent performing the work described here has been both transformational and deeply rewarding. I've gained a profound appreciation for the importance and complexity of researching clinical technology, and had the privilege of working with many incredible colleagues. This dissertation is dedicated to all the people in my life who helped to make this work possible.

To my advisor and thesis committee, whose mentorship and guidance taught me how to think like a scientist.

To all the people who participated in these studies, in particular Jan Scheuermann and Nathan Copeland, whose time and efforts allowed this research to exist.

To my friends, both in the Pitt Crew and the Nomads, who constantly reminded me of the joys of life outside of the lab.

And to my family: Clyde, Marianne, and Marina Royston, and my partner, Audrey Crompton, whose constant love and support have helped me through so many challenges and made me a better person.

1.0 Introduction

Our arms and hands are the primary method by which we interact with and shape the world around us, and are capable of highly complex and precise movements. This ability is driven by many brain areas working together to combine sensory and cognitive information into motor commands. In humans, the precentral gyrus is known as the primary motor cortex (M1) due to the predominance of its descending anatomical projections (Dum & Strick, 1991) as well as the direct relationship between its activity and generated movement (Wilder Penfield & Boldrey, 1937). Primary motor cortex, as well as many other sensorimotor brain areas, often display large-scale somatotopic spatial organization, where localized activity relates to movement of specific body parts (Cunningham, Machado, Yue, Carey, & Plow, 2013; W Penfield & Rasmussen, 1950). This organization appears to be partially reflected in the activity of individual neurons, such that neural activity recorded from "arm and hand areas" appear to correlate with the kinematics of intended arm movements (Georgopoulos, Kalaska, Caminiti, & Massey, 1982) and can be decoded to enable the control of computer cursors and neuroprosthetic limbs (Jarosiewicz et al., 2014; Kim, Simeral, Hochberg, Donoghue, & Black, 2008; Wodlinger et al., 2014). However, the activity of individual neurons throughout M1 are also known to display highly variable modulation during different movements (Griffin, Hoffman, & Strick, 2015; Kakei, Hoffman, & Strick, 1999; M. Schieber & Hibbard, 1993a), suggesting that single neurons may provide only a limited sample of the complex information encoded by neural populations.

This dichotomy highlights one of the central challenges in describing the function of specific cortical areas, which is that the neural correlates of cognition and behavior inherently operate across multiple spatial scales. A given cortical area perform certain computations, or participates in generating certain behaviors, as a result of its component circuits- the activity and anatomical connections of individual neurons. There is evidence describing the physiological relationship between recorded activity at these different scales (N K Logothetis, Pauls, Augath, Trinath, & Oeltermann, 2001; Nikos K. Logothetis & Wandell, 2004; Siero et al., 2014), but few results informing their computational relationship (i.e. what imaging activity predicts about the behavior of neurons in an area and vice versa). Therefore, if we wish to determine how neural populations in a specific cortical area encode information, we should consider both its meso-scale organization: the coarse activity of many neurons together, such as that measured with noninvasive neuroimaging, and the detailed activity of individual neurons within that area.

1.1 Recording Neural Activity

As individual neurons are generally considered the basic computational unit of the nervous system, the simplest way to study brain activity is to measure the activity of a given neuron. We can observe the activity of individual neurons by implanting microelectrodes within cortical tissue. These electrodes measure the extracellular voltage of local neural activity, composed of signals from nearby neural structures. This voltage signal can be processed to identify discrete action potentials (colloquially, “spikes”), which correspond to axonal output, and local field potentials (LFPs), which relate to broad changes in dendritic input (Nikos K.

Logothetis, 2012). Therefore, by identifying and analyzing these voltage signals, we can measure the information output of recorded neurons. With current human-implantable Utah microelectrode arrays (Maynard, Nordhausen, & Normann, 1997), it is possible to record from hundreds of neurons simultaneously in the human or monkey brain. While the ability to record directly from individual neurons at sub-millisecond temporal resolution offers significant advantages, these arrays can only sample from a relatively small ($16mm^2$) area of cortex.

Conversely, neuroimaging methods allow for the recording of activity across large portions of the brain, albeit with limited spatiotemporal resolution. Functional magnetic resonance imaging (fMRI) can be used to quantify the level of blood oxygenation (i.e. the BOLD signal) in a relatively small volume of cortex ($\sim 2mm^2$). This technology can thereby allow us to indirectly measure the amount of LFP modulation and therefore dendritic input (N K Logothetis et al., 2001; Nikos K. Logothetis, 2012; Nikos K. Logothetis & Wandell, 2004; Siero et al., 2014). While the BOLD signal relates more closely to input activity, our understanding of intracortical signals in humans is driven primarily by interpreting spiking output activity, which is directly responsible for generating movement and is therefore more closely related to movement parameters (Perel et al., 2015; Todorova, Sadtler, Batista, Chase, & Ventura, 2014). Therefore**,** analyzing sensorimotor activity using both fMRI and intracortical electrophysiology can allow us to study neural activity at a range of spatial and temporal scales, providing a basis for integrating computational results from separate domains of research.

1.2 Role of Sensorimotor Cortex in Generating Movement

One of the brain's primary purposes is to control the body as it moves through and interacts with its environment. In order for activity in the brain to drive muscle activity and generate movement, it must be transmitted "downstream" to the spinal cord and periphery (body). Therefore, we can define a cortical area as being "motor-related" if it contains neurons whose axons project out of the brain and down the spinal cord. Using viral tracers, anatomical studies in non-human primates have identified these descending corticospinal neurons in multiple cortical areas, providing evidence that movement is controlled by a widespread network of neural circuits (Dum & Strick, 1991; Picard & Strick, 1996; Jean-Alban Rathelot, Dum, & Strick, 2017). The precentral gyrus contains the majority of these descending white-matter tracts, supporting its role as the "primary motor cortex".

The significance of M1 in controlling movement is also supported by studies examining the activity of directly recorded single neurons. Georgopolous et al recorded from individual neurons in the "hand area" of M1 while macaques used their arms to perform a center-out reach task. They found that spiking activity was clearly modulated during arm movements, and that the behavior of individual neurons could be modeled with a "tuning curve", firing faster during reaches in a particular direction and slower during reaches in the opposite direction (Georgopoulos et al., 1982). Thus, by recording from multiple neurons and calculating a "population vector", it is possible to decode the direction of a movement purely by examining M1 activity (Georgopoulos, Schwartz, & Kettner, 2009). This principle of modeling linear relationships between movement direction and single-neuron firing rate has since been adapted and implemented in human participants, providing them with a brain-computer interface (BCI)

able to control the movement of computer cursors and robotic limbs (Collinger et al., 2012; Kim et al., 2008; Wodlinger et al., 2014) and demonstrating a direct relationship between M1 neural activity and the cortical representation of intended movement kinematics. However, these results are based on activity sampled during simple and highly-trained movements, from an extremely small portion of M1 during a limited range of movements. There remains an open question of how motor cortical activity relates to the varied parameters of complex ongoing movement. These population-vector results illustrate how single-neuron activity relates to end-point velocity, but other studies have demonstrated similar relationships to various movement-related variables such as grasp force (Intveld, Dann, Michaels, & Scherberger, 2018) and hand posture (Schaffelhofer, Agudelo-Toro, & Scherberger, 2015). It remains unclear how the activity of neurons in different areas of M1 coordinate to encode these and other parameters of ongoing movement.

1.3 Spatial Organization of Sensorimotor Representation in M1

Our understanding of the relationship between cortical activity and movement generation (described above) is robust, but built on recordings from spatially limited areas of cortex. Determining how the spatial organization of activity within M1 enables dexterous motor control remains a core question in neuroscience. Early studies by Penfield et al revealed orderly spatial organization, known as somatotopy, in M1/S1 by showing that stimulating different areas evoked movement of different body parts, often represented by a clear and orderly homunculus (W

Penfield & Rasmussen, 1950; Wilder Penfield & Boldrey, 1937). Based on these results, we might imagine that neurons in a "hand" area would be more active during hand movement compared to those from an "arm" area. However, even the authors here suggested that this is a simplified map of very overlapping patterns.

Many studies take large-scale somatotopy as a canonical truth, referring to anatomical "hand areas" (especially in non-human primate research) based on the movements evoked by stimulation and the peripheral targets (retrograde tracers from arm/hand muscles eventually mark neurons in this area of M1 (as well as multiple other brain areas, illustrating that motor control involves multiple cortical areas))(Dum & Strick, 1991). In humans, representations of specific body parts in M1 are often identified using fMRI, where areas displaying increased activity during movement production are labeled as their representation. Many neuroimaging studies investigating the spatial organization of M1 activity have found that while there does appear to be a large-scale somatotopic gradient, there is also substantial overlap between activity generated during different movements (Beisteiner et al., 2001; Choe et al., 2015; Dechent & Frahm, 2003; Hlustik, 2001; Lotze et al., 2000; Plow, Arora, Pline, Binenstock, & Carey, 2010).

While we have evidence that neurons from a "hand area" display activity related to hand movements, cortex is large and it is not clear how activity in a "hand area" differs from that in an "arm area", i.e. the degree to which M1 displays "spatial specialization". Indeed, it has been shown that neighboring neurons in the "hand area" display responses to movement (kinematics), muscles (EMG activity), and both (J.-A. Rathelot & Strick, 2006), indicating that even these basic parameters are not represented in strictly separated cortical areas.

Marc Schieber reviewed evidence of spatial organization in M1 and argued that rather than an orderly spatial mapping between cortex and muscles, M1 demonstrates distributed

organization with redundancy and overlaps between representations (M. H. H. M. H. Schieber, 2001). He argued that while the cortical sheet is 2D, the "number of dimensions represented in M1 is arguably much more than three, if each muscle, each degree of freedom at each joint, and each kinematic or dynamic parameter of movement constitutes a possible dimension". Furthermore, based on the demonstrated anatomical connectivity of M1 neurons, he suggested a "distributed system, networked by convergence, divergence, and horizontal connections", where frequently-used combinations of muscle activation, and therefore movement, can be represented redundantly. This interpretation suggests that the conventional model of somatotopy may be one dimension of representation, which overlaps with other gradients; therefore, a given area of cortex may encode multiple parameters, and a given parameter may be encoded similarly by multiple areas.

This view is supported by anatomical studies; Peter Strick et al have shown that the upper limb representation (as defined by conventional anatomical limits) is subdivided into "old and new M1" in an anterior/posterior axis based on the prevalence of direct corticomotoneuronal (CM) connections (J.-A. Rathelot & Strick, 2009). "Old M1" lacks direct CM neurons, projects to "integrative mechanisms of the spinal cord", is phylogenically older, and more related to coarse movements, while "New M1" has direct CM neurons, is phylogenically newer, and allows for refined control of skilled/precise movements (particularly of individual fingers). However, even these CM neurons, which directly affect muscle activity, display different activity when their target muscle is used in different contexts, demonstrating "functional tuning" even in directly-connected neurons (and providing evidence against "hard-wired" interpretations of motor encoding) (Griffin et al., 2015). Anatomical and functional studies have also demonstrated the presence of "parallel cortical networks", where different areas of M1 contain anatomical

connections to and from other cortical areas (premotor and parietal) in “clusters” (Dea, Hamadjida, Elgbeili, Quessy, & Dancause, 2016; Hamadjida, Dea, Deffeyes, Quessy, & Dancause, 2016). Furthermore, an extension of early stimulation studies showed that while short bursts of stimulation in a specific area of cortex evoked small movements, longer stimulation trains evoked more complex movements (Graziano, Taylor, & Moore, 2002). In other words, rather than simply causing muscle contraction, activity in a specific area of M1 evoked stereotyped and complex movements, suggesting that “actions” can be encoded in small areas of cortex (Graziano, 2016).

Together, these results indicate that while a large-scale somatotopic organization is present in M1, it is a simplified (1-dimensional) interpretation of what we now know to be an overlapping (high-dimensional) combination of multiple “layers” of organization. Based on this, we can expect that neurons recorded from an area shown to be active in fMRI (for example) during finger movement will likely display finger-related modulation; but since movement representations are complex and widespread, they are also likely to be modulated during other movements. This distributed organization poses a challenge for efforts to integrate our understanding of both large-scale organization (how different functions are represented by different areas of cortex) and micro-scale computation (how different functions are represented by a specific population of neurons).

This question is particularly relevant to the development of implanted BCI systems, which rely on placing a limited number of recording devices in cortical areas that produce activity relevant to the desired control parameters. Some groups have investigated the feasibility of using presurgical imaging to map the behavior-related activity underlying BCI control for planning purposes (Collinger et al., 2014; Yoo et al., 2018). To maximize the utility of this pre-

surgical imaging and planning, it is important to improve our understanding of the relationship between the large-scale activity recorded using neuroimaging and the fine-grained activity recorded using electrophysiology. Additionally, the complex organization observed in M1 indicates that it may be both important and valuable to investigate the differences and similarities between the behavior of univariate measures (such as simple task-related neuroimaging and single-neuron recordings) and multivariate models which integrate the concept of high-dimensional representations.

1.4 Analyzing Population-Level Activity Patterns

Much of our understanding of the neural correlates of cognition and behavior (including the work described above) focuses on analyzing the activity of individual neurons. As discussed previously, single neurons are often thought of as the "basic computational unit" of the nervous system. Correspondingly, much of the research aiming to identify relationships between motor cortex activity and movement parameters is framed in a "representation model", which posits that the temporal firing activity of single neurons represents the temporal profile of movement kinematics and/or muscle activity. Experimental results based on this representational model have proven valuable and enabled the development of highly capable BCI systems. However, as discussed above, this framework may be insufficient to fully explain the encoding of multivariate movement parameters.

Alternatively, modern theories of neural computation have shifted away from exclusively interpreting the activity of individual neurons, instead focusing on describing the coordinated activity of neural populations. This framework posits that populations of neurons serve to generate an overall pattern of descending activity by functioning as a distributed system (Shenoy, Sahani, & Churchland, 2013). As the population-level activity pattern encodes the kinematic and muscle parameters necessary for generating movement, these variables may be observed in the activity of individual neurons within the population. These representational models utilize dimensionality reduction techniques, which identify patterns of variance (i.e. principal components, neural factors) in temporal activity shared across populations of neurons, to identify the degree to which each neuron displays each component. We can then use this transformation to describe the shared population activity as a single "neural state", i.e. the position of each timepoint in a space defined by the components which explain the largest portion of the overall observed variance in neural activity.

Focusing on this high-dimensional perspective reveals many novel insights into how populations of neurons use coordinated activity to generate and regulate movement production. State-space models have been used to reveal how complex task information (object shape, hand posture) is represented differently across sequential cortical areas in the motor-control network (parietal, premotor, M1) (Menz, Schaffelhofer, & Scherberger, 2015; Schaffelhofer et al., 2015; Schaffelhofer & Scherberger, 2016), provide a potential explanation for how kinematically-similar movements can be uniquely represented in the same cortical area through "untangled" population dynamics (Russo et al., 2018), and determine the natural constraints on which types of behavior can be learned (Sadtler et al., 2014).

Additionally, similar population-level analyses have also proven valuable for interpreting large-scale neuroimaging data. Multiple studies investigating the spatial distribution of activity during individual finger movements have observed that per-finger BOLD activity is broadly somatotopic but displays high variability between individuals (Ejaz, Hamada, & Diedrichsen, 2015; Kikkert et al., 2016). Analyzing the "pairwise digit representational similarity of multivoxel patterns", i.e. quantifying the statistical distance between the high-dimensional neural activity throughout M1/S1 (Kriegeskorte, 2008; Oosterhof, Wiestler, Downing, & Diedrichsen, 2011), revealed a "representational structure" which reflected the statistics of natural finger movement and was consistent across individuals. While univariate BOLD activity demonstrated some spatial organization, interpreting multi-voxel activity as components of a unified population-level pattern revealed a more complex and behaviorally-relevant representation of movement.

1.5 Mapping Cortical Sensorimotor Representations in Chronic Spinal Cord Injury

As discussed above, intracortical brain-computer interfaces (BCIs) have been successfully used to allow individuals with tetraplegia due to spinal cord injury (SCI) to control prosthetic arms and hands (Collinger et al., 2012; Hochberg et al., 2006; Wodlinger et al., 2014). In addition to their clinical value, these BCI systems also provide an opportunity to directly study the behavior of populations of neurons in the human cerebral cortex during natural motor control. However, as participants in such studies are recruited specifically for clinical trials as a

result of their impairment conditions, it is important to consider the potential neurological effects of chronic tetraplegia when interpreting such results. In chronic SCI, descending efferent motor connections and ascending somatosensory afferent connections are physically disrupted, which can lead to anatomical and functional reorganization throughout the nervous system, but primarily in subcortical structures (Jones & Pons, 1998). Numerous neuroimaging studies have found that while somatotopic sensorimotor representations are generally preserved after SCI (i.e. significant activity is still observed during natural motor tasks), they often display higher variability in magnitude and spatial extent (K. J. Kokotilo, Eng, Curt, & Boyd, 2009; Urbin, Royston, Weber, Boninger, & Collinger, 2019). There is evidence that these representations may undergo a degree of reorganization, such as activity during preserved movements extending into cortical territory previously relating to impaired movements (Henderson, Gustin, Macey, Wrigley, & Siddall, 2011) and decreases in cortical activity during completely impaired but not partially impaired movements (Foldes, Weber, & Collinger, 2017). However, another study in upper-limb amputees revealed that the underlying structure of disconnected finger representations was largely preserved (Kikkert et al., 2016), suggesting that the use-based structure of sensorimotor representations are generally intact even after chronic disconnection. Additionally, the use of cortical sensorimotor activity to operate limb-related intracortical BCIs (Wodlinger et al., 2014) and drive muscle-specific stimulation to restore motor function (Ajiboye et al., 2017) suggests that the detailed encoding of intended limb movements is preserved after injury, further supporting the study of natural movement encoding in BCI participants with tetraplegia.

1.6 Task Context and Multisensory Enrichment

Although the fundamental structure of cortical sensorimotor representations appears to be preserved after chronic SCI, they often display increased variability in the magnitude and spatial extent of activity (K. Kokotilo, Eng, & Curt, 2009; Urbin et al., 2019). This variability may relate to the prolonged lack of sensory feedback during movement. Studies of arm movements in patients without proprioception have shown that without feedback, reaching movements become less controlled and more variable, indicating that the continuous somatosensory feedback is involved in constraining ongoing movements (Gordon, Ghilardi, & Ghez, 1995). This variance was especially pronounced when patients could not see their limbs, but reduced with both simple cursor feedback and vision of their arm's position prior to movement (Ghez, Gordon, & Ghilardi, 1995), indicating that visual information alone could be integrated and used to control the kinematics of intended movement. These results suggest that multisensory information may be integrated by the motor control network and used to maintain the overall pattern of activity necessary for limb control by selectively enhancing relevant activity while suppressing unnecessary variance (Mahan & Georgopoulos, 2013).

As this multisensory feedback is disrupted in SCI, it may be possible to leverage additional sensory cues to restore this feedback and increase the robustness of movement encoding. This idea is supported by neuroimaging results demonstrating that individuals with SCI display more activity in widespread sensorimotor areas during attempted movement compared to imagined (Hotz-Boendermaker et al., 2008), suggesting that these cortical networks may recruit additional neural resources when processing incongruent motor and sensory signals. Other studies examining the embodiment of artificial limbs have shown that both sensorimotor

activity and subjective embodiment are maintained by congruent visual and somatosensory stimulation, but disintegrate when the sensory cues are conflicting, demonstrating the significance of such multisensory information for limb representation (Gentile, Guterstam, Brozzoli, & Ehrsson, 2013). Additionally, recent results have shown that somatosensory finger representations evoked through purely visual stimulation (Kuehn, Haggard, Villringer, Pleger, & Sereno, 2018) and active movement (Sanders, Wesselink, Dempsey-Jones, & Makin, 2019) are both spatially and structurally similar to those elicited through tactile stimulation. These results indicate that the underlying structure of sensorimotor representations are robust and inherently multisensory, supporting the potential utility of contextual sensory cues to drive strong movement representations.

As discussed above, M1 receives input from multiple premotor and parietal areas (Dea et al., 2016), suggesting that higher-order multisensory and cognitive processes may affect activity in M1. Several studies examined the activity of neural populations from these three areas while macaques performed reach-to-grasp tasks towards a variety of objects and showed that visual object properties are sequentially transformed into motor commands for specific hand postures (Menz et al., 2015; Schaffelhofer et al., 2015; Schaffelhofer & Scherberger, 2016), demonstrating that context-related visual information informs activity in M1. Additionally, recent results have shown that during neuroprosthetic limb control, M1 neurons displayed increased activity when reaching towards an object compared to similar reaches to empty space (Downey et al., 2017), and that providing task-related tactile information via intracortical microstimulation (Flesher et al., 2016) in conjunction with visual feedback improves arm control compared to purely visual feedback (Flesher et al., 2019). Together, these results suggest that

multisensory contextual information can be used to facilitate robust limb representations in individuals with SCI.

1.7 Summary of Work

The spatial organization of movement-related activity in primary motor cortex has been studied extensively in humans using noninvasive neuroimaging and in non-human primates using intracortical electrophysiology. While large-scale somatotopic organization has been frequently observed in neuroimaging results, recordings from single neurons indicate that sensorimotor encoding is widely distributed across M1. Additionally, individual neurons display variable tuning to different movement parameters based on task context, suggesting that neural populations display more complex computational organization than previously thought. In order to reconcile findings from these disparate fields, it is necessary to develop interpretive frameworks that integrate the behavior of neural populations from cortical areas displaying different large-scale patterns of activity. Elucidating the nature of these multi-scale relationships is particularly important for understanding neural activity in humans, which are capable of performing dexterous sensorimotor tasks in highly variable behavioral contexts.

The recent development and clinical testing of intracortical brain-computer interfaces in human participants provides a unique opportunity to examine the activity of human neural populations. This dissertation seeks to identify novel insights into the correspondence between large-scale cortical organization and the function of spatially separate neural populations in

human M1 during arm and hand movements under various sensory contexts. First, functional neuroimaging was used to characterize how the spatial organization of activity in primary sensorimotor cortex is affected by contextual multisensory enrichment of different upper-limb movements and sensations (Chapter 2). Next, intracortical recordings from human motor cortex were compared during arm and hand tasks to determine how spatially separate neurons contribute to encoding different movements (Chapter 3). Finally, a separate set of intracortical recordings were compared during multisensory enrichment of different upper-limb tasks to determine whether spatially separate neural populations are affected by multisensory information (Chapter 5).

2.0 Mapping Mesoscale Sensorimotor Representations Using Enriched Covert Imagery

The work described in this chapter focuses on determining how cortical activity during motor and sensory imagery is affected by supplementary multisensory cues. Determining how sensory information influences activity in sensorimotor cortex is vital to understanding the neural correlates of goal-driven behavior. It is also particularly relevant for integrating neuroimaging and electrophysiological domains. Text for this chapter is adapted from a manuscript in preparation.

2.1 Introduction

There is significant scientific and clinical value in mapping the cortical activity underlying motor and sensory imagery, particularly in individuals with impairments such as spinal cord injury. This activity can be used as a biomarker for identifying and tracking rehabilitative treatments (Urbin et al., 2019), as well as identifying desirable locations for implantable BCI systems (Collinger et al., 2014; Yoo et al., 2018). As such systems generally target the primary motor (M1) and somatosensory (S1) cortices, there is a specific need to develop effective ways to map the spatial distribution of activity within primary sensorimotor cortex (SMC). Due to the "canonical" somatotopic organization frequently observed in SMC (Wilder Penfield & Boldrey, 1937), many studies use simple "localizer" tasks to map the areas which are most responsive to a given movement/sensation/body part (Alkadhi et al., 2002).

However, there is no current "standard" behavioral task used to identify specific representations; different studies use a wide range of different paradigms to elicit sensorimotor activity (K. J. Kokotilo et al., 2009). Interpreting activity elicited during different behaviors as the "same" representation can cause uncertainty about what information is represented in a given brain area.

Mapping sensorimotor representations in patient populations compounds these challenges, due to impaired ability to overtly perform motor and sensory tasks. In individuals with spinal cord injury (SCI), there is disagreement about whether SMC remains active during engagement of impaired body parts. While there is evidence that the nervous system can "reorganize" and display altered sensorimotor activity (Urbin et al., 2019) after SCI, studies demonstrating altered activity during attempted or imagined movements often instruct subjects to perform self-paced movements without any visual or temporal cues (Hotz-Boendermaker et al., 2008). Many results have demonstrated that SMC activity can be affected by goal-related multisensory information (Kuehn et al., 2018; Schaffelhofer & Scherberger, 2016), meaning that in chronic SCI, it may be possible to enhance individuals' subjective embodiment and cortical activity by supplementing motor and sensory imagery tasks with additional multisensory cues (Gentile et al., 2013; Ratcliffe & Newport, 2017).

Here we seek to determine how large-scale sensorimotor representations in SMC are affected by goal-directed multisensory information (i.e. "enrichment") by developing and testing an effective paradigm to elicit sensorimotor activity during covert motor and somatosensory imagery supplemented with additional sensory cues, such as visual object interaction (Fabbri, Stubbs, Cusack, & Culham, 2016) and auditory and tactile timing cues. The primary goal of this study was to quantify changes in the volume, magnitude and location of sensorimotor cortex activity by comparing fMRI activity from able-bodied control subjects and participants with SCI

during tasks enriched with goal-related visual, auditory, and vibrotactile stimulation. We hypothesized that enriching sensorimotor imagery tasks with context-related sensory cues (visual, audio, and vibrotactile) would increase the volume and magnitude of cortical activity in both AB controls and participants with SCI.

2.2 Methods

2.2.1 Participants

In order to examine sensorimotor enrichment, we collected fMRI data from 8 participants with chronic tetraplegia due to SCI (see Table 1 for demographics) and 20 age-matched able-bodied control subjects while they performed a novel covert imagery task.

Table 1: Subject demographics for SCI group

Subject	Age	Years since injury	ASIA Level	ASIA Scale
CMS01	30	12	C3	A
CMS02	48	20	C3	A
CMS03	47	15	C4	A
CMS04	24	9	C4	B
CMS06	30	5	C5	B
CMS07	23	6	C6	B
CMS09	52	25	C5	B
CMS13	60	11	C4	C

2.2.2 Behavioral task design

The goal of this experiment was to determine how varying levels of multimodal sensory information alter the sensorimotor activity generated during motor and somatosensory imagery. To that end, we created a novel behavioral paradigm based on enriching simple motor imagery with additive levels of goal-directed sensory information (**Figure 1**). To identify cortical areas likely to be active during enriched imagery, we first designed "Overt" conditions for each task type. The Overt-Motor task consisted of 5 movements (lip purse, wrist flex, hand grasp, finger tap, ankle flex), cued with simple looped videos of each movement, which all subjects were instructed to attempt to perform (i.e. "imitate") as much as they were physically able. The Overt-Sensory tasks consisted of 2 somatosensory stimuli (passive wrist movement, fingertip brushing) which were delivered while subjects were instructed to focus on the sensation.

To examine the effects of multisensory enrichment, we then designed 5 "Covert" paradigms which consisted of 3 motor imagery tasks (wrist flex/extend, hand grasp, sequential finger taps) and 2 somatosensory imagery tasks (passive wrist movement, tactile fingertip stimulation). Each of these Covert imagery tasks consisted of 4 enrichment conditions: Simple (unenriched), Goal (visual context), Audio (Goal + auditory timing cue), and Stim (Goal+ Audio + vibrotactile stimulation). The "Simple" conditions were defined by videos of simple rhythmic movements being performed against a featureless background. "Goal" conditions were defined by videos of similar movements directed towards a specific object/goal. "Audio" conditions were defined by the "Goal" condition videos and additional auditory cues synched to the moment of peak object contact. "Stim" conditions were defined by the "Audio" stimuli (video + sound) and additional vibrotactile stimulation synched to the moment of peak object contact, delivered using

piezoelectric stimulators (Dancer Designs). Since subjects with SCI were generally unable to detect somatosensory stimuli on the hand, we placed these stimulators on the clavicle (where sensation was generally preserved) in order to ensure the detection of timing-related tactile information. To control for potential differences in the location of this "referred" sensation, the AB subject group was split into two subgroups based on the location of the vibrotactile stimulation: "hand sensation", where stimulation was delivered to the hand; and "referred sensation", where stimulation was delivered to the clavicle.

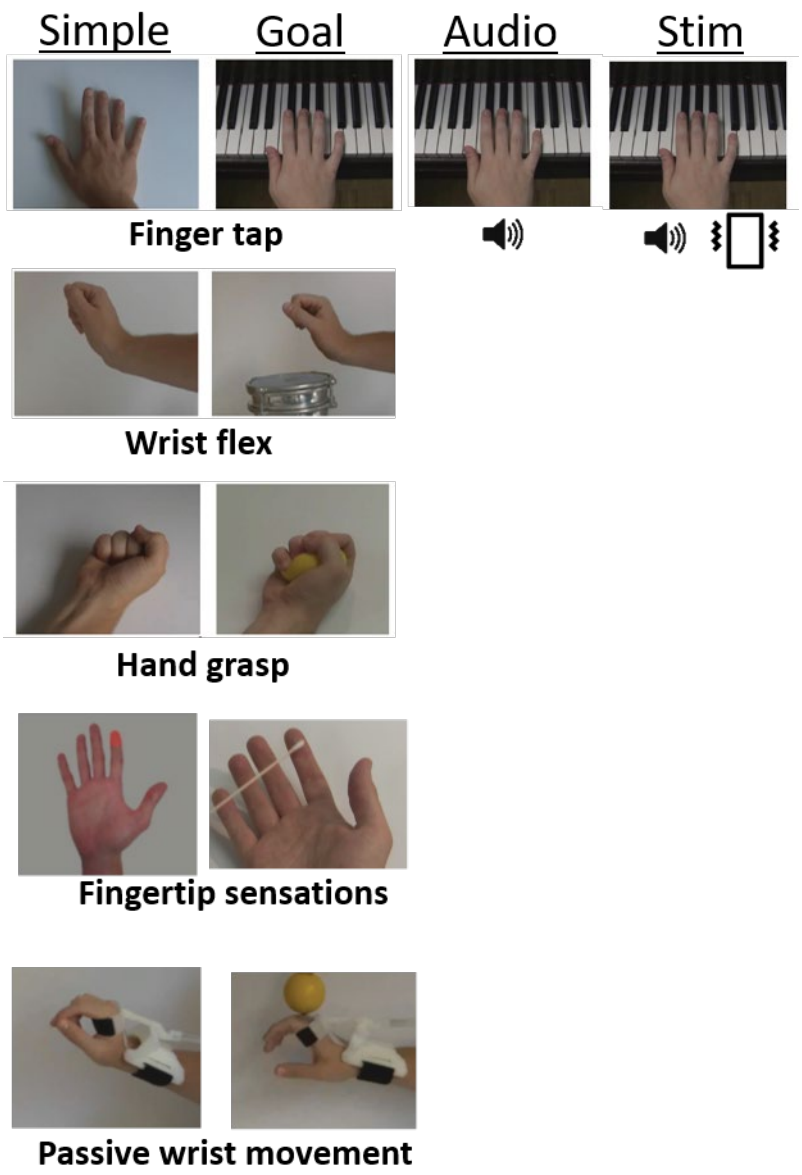

Figure 1: fMRI behavioral paradigm. Multisensory enrichment stimuli used in the fMRI behavioral paradigm to cue motor (finger tap, wrist flex, hand grasp) and somatosensory (fingertip sensation, passive wrist movement) imagery.

fMRI data were collected while subjects viewed stimulus videos of rhythmic movements being performed and were instructed to simulate the movements/sensations in time with the videos. For able-bodied subjects, who were able to physically perform the movement tasks, we wished to examine the effects of the goal-directed enrichment without involving the actual somatosensory feedback inherently produced during overt movement production. As such, the AB subject group was instructed to attempt to physically execute the "Overt" movements, and to imagine (without actually moving) all "Covert" movement conditions. For subjects with SCI, who all had impaired hand function, we wished to elicit the maximum amount of sensorimotor activity. As such, the SCI subject group was instructed to attempted to physically execute (as much as they were able) both Overt and Covert movement tasks. All subjects were asked to verbally confirm their understanding of each task's movement instruction before and after the scans.

2.2.3 Scan parameters

Imaging data was collected using a 3T Siemens Trio scanner with a 32-channel head-coil. Anatomical images were collected using T1-weighted scans at $1mm^3$ isovoxel, 176 slices, 256x256 in-plane resolution. Whole-brain functional data were collected using T2*-weighted echo-planar imaging (EPI) sequences (TR=2000ms, TE=29ms, voxel size = 1.964x1.964mm, slice thickness=2mm, image dimensions=112x112x60mm, 20 slices, GRAPPA multi-band=3).

2.2.4 fMRI processing

Functional MRI data were processed through SPM12 using a standard set of preprocessing operations; functional data were spatially realigned to the mean using a rigid-body transformation, co-registered to the anatomical image, segmented into gray matter/white matter/CSF, normalized into MNI-152 space , and spatially smoothed with a 6mm FWHM Gaussian kernel. We performed a general linear model (GLM) analysis to produce per-movement activity maps for each subject. Movement conditions were fitted with a boxcar predictor and convolved with a canonical hemodynamic response function, with motion nuisance regressors subtracted. This GLM can be summarized by the following equation:

$$\mathrm{BOLD} = (\mathrm{D} * \mathrm{HRF}) * \beta + \mathrm{E} \qquad (2-1)$$

Each voxel can be described with a time-series (BOLD), representing the recorded fMRI signal. The GLM seeks to explain this signal by identifying the regression beta-value (β) relating to the design matrix (D), convolved with a hemodynamic response function (HRF) accounting for the physiological delay between neural activity and BOLD signal (Devor et al., 2005), and removing any motion-related signal (E). This model produces a 3D image where each voxel is related to a given task by its beta-value, which can then be used for subsequent analysis, and a T-statistic (student's t-test) conveying its significance.

2.2.5 Group-level image statistics

Task-related activity was quantified by extracting voxel data from the anatomically-defined regions of M1/S1 (i.e. the precentral and post-central gyri, which together include the banks of the central sulcus) (Desikan et al., 2006; Tzourio-Mazoyer et al., 2002). In order to further segment the spatial distribution of activity in these areas, we divided each ROI into its dorsal and ventral halves, and report quantitative values (activation volume and amplitude) separately for each aspect. We defined "activation volume" as the number of voxels with a T-statistic above a given threshold. Since the group-level T-statistic images were calculated independently (i.e. each condition is generated from a separate set of beta-coefficients) and yielded slightly different distributions, they each displayed a different "significance threshold" as calculated using the false-discovery rate (FDR, $p< 0.05$). To allow data from different conditions to be compared, we defined a common significance threshold as the mean of each condition's individual threshold, in this case $T>2$. I then defined "activation amplitude" as the distribution of beta-coefficient values from the voxels significantly active in each condition. Since these beta-coefficient values correspond to the degree of correlation between a voxel's BOLD time-series activity and movement periods relative to rest, they can be either positive or negative (i.e. correlated or anti-correlated). However, since our hypotheses are structured to be one-directional (i.e. determining whether an area displays increased activity during a given task), we focused on only comparing the distributions of significantly positive beta-coefficient values. This procedure means that the number of samples (beta-coefficients) is different in each condition; thus, in order to determine significant differences between these distributions, we determined between-condition significance using the Wilcoxon rank-sum test.

2.2.6 Quantifying between-condition enrichment

While the technique of calculating group-level images are valuable for estimating the overall task-related activity during a given condition, it is less ideal for assessing differences between similar conditions. In order to determine how the addition of contextual sensory information affected activity during a specific sensorimotor task, we focused on analyzing this "enrichment effect" directly. For each individual subject, we calculated the difference in beta-coefficient values between each pair of conditions:

$$\Delta\beta = \Delta\beta\,(C) - \Delta\beta\,(C-1) \qquad (2-2)$$

To determine how increasing levels of enrichment altered activity, differences were calculated between additive enrichment conditions (i.e. Goal – Simple, Audio – Goal, etc). This produced 6 enrichment images for each subject, which were then averaged across subjects to create 6 group-level enrichment images. In this image, each voxel's value describes the across-subject enrichment effect between conditions.

2.3 Results

2.3.1 Analyzing sensorimotor fMRI activity

Full sets of task data were collected from 20 AB and 8 SCI subjects. Although it is important to determine whether there are any significant differences between the AB and SCI subject groups, the primary focus of this research was to identify consistent effects within each group. Therefore, data from each group was processed and analyzed separately.

We calculated a group-level image for each task-condition by normalizing each subject's functional data into a standardized coordinate space and averaging the whole-brain 3D beta-coefficient matrices across all subjects in a group. we then used this 4D matrix to calculate a T-statistic image across each subject group, indicating the areas which displayed significant task-related activity. Since each voxel's significance in the group-level image is calculated using data from each subject, this group image reveals areas that may not be highly active in each individual, but which are significant at the group level (citations).

2.3.2 Overt movement representations

First we characterized motor-related activation using a block-design Overt movement paradigm, as it is often used as a localizer task (Caspers, Zilles, Laird, & Eickhoff, 2010). Inspecting how basic attempted movements are represented provides a frame of reference for comparing these results to more conventional sensorimotor mapping studies. In this condition,

both subject groups (AB and SCI) were instructed to attempt to perform different simple movements in time with the stimulus videos. **Figure 2** shows the group-level activity from the AB group during each task. This activity reveals the expected large-scale somatotopic organization, with hand-related representations located between face (ventral) and leg (dorsal) activity. The areas of peak activation for wrist, grasp, and finger movements are each distributed across a common region of sensorimotor cortex, consistent with the anatomical "hand knob" (**Figure 2B**).

Since overt production of these three movements involves the activation of similar distal arm muscles, this overlapping "hub" of activation supports the idea that movements involving similar muscle activation are represented by similar cortical areas (Kakei et al., 1999). However, each movement also displays different areas of activation beyond this shared hub; clusters of wrist and grasp activity appear to be more prevalent in the dorsal aspect of SMC, while finger activity appears more widespread, especially in ventral areas (**Figure 2C**). While these three movements involve recruiting a similar pool of muscles, each task requires different spatiotemporal patterns of muscle activation. As such, we might expect that these movements are encoded by different combinations neurons, thereby displaying BOLD activity in different areas of PSMC. To quantify the degree of these differences in spatial activation, we divided both M1/S1 into dorsal and ventral halves, and compared the volume and amplitude of task-activated voxels in each sub-ROI.

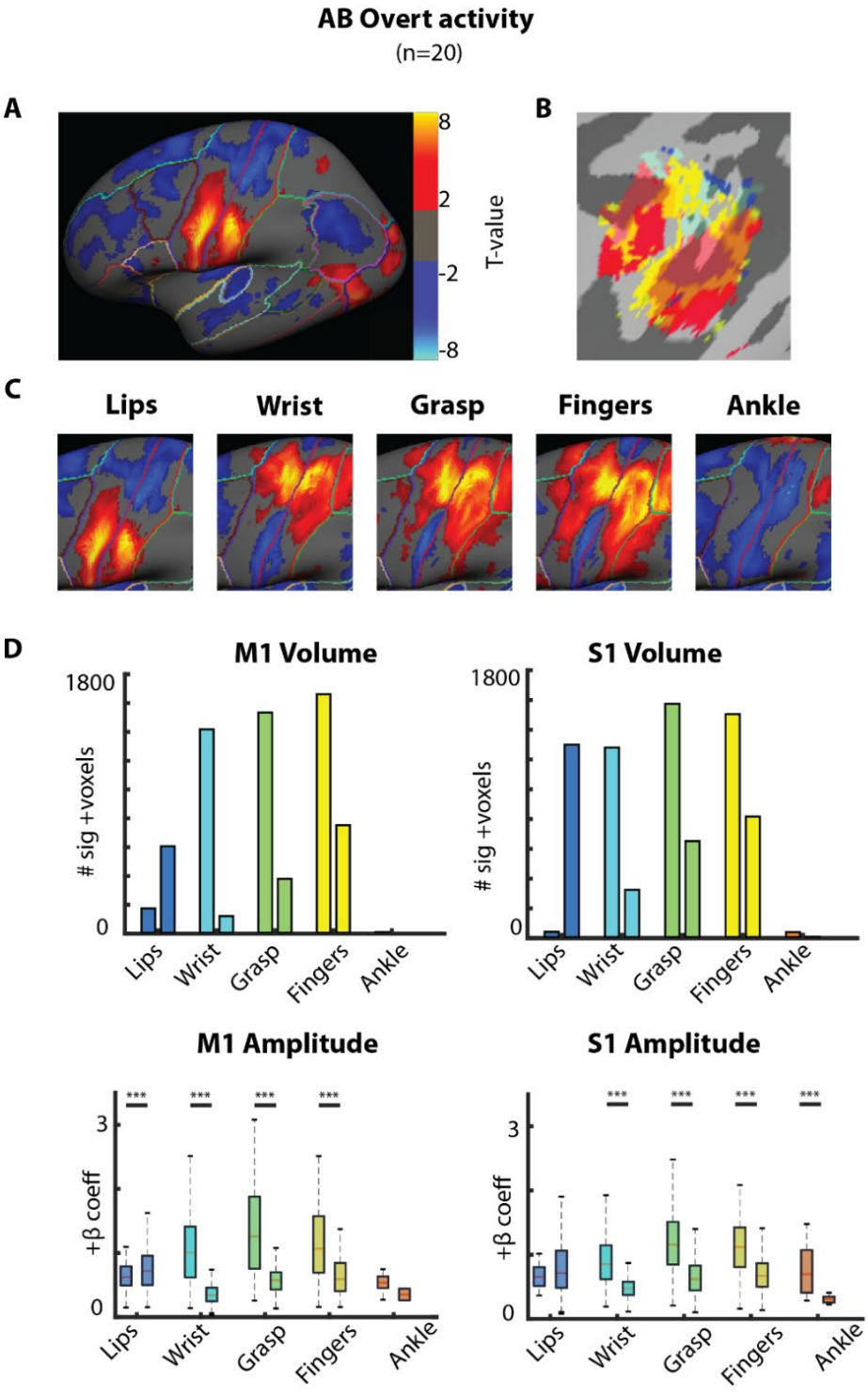

Figure 2: AB group-level activity during overt movement. **(A)** Combined average activity from AB group (n=20) during overt lip movement, projected onto inflated cortical surface (thresholded at T>2). **(B)** Overlaid peak activation during hand-related movements (wrist/hand/fingers, T>7). Blue = wrist, yellow = grasp, red = fingers. **(D)** Volume and amplitude of significant (T>2) positive activity in dorsal (left) and ventral (right) aspects of SMC.

Figure 2D depicts the volume and amplitude of activation in the dorsal and ventral aspects of SMC during each condition. The dorsal aspects of both ROIs (which contain the majority of the anatomical hand knob) displayed both high volume and amplitude during all three hand-related conditions, confirming the qualitative observation of substantial overlap in these areas. These areas also contained low levels of activity during lip and ankle movement, illustrating that while the activation peaks are spatially separated, such activity can be widely distributed throughout SMC. It is worth noting that while ankle-related activity is clearly present in the surface renders, it is minimally captured in the dorsal sub-ROI statistics. This is due to the anatomical boundaries used to define the M1/S1 ROIs, which do not fully extend to the hemispheric fissure (Tzourio-Mazoyer et al., 2002).

In contrast, the ventral aspects displayed more dramatic differences between condition activity. Lip-related activity showed very high volume and amplitude in both ROIs, consistent with the ventral aspects' greater proximity to Broca's area and speech-related representations (Anumanchipalli, Chartier, & Chang, 2019). All 3 hand-related movements displayed significant activity, indicating a wide spatial distribution from the peaks observed in the dorsal aspects. Finger activity was represented most strongly in both M1/S1, followed by grasp and wrist, consistent with the widespread activity observed in the surface renders.

Comparing the relative strength of this activity in dorsal and ventral SMC reveals a degree of large-scale somatotopy, with hand-related activity located in cortical areas bracketed by face and leg representations, consistent with the classical interpretation of spatial organization in M1 and S1. However, this data demonstrates that hand-movement representations are both significantly overlapping (particularly in the dorsal aspects) and widespread (as seen in the ventral aspects). The substantial overlap between hand-related representations indicates that

while each movement is encoded by separate areas (voxels that were only significant during one condition), they also involve activity in cortical areas which contribute to encoding multiple movements. Similarly, the large spatial extent of each movement's activation suggests that while there may be a "hub" where these commands are predominantly represented, large areas of PSMC may participate in encoding ongoing movements.

Next, we examined Overt movement activity in the SCI group. **Figure 3** shows the group-level activity from SCI subjects during attempted Overt movements. The surface visualizations (**Figure 3C**) reveal striking differences in the extent of activation compared to the AB group, with each task's activity appearing less "focal", with high-amplitude activity less tightly clustered and more widely distributed throughout SMC, especially during the three hand-related tasks. This spatial expansion is apparent in the ventral aspects of M1 and S1, where hand-related activity displays substantial volume and amplitude (**Figure 3D**). Indeed, we found that the SCI group displayed significantly stronger activity in both aspects of M1/S1 during each Overt hand-condition, except in dorsal M1/S1 during the Hand condition ($p<0.05$, Wilcoxon rank-sum).

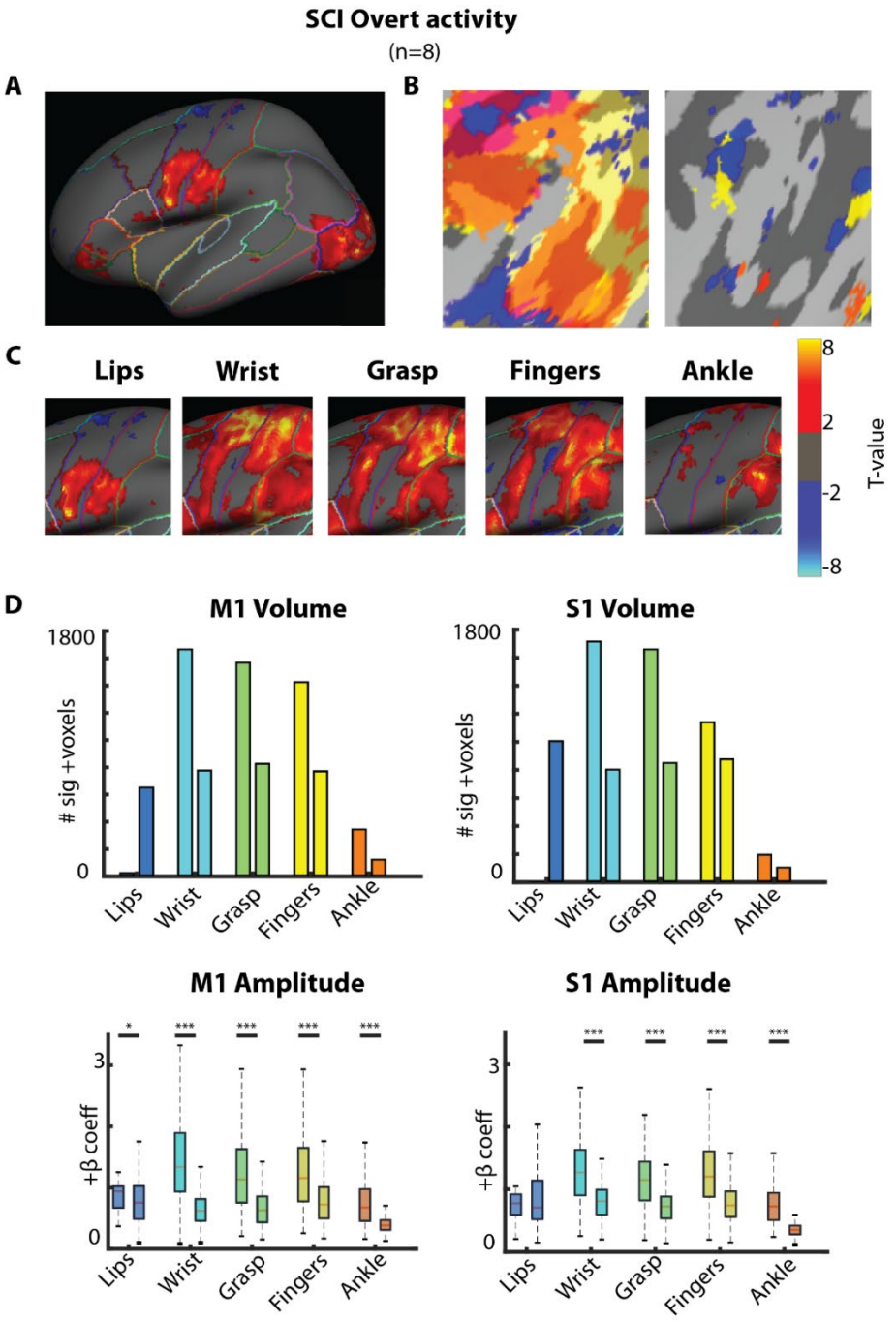

Figure 3: SCI group-level activity during overt movement. **(A)** Combined average activity from SCI group (n=8) during overt lip movement, projected onto inflated cortical surface (thresholded at T>2). **(B)** Overlaid peak activation during hand-related movements (wrist/hand/fingers, T>7). Blue = wrist, yellow = grasp, red = fingers. **(D)** Volume and amplitude of significant (T>2) positive activity in dorsal (left) and ventral (right) aspects of SMC.

2.3.3 Group-level activity during covert Motor enrichment

To investigate the extent to which sensorimotor activity in SMC is affected by enrichment, I repeated these analyses on fMRI data collected while subjects performed covert movements with varying degrees of multisensory enrichment. For each of the hand-related tasks (wrist flex/extend, whole-hand grasp/open, sequential individual finger tapping), we compared the volume and amplitude of group-level activity in dorsal and ventral SMC during each of the 4 enrichment conditions (Simple, Goal, Audio, Stim). **Figure 4A** shows surface maps of AB group-level activity for each condition during enriched covert movements. Although these AB subjects were performing motor imagery and thus not moving overtly, significant activation was observed throughout SMC during each covert condition, both within and extending beyond the areas displaying activity during Overt performance of the same movements. Within each task, areas of cortex can be seen which are consistently active across conditions, while others are selectively active depending on enrichment.

Figure 4B shows the volume and amplitude of activity in dorsal and ventral SMC for each condition. In almost all tasks and areas, the Simple condition displayed the least activity, while both volumes and amplitudes increased with additive enrichment. The Wrist task displayed the most dramatic increase from Simple to Goal, with Audio and Stim activity below Goal but still above Simple. The Grasp task displayed largely linear increases in activity across enrichment conditions, particularly in both aspects of S1. The Finger task displayed less ordered changes in activation across conditions, with Stim and Goal displaying overall increases across most regions.

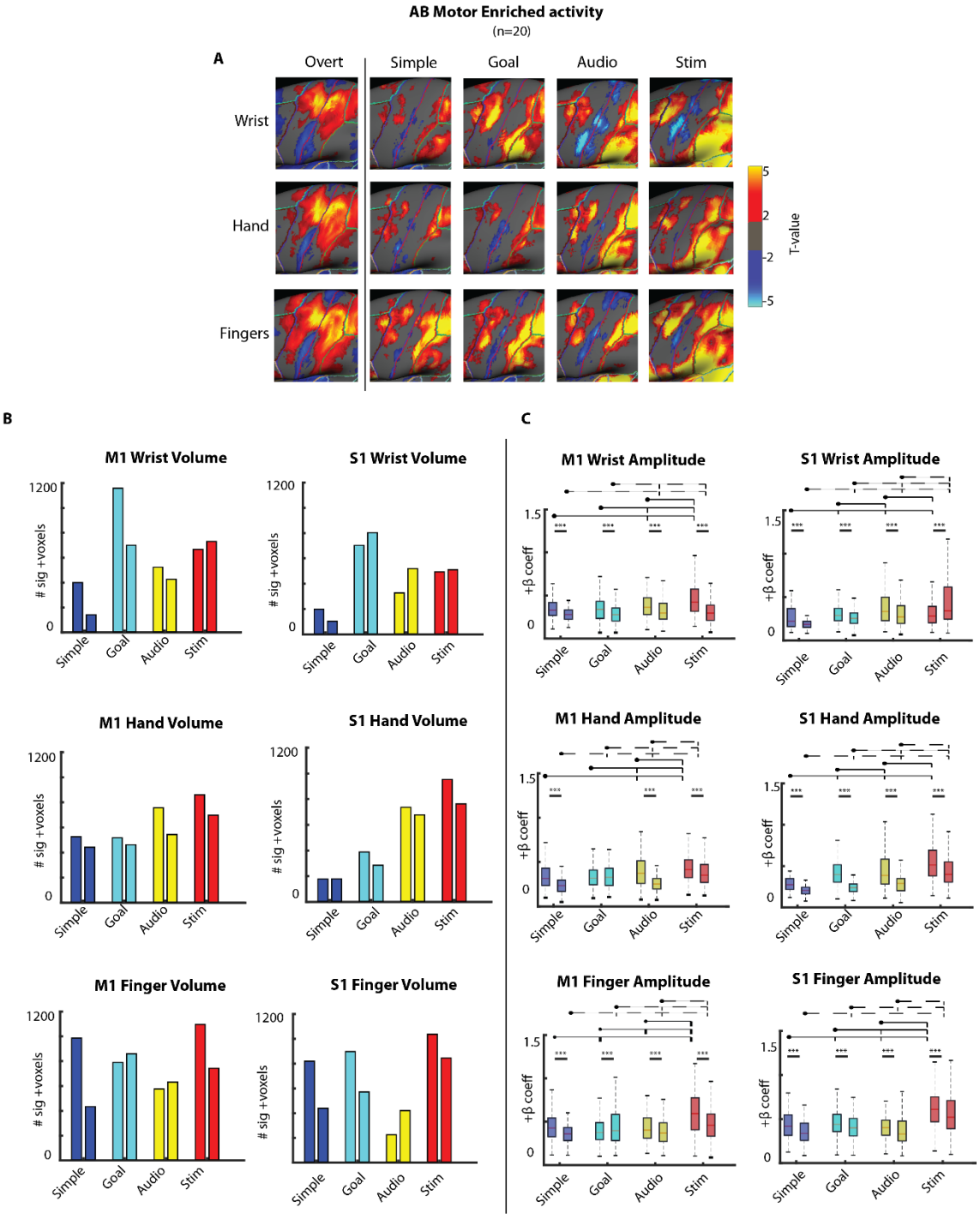

Figure 4: AB group-level activity during enriched Motor tasks. (**A**) surface renders (T-vals thresholded at FDR>0.05, T>2)). (**B**) Volume and beta amplitude of significant voxels (T>2)

Figure 5 shows the spatial distribution (**A**) and quantitative comparisons (**B**) of SCI group-level activity during each the enriched covert hand-related tasks. In all task conditions, activity was widely distributed throughout SMC, consistent with the activity seen during Overt attempted movement. Interestingly, the SCI group displayed a strong spatial disparity between activity in dorsal and ventral aspects. While dorsal M1/S1 displayed similar or greater activity across enrichment conditions compared to Simple for each task, Goal and Audio conditions appeared to significantly decrease activity in ventral areas during the Wrist and Grasp. This effect was not observed during the Stim conditions, where activity volume and amplitude was similar or greater than Simple for each task. Such decreases were also much less pronounced in the *Fingers* task. When we compared each condition's +β-value distribution between subject groups, we found that the SCI group displayed significantly greater activation in every region and condition ($p<0.001$, Wilcoxon rank-sum).

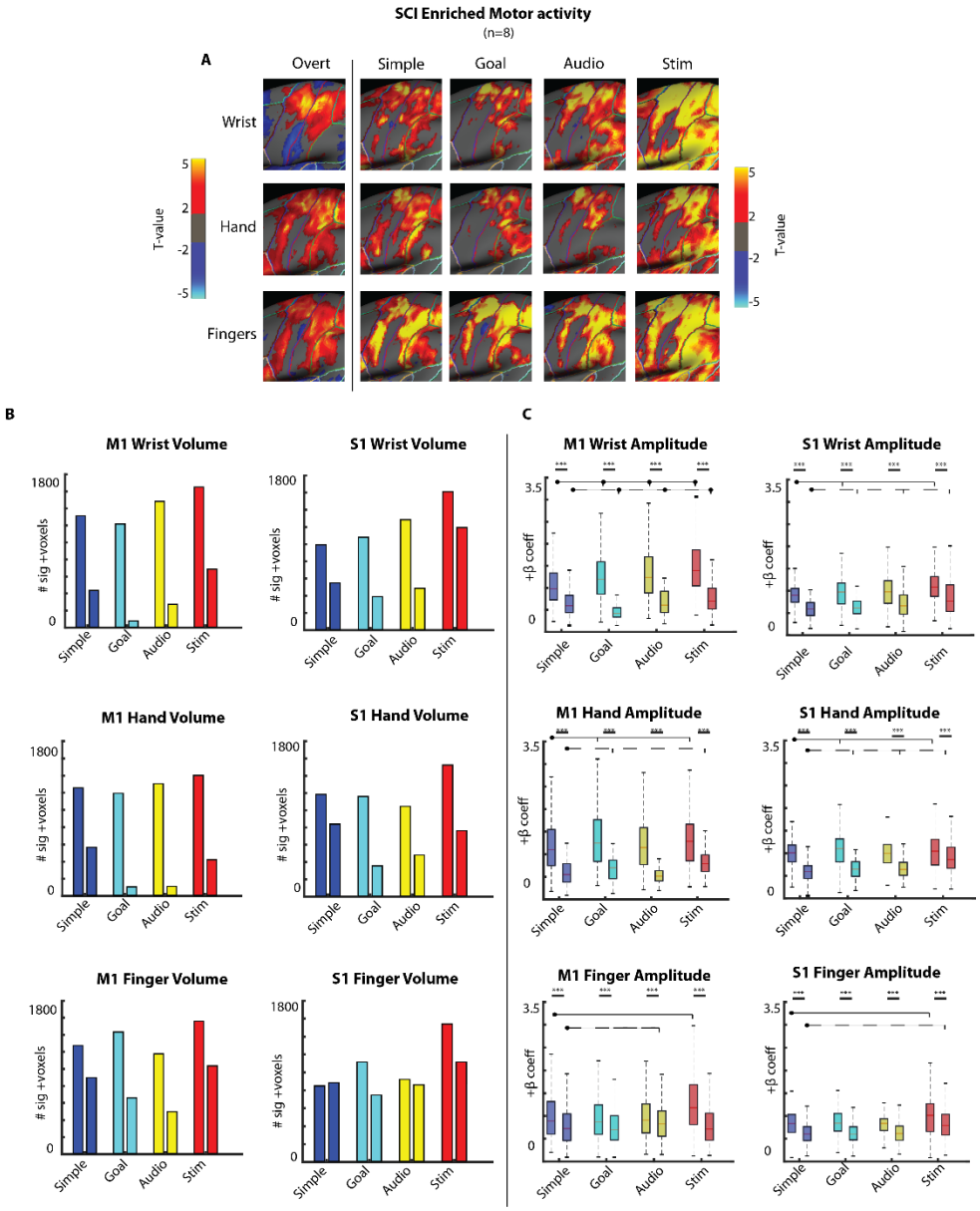

Figure 5: SCI group-level activity during enriched Motor tasks. (**A**) surface renders (T-vals thresholded at FDR>0.05, T>2)). (**B**) Volume and beta amplitude of significant voxels (T>2)

2.3.4 Directly calculating enrichment effect

These results illustrate that group-level activity during each hand-related task displays significant changes across different multisensory contexts, generally increasing in volume and amplitude with additive enrichment. To explore how activity changes between each condition, we then sought to directly quantify the effects of enrichment across individual subjects.

Figure 6 shows the AB group-level enrichment values ($\Delta\beta$) for each pair of conditions within each motor task. The Wrist task displayed substantial enrichment in all SMC areas during all 3 conditions compared to Simple, consistent with changes observed in the group-level activity. Both Audio and Stim displayed negative enrichment from Goal, indicating that much of the observed increases in activity across conditions derive primarily from the Goal condition. The Hand task displayed more diverse enrichment effects, with the Audio condition displaying the greatest enrichment, especially in S1. The Fingers task displayed little enrichment in either Goal or Audio conditions, but showed dramatic increases in the Stim condition relative to all others.

Overall, these results demonstrate that in able-bodied subjects, multisensory enrichment increased task-related activity throughout SMC during motor imagery. This elevated activation was not spatially limited to the cortical areas involved in driving overt movements, but was instead distributed throughout SMC. Indeed, the areas most consistently active during enriched covert tasks displayed different spatial trends in motor and somatosensory cortices. Enriched activity in M1 was frequently observed in more anterior and ventral areas, as well as the dorsal and posterior areas dominant in Overt tasks, while enrichment in S1 was generally located in more posterior areas relative to Overt activity.

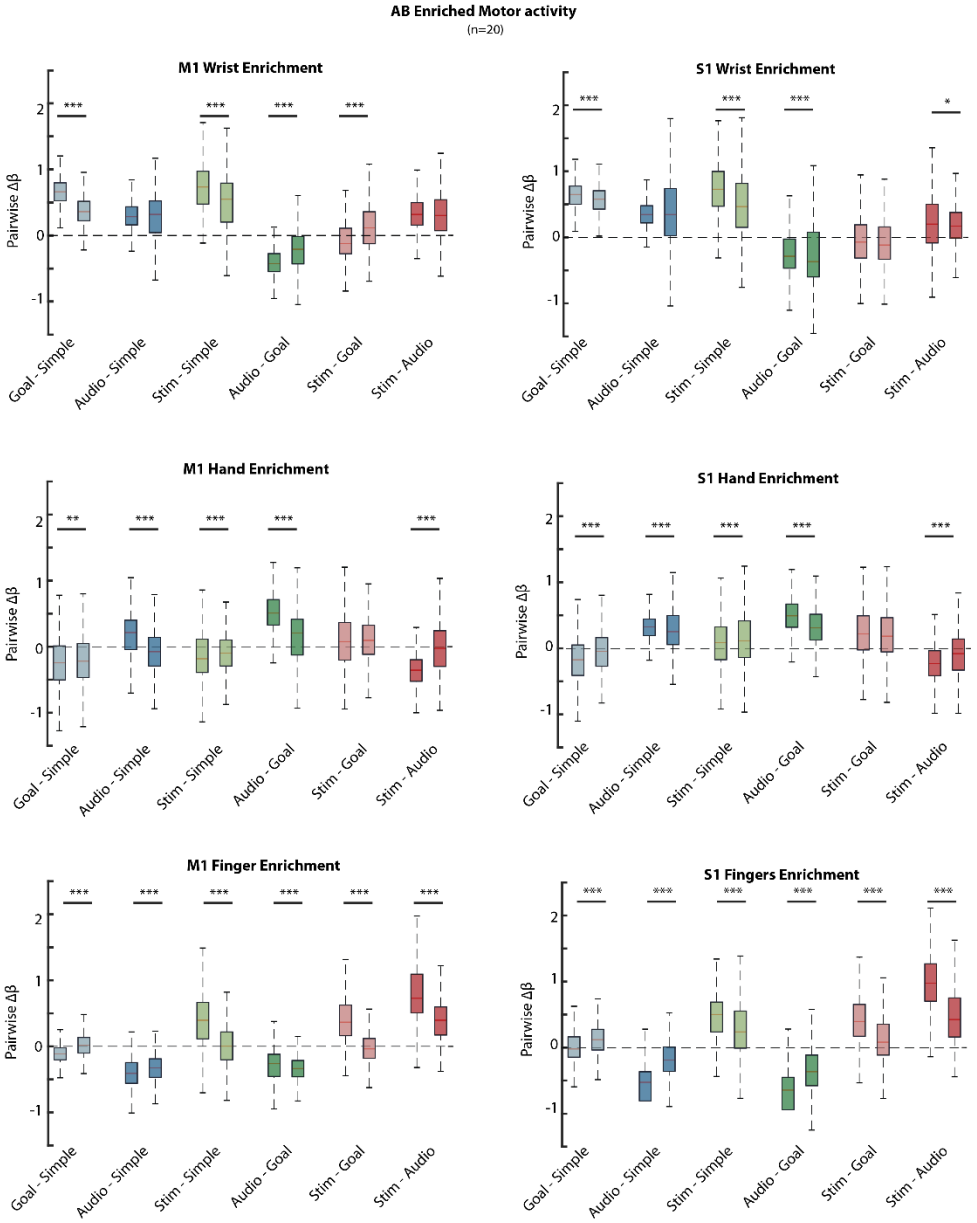

Figure 6: AB group-averaged per-voxel enrichment effects between pairwise conditions. Boxes show median, interquartile range, and 5/95%. *** = significance between arrays, $p<0.05$ Wilcoxon rank-sum

We then examined the per-voxel enrichment effect in the SCI group. **Figure 7** shows the distribution of per-voxel Δβ for each task's pairwise enrichment. The Wrist task displayed substantial positive enrichment during the Audio and Stim conditions, while Goal enrichment was negligible. Interestingly, strong Audio enrichment was present in dorsal but less so in ventral aspects, while Stim enrichment was present in all regions and especially pronounced in ventral aspects (especially S1). The Hand task generally displayed only minor enrichment in Goal and Audio conditions, but strong positive enrichment in all areas during the Stim condition, particularly in both ventral regions. The Fingers task displayed a similar pattern, where activity did not change substantially in Goal and Audio conditions, but increased dramatically in all areas with Stim enrichment. In comparison to the AB group, SCI subjects displayed similar patterns of conditional enrichment across tasks, with less overall response (positive enrichment) during Goal and Audio conditions, but much more response to Stim conditions.

This dichotomy was confirmed when we directly compared each region's pairwise enrichment between groups. Within Wrist and Hand conditions, we found that baseline enrichment (Enrich – Simple) was significantly greater in the AB group across regions, while cumulative enrichment ($Enrich_N$ – $Enrich_{N-1}$) was greater in the SCI group across regions. Within Finger conditions, the SCI group displayed greater enrichment in almost every region and condition pair (18/24) $p<0.001$, two-tailed t-test).

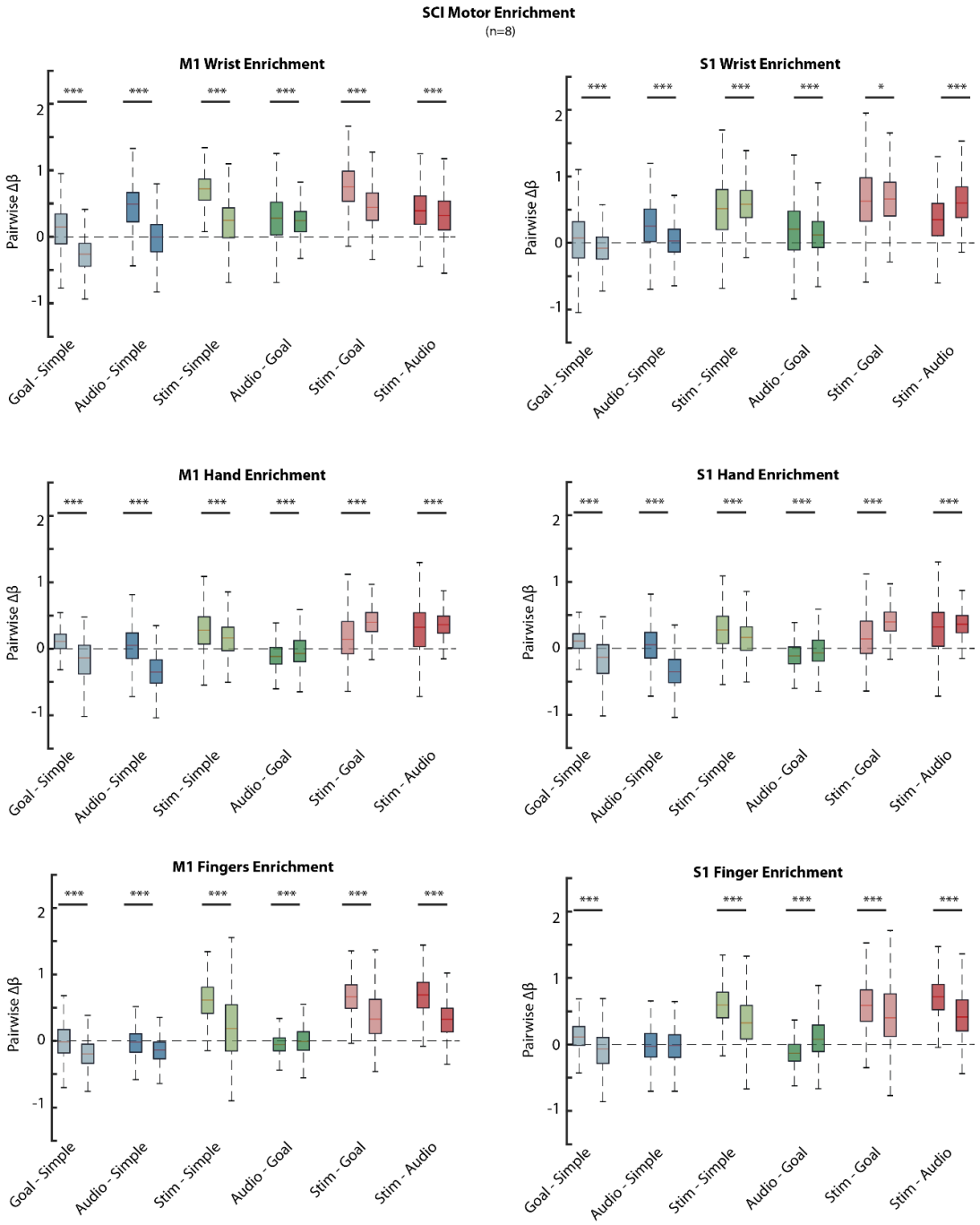

Figure 7: SCI group-averaged per-voxel enrichment effects between pairwise conditions. Boxes show median, interquartile range, and 5/95%. *** = significance between arrays, p<0.05 Wilcoxon rank-sum.

2.3.5 Group-level activity during covert Sensory enrichment

We next examined the effect of contextual enrichment during Sensory tasks, which were designed to elicit somatosensory-related activity rather than motor imagery. **Figure 8** shows the AB group-level activity during enrichments of passive wrist movement and fingertip stimulation. Although these tasks are focused on somatosensory sensations, we observed significant activity in M1 as well as S1 during each task-condition. During Sensory-Wrist imagery, we found that the volume and amplitude of activity in each enrichment condition was decreased relative to Simple, contrasting the effects seen during Motor-Wrist imagery. Activity volume during the Sensory-Finger task appeared to increase most dramatically with Goal enrichment, while amplitude was significantly greater across regions in each condition compared to Simple.

Conversely, during Sensory-Wrist imagery the SCI group (**Figure 9**) displayed higher activity volume and amplitude in M1 compared to S1, with significantly stronger activity during the Goal condition, particularly in dorsal aspects. During the Sensory-Fingers task we observed substantial activity in each condition, but surprisingly found that each enrichment condition reduced the amplitude of activity relative to simple. As in the Motor tasks, directly comparing each condition's amplitude between groups revealed stronger SCI activity in a majority of regions and conditions (14/16 comparisons, $p<0.05$ Wilcoxon rank-sum).

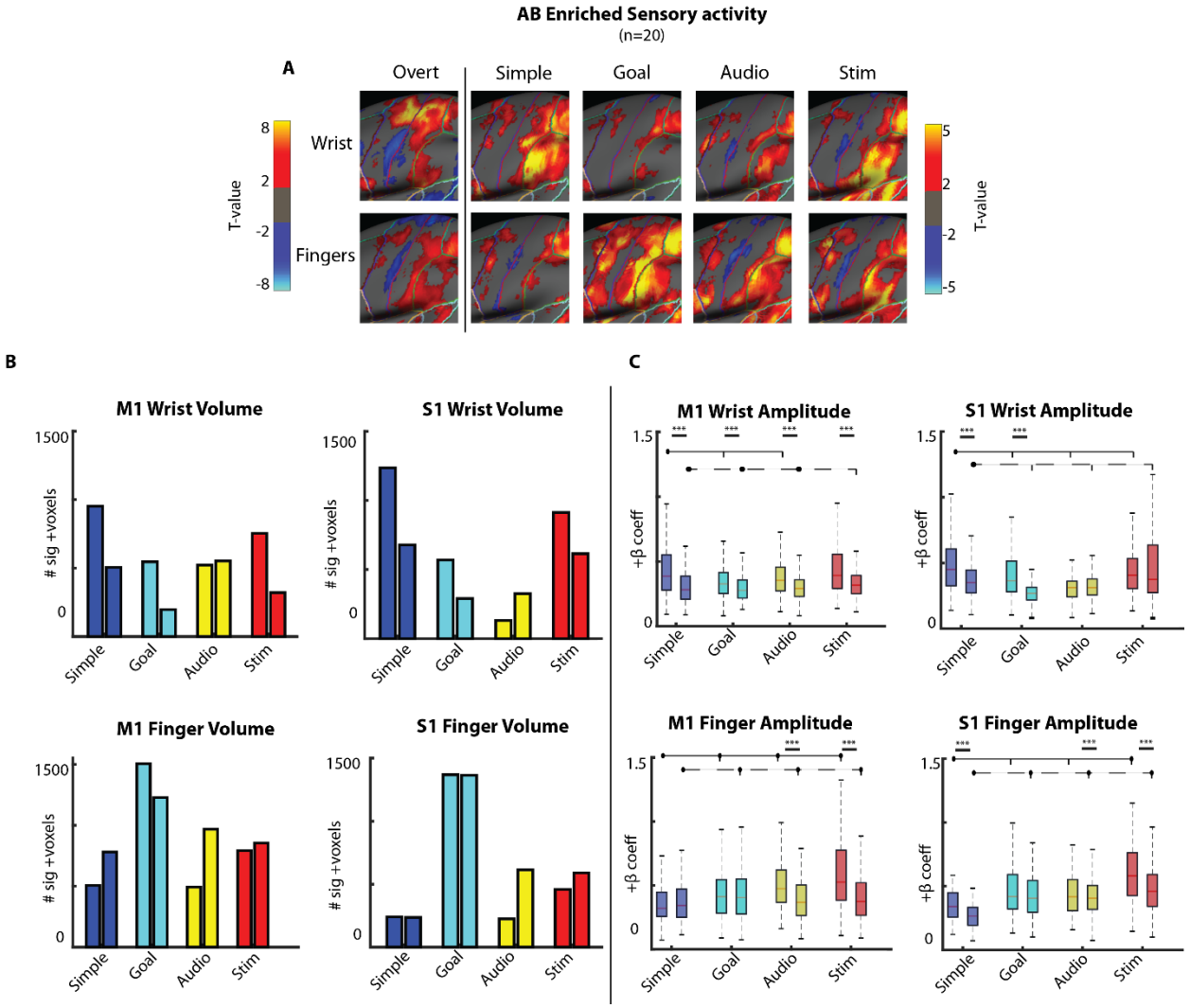

Figure 8: AB group-level activity during enriched Sensory tasks. (A) surface renders (T-vals thresholded at FDR>0.05, T>2)). (B) Volume and beta amplitude of significant voxels (T>2)

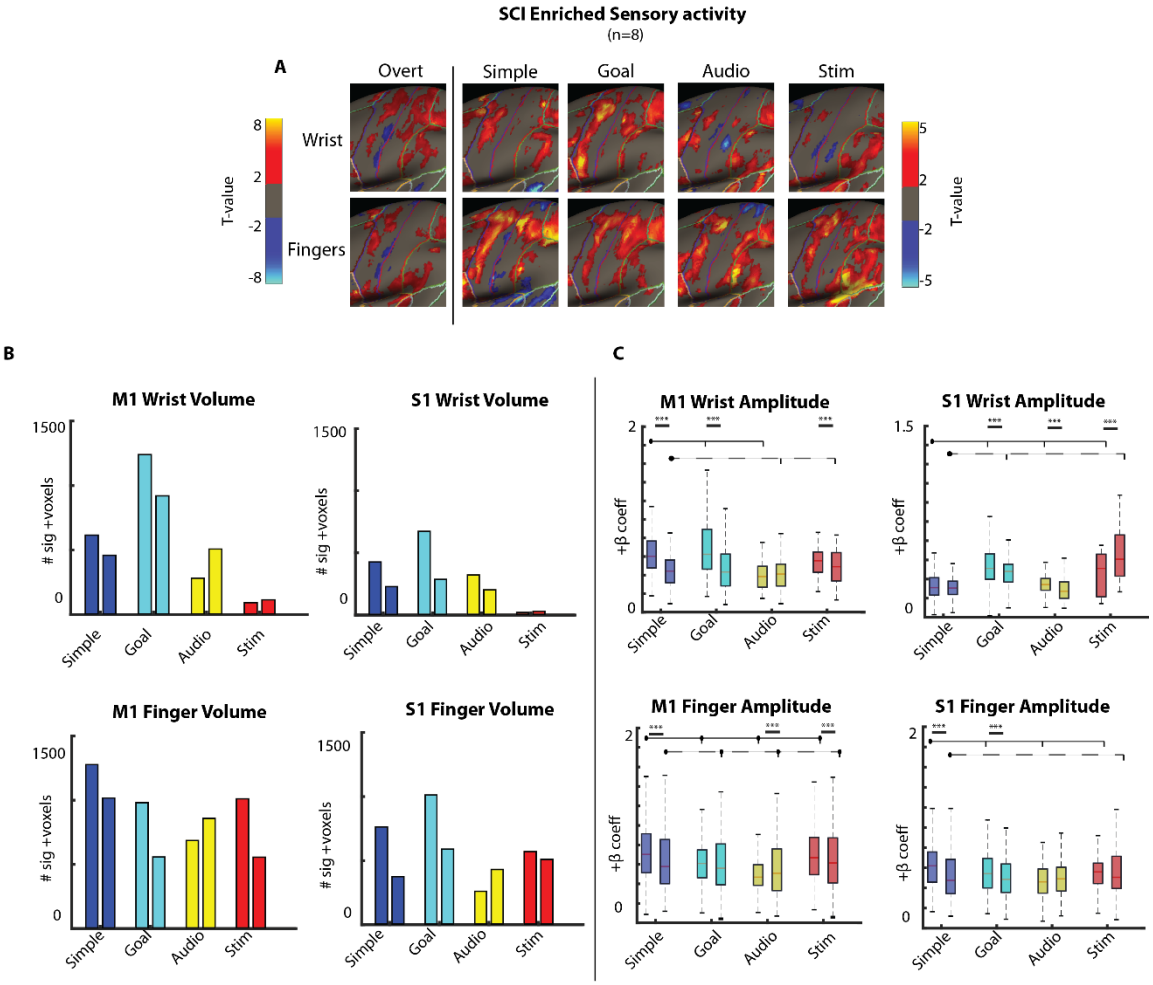

Figure 9: SCI group-level activity during enriched Sensory tasks. (A) surface renders (T-vals thresholded at FDR>0.05, T>2)). (B) Volume and beta amplitude of significant voxels (T>2)

When we directly calculated each group's pairwise per-voxel Δβ we found that within the Sensory-Wrist task, the AB group (**Figure 10**) only displayed substantial increases specifically in the Stim condition, predominantly in dorsal SMC. During the Sensory-Finger task, we observed greatly increased activity with Goal enrichment in both aspects of SMC , with additional increases due to Audio (particularly in ventral aspects) and Stim (particularly in dorsal aspects). In the SCI group (**Figure 11**), we found strong Goal-driven increases in both regions (particularly dorsal) during the Sensory-Wrist task, while additional enrichment appeared to reduce this effect. We found more complex changes during the Sensory-Finger task; ventral S1 activity increased relative to Simple in each enrichment condition, while dorsal S1was reduced by Audio cues but increased again with Stim. Activity in M1 was either unchanged or decreased with enrichment, with the exception of an increase in the dorsal aspect during the Stim condition. Directly comparing per-voxel distributions between groups revealed that while both groups displayed only moderately increased activity during Sensory tasks, these effects were greater in the AB group across a majority of task-condition pairs (16/24, $p<0.05$, Wilcoxon rank-sum).

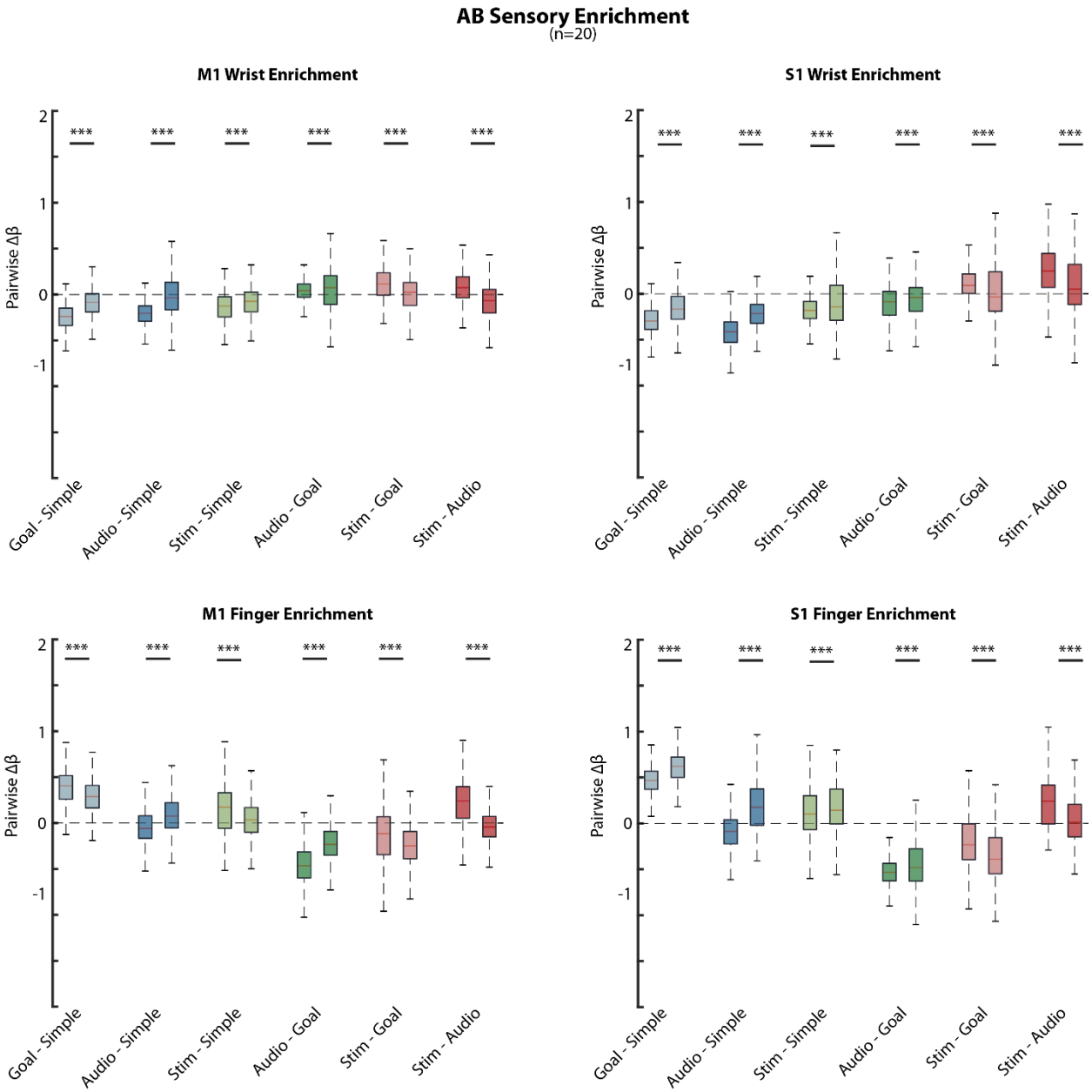

Figure 10: AB enrichment during Sensory tasks. Boxes show median, interquartile range, and 5/95%. *** = significance between arrays, $p<0.05$ Wilcoxon rank-sum.

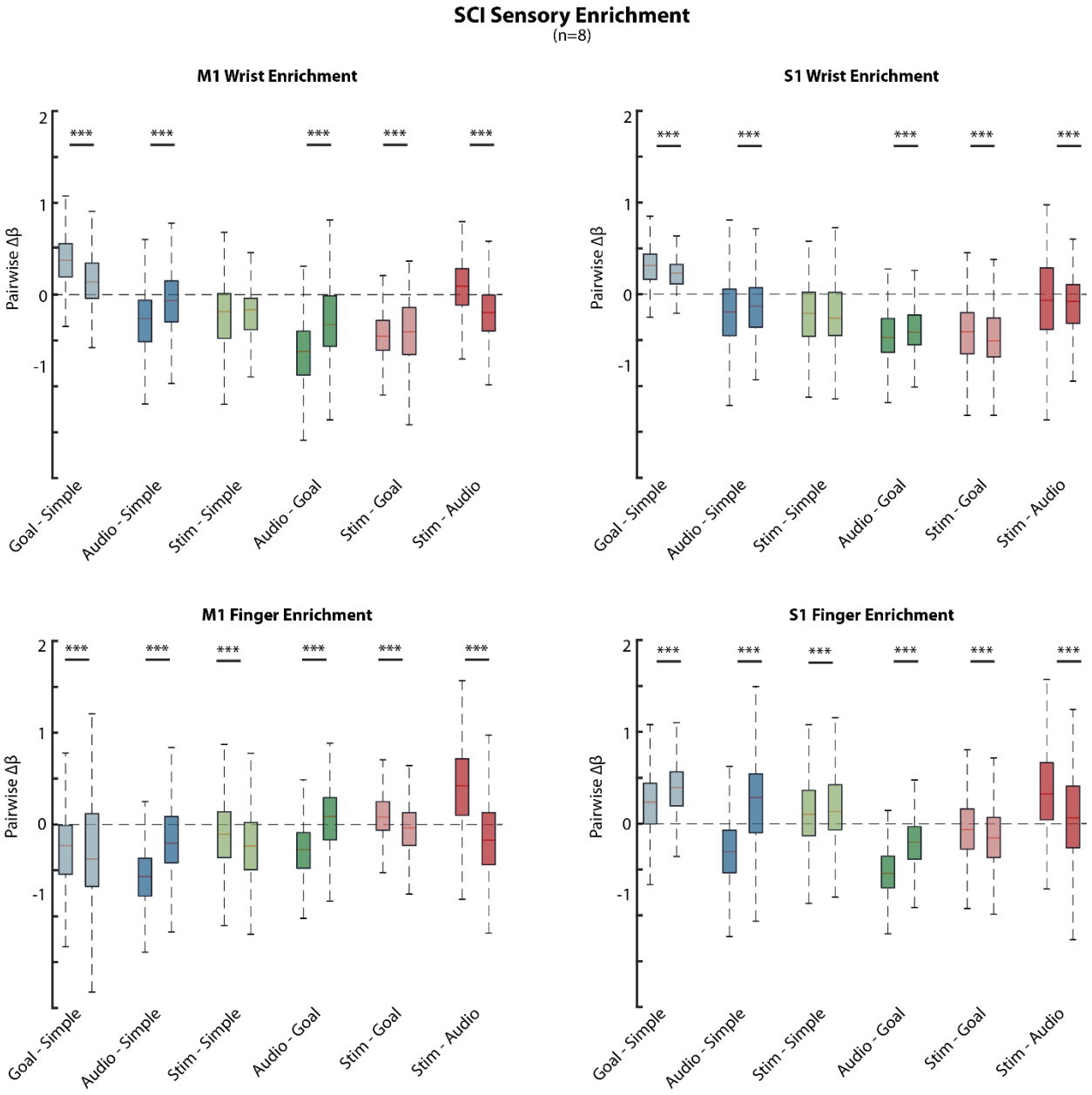

Figure 11: SCI enrichment during Sensory tasks. Group-averaged per-voxel enrichment effects between pairwise Sensory conditions in dorsal (left) and ventral (right) aspects. Boxes show median, interquartile range, and 5/95%. *** = significance between arrays, $p<0.05$ Wilcoxon rank-sum.

2.4 Discussion

We designed and tested a novel behavioral paradigm to determine how cortical sensorimotor activity during motor and somatosensory imagery is affected by additional multisensory cues. We observed substantial activation throughout M1 and S1 during each covert task in both able-bodied subjects and individuals with SCI. This Covert activity partially overlapped with the representations seen during Overt movement, but was also frequently observed in more ventral regions of cortex.

The activation profiles observed during overt movements suggests that even in "simple" tasks, hand-related sensorimotor control involves significant portions of M1 and S1, which can be both selective (preferentially active during certain conditions) and shared (active during multiple conditions). Since the three upper-limb overt conditions (wrist flex/extend, hand grasp/open, sequential finger tap) differ primarily in the specific patterns of muscle contraction necessary to perform them, these spatial trends suggest that rather than being tightly clustered, the neural circuits underlying hand use involve activity throughout SMC, and that activity in a given area may contribute differently to encoding similar motor commands under different behavioral contexts.

During enriched Wrist movement, the AB group displayed substantially increased activity in the Goal condition compared to simple, particularly in the dorsal aspects of both M1/S1. Both group-level activity and per-subject enrichment increased with enrichment, suggesting that Goal enrichment may drive increased activity in a relatively small cortical area. AB-group activity primarily rose with Audio enrichment during Hand movement and with Stim enrichment during Finger movement, indicating that while Goal enrichment may not increase

activity during all movements, the additional timing information provided by Audio and Stim enrichment can still be integrated, driving increased activity in M1 but particularly in S1.

The SCI group displayed significantly increased activity in Overt movements compared to the AB group, as well as in a majority of Covert conditions. SCI-group activity during enriched Motor was stronger in dorsal aspects of M1/S1, indicating that post-injury reorganization may result in the expanded recruitment of disconnected cortical territory by partially preserved movements (K. J. Kokotilo et al., 2009; Urbin et al., 2019). In addition, the SCI displayed less Goal-related increases in activity but consistent increases in both M1 and S1 during Audio and Stim conditions (most notably Stim), suggesting that the additional timing information conveyed by auditory and vibrotactile stimulation may aid in embodying attempted movements (Gentile et al., 2013; Ratcliffe & Newport, 2017).

During enriched Sensory tasks, we found that S1 activity was significantly increased during Goal and Stim enrichment, especially during covert Finger stimulation. While M1 activity was either maintained or decreased, the increases in S1 during Goal enrichment demonstrates that purely visual information can be used to increase the strength of somatosensory representations, consistent with other recent results (Kuehn et al., 2018).

Taken together, our results demonstrate that motor and somatosensory imagery tasks can be enriched with multisensory cues to increase the intensity of activity in sensorimotor cortex. Different combinations of enrichment elicited peak activation during different upper limb tasks, suggesting that while these cues can be integrated by the sensorimotor network, their effect can vary based on the behavioral context of the task. While enriched covert activity was frequently observed to spatially overlap with Overt activity, we also observed significant enrichment-related increases in more ventral and anterior areas. As these areas may be more likely to receive input

from premotor and parietal areas, this localized Covert activity may indicate cortical areas which are more strongly involved in integrating contextual multisensory information. Such areas may be potential targets for the future development of intracortical BCI, which could benefit from access to more context-sensitive neural activity (Downey et al., 2017).

In order to ensure that this enrichment paradigm can be successfully used for mapping activity in individuals with SCI, we analyzed data from 8 participants with chronic SCI-induced tetraplegia. Subjects with SCI were instructed to attempt to perform covert movements in order to maximize the intensity of elicited cortical activity, while AB subjects were instructed to imagine performing covert movements in order to minimize actual somatosensory input. This difference makes it difficult to directly compare the distribution of activity and the effects of enrichment between groups. As subjects with SCI display different activity when instructed to attempt and imagine performing movements (Foldes et al., 2017), our data may suggest that future studies comparing activity between able-bodied subjects and subjects with tetraplegia could achieve better similarity by having both subject groups "attempt" to perform tasks rather than imagining.

Our results demonstrate the potential effectiveness of using contextual multisensory cues to enrich behavioral tasks and increase the utility of sensorimotor mapping. However, our observations that enriched activity was often widely distributed throughout SMC, as well as frequently overlapping in specific areas, suggests that contextual sensory information may be preferentially processed by different areas of cortex. It may be possible to determine how sensorimotor task activity is represented in a given area by applying multivoxel analyses to quantify the representational similarity between conditional activity (Ejaz et al., 2015; Kriegeskorte, 2008). While such analyses require a large amount purpose-collected data, using

this kind of decoding-based approach could be used to identify cortical areas with maximally separable activity, which could be invaluable for pre-surgical planning of invasive recordings (Collinger et al., 2014; Yoo et al., 2018).

3.0 Somatotopic Biases in the Broad Tuning of M1 Neurons

Figures and text in this chapter have been reproduced with permission from a paper submitted to the journal Neuron by: Dylan A. Royston, Brian M. Dekleva, Stephen T. Foldes, Elizabeth C. Tyler-Kabara, Michael L. Boninger, Timothy D. Verstynen, Robert A. Gaunt, Aaron P. Batista, and Jennifer L. Collinger.

Human primary motor cortex is grossly somatotopically organized, similar to the organization found in animal investigations of single-neurons. However, the human hand possesses a unique degree of individuated dexterity, and it is unclear how this control is reflected in the behavior of individual neurons. We recorded single-neuron activity from two microelectrode arrays placed centimeters apart within the M1 upper limb representation in two human participants with tetraplegia as they attempted arm and hand movements, many of which could not be performed overtly. We found that single neurons were broadly modulated by arm and hand movements, often displaying similar firing rate ranges during all tasks. However, neurons in more medial areas of M1 displayed more selective firing during arm movements but were also active during individual finger tasks. Neurons in lateral areas of M1 displayed broad tuning to both arm and finger movements. We conclude that macro-level somatotopy reflects local biases in the activity of broadly-tuned neurons, consistent with modern theories of population-level encoding models.

3.1 Introduction

The relationship between the location of activity in primary motor cortex (M1) and corresponding movement production has been a subject of investigation and debate for over half a century. While it is clear that mesoscale somatotopy (causal correlation between localized activity and the production of specific movements) is present in humans, there is ongoing debate regarding whether this organization is observed across spatial scales, and how broadly these movement representations are distributed across populations of individual neurons within M1. Early cortical stimulation studies yielded an orderly "homunculus", where evoked movements in different areas of the body were organized in a mediolateral gradient across M1 (W Penfield & Rasmussen, 1950; Wilder Penfield & Boldrey, 1937). This large-scale somatotopy has since been observed in human neuroimaging data (Alkadhi et al., 2002; Cunningham et al., 2013; Plow et al., 2010; Stippich, Ochmann, & Sartor, 2002), but such studies also reveal that rather than the clear separation portrayed by early "homunculus diagrams" (Wilder Penfield & Boldrey, 1937), cortical representations display substantial overlap (Ejaz et al., 2015; Hlustik, 2001; Sanes, Donoghue, Thangaraj, Edelman, & Warach, 1995). However, the signals measured by imaging and cortical surface recordings are generated by millions of neurons simultaneously (N K Logothetis et al., 2001), so it remains unclear how these mesoscale findings extend to the individual neurons responsible for controlling movement. This question is particularly relevant to the study of upper-limb sensorimotor control in humans, where a broad spectrum of dexterous hand and finger control is represented in a large area of cortex.

It is well-established that the activity of M1 neurons is strongly involved in generating upper limb movements (Kakei et al., 1999). Spiking activity from cells throughout M1 have

demonstrated “tuning” to (activity correlated with) a variety of movement parameters (Georgopoulos et al., 1982, 2009), and many M1 neurons project to motor neurons in the spinal cord, allowing their activity to directly influence motor production (Griffin et al., 2015). Retrograde tracer studies have shown that these corticomotoneurons projecting to shoulder and finger muscles are spatially intermixed in non-human primates (J.-A. Rathelot & Strick, 2009), indicating a high degree of physical coordination and spatial overlap between the neural populations involved in controlling different muscle groups. In addition to this spatial intermixing of functionally-distinct descending neurons, electrophysiology studies in non-human primates (NHPs) have shown that individual neurons in the hand area of M1 display similar activity during individuated movement of each finger (Irwin et al., 2017; Kirsch, Rivlis, & Schieber, 2014; M. Schieber & Hibbard, 1993b). This suggests that the overlapping representations observed at a gross level are not only caused by spatially intermixed populations, but also broad functional tuning in individual neurons. Additionally, as NHPs do not naturally display individuated finger movements, most such studies have not examined the functional relationship between neural encoding of both arm movements and hand/finger control, which is a dominant behavioral trait in humans.

Neuroimaging studies in humans have shown substantial overlap in the activity underlying different upper limb movements, particularly within areas related to individual finger movements (Beisteiner et al., 2001) but also between hand and arm representations (Meier, Aflalo, Kastner, & Graziano, 2008; Plow et al., 2010). These overlapping representations have frequently been interpreted in the framework of a “functional somatotopy” Cunningham et al., 2013), wherein the neural circuits underlying motor production are shared between different movements in order to facilitate within-limb coordination. Such results suggest that a given

overlap area of cortex may contain individual neurons involved in producing different movements, and many overlap areas together may create a somatotopic gradient of neural populations with different tuning properties. Results from sequentially recorded single neurons in NHP hand areas revealed significant overlap and minimal separation between neurons modulated by individual finger movements (M. Schieber & Hibbard, 1993b), supporting the concept of neural circuits being involved in multiple movement representations.

The fact that activity related to multiple movements is contained within a relatively small cortical volume raises the question of whether motor cortex contains multiple behaviorally-independent, but spatially-intermixed, neural populations, or a single population capable of producing many behaviors through distinct patterns of activity. Since the local and long-range connectivity of M1 means neighboring neurons are unlikely to be functionally independent, we aimed to characterize the degree to which individual neurons selectively encode different types of movement, and whether neurons from spatially separate cortical areas display different "tuning" profiles. We recorded from microelectrode arrays chronically implanted in M1 of two human subjects (2 arrays in each subject) participating in an ongoing brain-computer interface (BCI) study. Simultaneous recordings were made from both arrays while participants attempted to perform arm(arm) and finger (finger) movements. Both participants have chronic tetraplegia as a prerequisite for participation in this study. While this limited their performance of most movements, there is substantial evidence showing that the large-scale organization of upper limb representations is preserved even after chronic injury (Degenhart et al., 2017; Foldes et al., 2017; Kikkert et al., 2016; K. J. Kokotilo et al., 2009; Makin & Bensmaia, 2017; Urbin et al., 2019). By characterizing the behavior of individual neurons from separate areas during a range of

different movement types, we can determine how large-scale somatotopy is reflected in the activity of neural populations throughout M1.

3.2 Materials and Methods

3.2.1 Study participants and surgical procedures

The studies allowing the collection of this data were approved by the institutional review boards at the University of Pittsburgh (Pittsburgh, PA, USA) and the Space and Naval Warfare Systems Center Pacific (San Diego, CA, USA). We obtained verbal informed consent from both participants before their enrollment in these studies, and consent was signed by their legal representatives. We collected and analyzed data from two individuals implanted with platinum-coated silicon intracortical microelectrode arrays (Blackrock Microsystems, Salt Lake City, UT, USA) in left primary motor cortex.

Participant 1 was a 52-year old female at time of implant, with chronic tetraplegia due to spinocerebellar degeneration diagnosed 13 years before participating in this study. Due to the nature of this condition, the subject has complete loss of motor function below the neck while retaining intact somatosensation. Participant 1 was implanted with two 4mm x 4mm x 1.5mm, 96-channel arrays in motor cortex. Participant 2 was a 28 at time of implant, with chronic tetraplegia due to a C5-motor/C6-sensory ASIA-B spinal cord injury (due to automobile accident) approximately 10 years before implantation. Due to the level of injury, this participant

retains full use of his shoulder and elbow, partial use (extension) of his wrist, while his hand is completely paralyzed and desensate in the medial part of his hand innervated by the median nerve. Participant 2 was implanted with two 4mm x 4mm x 1.5mm, 88-channel arrays in motor cortex. He was also implanted with two 2.4mm x 4 mm x 1.5mm, 60-channel arrays in primary somatosensory cortex ((Flesher et al., 2016)), but data from these arrays were not included in this study.

3.2.2 Presurgical neuroimaging

MRI data were collected on a Siemens Technology (Munich, Germany) Trio 3T scanner. Participant 1 received a T1-weighted whole-brain anatomical scan (1x1x1.2 mm voxels, 160 slices, 240x256 mm in-plane resolution). Functional scans were collected from dorsal sensorimotor cortex using T2*-weighted echo-planar imaging (EPI) sequence (TR = 2000 ms, voxel size = 2 mm^3 isovoxel, 128x128 mm in-plane resolution, 27 mm field of view). Participant 2 received a T1-weighted whole-brain anatomical scan (1 mm^3 isovoxel, 176 slices, 256x256 mm in-plane resolution). Functional scans were collected from dorsal sensorimotor cortex using T2*-weighted echo-planar imaging (EPI) sequence (TR = 2000 ms, TE = 29 ms, voxel size = 2.156 x 2.156 mm, slice thickness = 2 mm, 128x128 mm in-plane resolution, 26 mm field of view).

Functional data were collected using a block design (**Figure 12A**), wherein a 20 second baseline period was followed by 4 alternating 20 second blocks of rest and movement condition. Each run consisted of 4 blocks of rest/move conditions. Rest periods were cued by a gray fixation cross, while movement conditions consisted of a green/red fixation cross changing color

at 0.5 Hz, cuing subjects to alternatively grasp and relax with their dominant hand, respectively. During the movement condition, the participant was instructed to "attempt" to physically execute each movement. fMRI data were pre-processed using SPM12 (Ashburner et al., 2013). fMRI images were spatially realigned using a rigid-body transformation, spatially smoothed (6 mm FWHM), and coregistered to the anatomical scan. BOLD responses were determined with a box-car general linear model (GLM) convolved with a canonical hemodynamic response function. The resulting T-contrast images were then projected onto a cortical surface render (created using Freesurfer (Fischl, 2012)) for visualization(Collinger et al., 2014).

3.2.3 Array placement based on presurgical neuroimaging

In order to record the cortical activity most directly related to upper limb movements, fMRI was used to localize the cortical areas active while the subjects attempted to perform various upper limb movements. These functional images served to guide the placement of the microelectrode arrays implanted in each subject's primary motor cortex (**Figure 12B/C**). Final positioning was determined intraoperatively based on the cortical surface topography and vasculature. Array position was estimated using post-implantation high-resolution CT and co-registered to the pre-surgical MRI. For participant 1, one array was placed in a lateral area active during grasp and finger tapping tasks ("lateral motor array"), while the other was placed more medially in an area of grasp-related activity and adjacent to shoulder-related activity ("medial motor array"). For participant 2, one array was placed in a lateral area of finger- and grasp-related activity, while the second array was placed in a more medial area thought to be more related to arm movement, although this was not mapped explicitly.

3.2.4 Behavioral task design

We designed a rhythmic movement task to provide a behaviorally simple task for subjects to perform in order to generate clear movement-related neural activity. The participants were presented with videos of movements and instructed to attempt, as much as physically possible, to perform each movement in time with the videos. Although neither participant was able to overtly perform all movements, subjects were asked to attempt the movements in order to maximize the magnitude of movement-related neural activity (Szameitat, Shen, Conforto, & Sterr, 2012).

Participant 1 performed 5 tasks: shoulder raise/lower, elbow flex/extend, wrist flex/extend, whole-hand grasp, and sequential thumb-finger tapping. Participant 2 performed 9 tasks: shoulder raise/lower, elbow flex/extend, wrist flex/extend, whole-hand grasp, and flex/extend all 5 individual fingers. To facilitate our ability to quantify neural modulation during different movement types, we split these tasks into "gross" (shoulder/elbow/wrist/grasp) and "fine" (individual finger) movements for several analyses.

These movements were paced at ~0.5Hz, such that one movement was performed every 2 seconds. For participant 1, movements were presented in individual blocks of 4 trials, where a trial consisted of 20 seconds of movement separated by 10 seconds of rest cued with a fixation cross. For participant 2, movements were presented in individual blocks of 8 trials, where a trial consisted of 10 seconds of movement separated by 5 seconds of rest cued with a fixation cross. Each test session consisted of one set of each movement. For participant 1, one testing session was performed one month after implantation. For participant 2, 12 testing sessions were

performed approximately every 1-2 months, beginning one month after implantation, for 44 months (**Figure 13**).

3.2.5 Neural recording/electrophysiology

Neural data were recorded from Utah microelectrode arrays implanted in the arm/hand area of M1. Raw voltage signals were sampled at 30KHz with a 250-4500 Hz bandpass filter. Spikes were defined as 48-sample (1.6ms) events where the voltage signal crossed a fixed threshold above the baseline root-mean-square (RMS) voltage for each channel (-5.25*baseline RMS for participant 1, -4.50*baseline RMS for participant 2).

To examine the activity of individual neurons, we sorted spike snippets into 'neurons' using the principal component analysis (PCA)-based method described previously ((Downey, Schwed, Chase, Schwartz, & Collinger, 2018)). Briefly, we used PCA to visualize each channel's snippets in the first two components based on waveform shape. Separable clusters were manually identified and used to initialize a Gaussian mixture model expectation-maximization algorithm, which created the specified number of clusters and assigned each snippet to the most likely unit.

To further isolate activity from individual neurons, neurons primarily containing noise events, i.e. snippets diverging from the stereotyped action potential waveform, were then manually identified and excluded from further analysis. Neurons that displayed any inter-spike intervals (ISI) less than 1ms were also excluded. We then calculated a consistency metric to identify neurons with consistent waveform shapes by taking the dot product of sequential

normalized snippets ((Fraser & Schwartz, 2012)). We fit the resulting "consistency" histogram with two normal distributions and identified the threshold separating neurons with low and high consistency, and only included those neurons with waveform consistency above this threshold.

3.2.6 Quantifying neural modulation during single movement repetitions

The behavioral task performed here was used in part to match the task used during presurgical neuroimaging. For this study, as we wanted to examine the neural activity underlying individual movement repetitions, we processed the raw timeseries activity to isolate each individual attempted movement. Using the stimulus videos provided to subjects, the start and end time of each single repetition was marked manually. As the stimulus videos were recorded continuously, each repetition had a slightly different duration, so we used the mean duration to define the length of each movement period. To make data between subjects as directly comparable as possible, we leveraged this repetition isolation to separate out individual finger movements from participant 1's sequential finger task. To calculate a given unit's activity during movement, we calculated a peristimulus time histogram (PSTH) of spike times during each movement repetition. We then smoothed this trial-averaged spike count with a Gaussian kernel (σ=50ms, width=300ms) to generate smooth instantaneous firing rates for each unit. In order to quantify the degree to which a given neuron was "tuned" to a specific movement, we extracted the firing rate activity from each neuron during these repetitions and calculated the modulation depth (MD) as the mean of the difference between maximum and minimum firing rate during the stacked repetitions.

3.2.7 Modulated neuron identification

To identify neurons that displayed modulated activity during attempted movement, we compared each neurons' firing rate distributions during movement and rest. To filter out spurious activity, only neurons with mean firing rates >1Hz during both movement and rest were analyzed. For each task, firing rate activity during rest (defined as the 2s prior to movement onset) and movement (defined as the 10s following movement onset) was concatenated across all trials and compared using a two-tailed Kolmogorov-Smirnov test ($p<0.001$). Any "valid" neuron that was significantly modulated during at least one task was included for further analysis.

3.2.8 Neural selectivity index

To examine how broadly a given neuron participated in encoding different movements, we calculated a "selectivity index" (SI) based on finger-movement individuation studies ((Lang & Schieber, 2003, 2004)). Selectivity (II_J) was calculated as:

$$II_j = \left[\sum_{i=1}^{n} \left|FR_{ij}\right| - 1\right] / \ (n-1) \qquad (3-1)$$

where *FR* is the modulation depth during each task (normalized for each neuron to its maximum task) and *n* is the number of tasks. By this metric, a neuron with an SI of 1 would be perfectly selective and only fire during one task, whereas a neuron with an SI of 0 would display the same activity during every task.

3.2.9 Movement type selectivity interaction

To account for potential type-wide differences in firing rate and determine whether neurons recorded from different areas were preferentially selective to one type of movement, we recalculated each neurons' SI for arm and finger movement types separately, and split neurons by array. We then used each neurons' SI to arm and finger movements to create a "bias distance" by plotting its selectivity to each movement type and calculating the Euclidean distance between that point and the midline (y=0, m=1), where neurons below this line displayed more selectivity to arm than finger movements and vice versa. We then calculated a "bias ratio" for each array by dividing the distribution of positive (below unity line) and negative (above unity line) distances.

3.2.10 Electromyogram recording

To evaluate participant 2's ability to overtly perform the attempted upper limb movements, we recorded surface EMG activity using an Intan recording controller (Intan Technologies, Los Angeles, CA, USA) while he performed each movement task (simultaneous with neural data included here on day 12). Recordings were made using bipolar electrode pairs

placed serially along the belly of each muscle. To examine upper limb movement activity, we recorded from the following muscles: trapezoid, posterior deltoid, mid deltoid, anterior deltoid, bicep, tricep, wrist extensor, wrist flexor. Raw voltage signals were passed through a band-pass filter (20-1000 Hz), rectified, and passed through a smoothing low-pass filter (2^{nd}-order Butterworth filter at 10 Hz), and de-noised to remove linear drift and outlier spikes. Activity during individual repetitions was reorganized in the same manner as the neural data described above.

3.3 Results

3.3.1 M1 neurons are broadly modulated during movement

We aimed to determine whether single neurons recorded from spatially separate areas of human M1 display different patterns of activity during arm and hand movements. Participants performed an attempted movement task where they viewed videos of simple rhythmic arm/hand movements and were instructed to attempt to perform the same movements with their own limbs (**Figure 12A**). All instructed movements used the right arm, contralateral to the implanted microelectrode arrays. Participant 1 performed 5 tasks (shoulder, elbow, wrist, grasp, sequential finger-tapping), while participant 2 performed 9 tasks (shoulder, elbow, wrist, grasp, and 5 individual finger movements). To determine the degree to which M1 activity displays somatotopic bias, we grouped these 9 movement tasks into “proximal” arm and hand movements

(shoulder, elbow, wrist, grasp) and "distal" individual finger movements (thumb, index, middle, ring, pinky for participant 2). For participant 1, sequential finger-tapping and grasp were classified as a "fine" movement due to the smaller range of movements performed. While the primary experiment was conducted with participant 2, we have included data from participant 1 since a similar dataset was collected.

Figure 12B/C shows the location of microelectrode arrays on the cortical surface. Array placement was in part guided by presurgical neuroimaging (see Methods); arrays for participant 1 were located within medial and lateral areas of the anatomical "hand knob", while participant 2 had one array located in a lateral hand-related area and another in a more medial arm-related area.

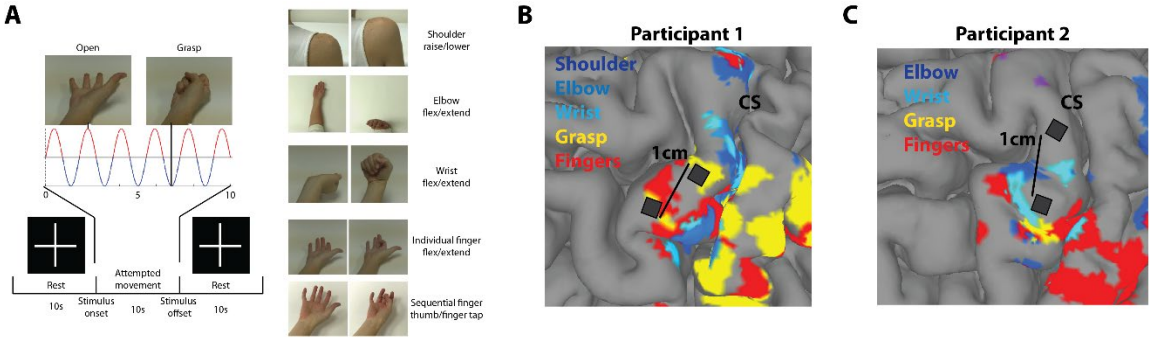

Figure 12: Behavioral task and electrode localization. (A): Left, task structure. 10s of rhythmic movement videos separated by 10 second rest periods. Right, example movement stimuli at peak phases of each task. (B and C): Electrode array locations and fMRI activation maps for participant 1 (B) and participant 2 (C) overlaid on individual cortical surface renders. Scale bars determined from intraoperative markers.

For participant 1, neural data were collected during one test session approximately 3 months after implantation. We recorded from 62 well-isolated single neurons (18 from the medial array, 25 from the lateral array). For participant 2, neural data were collected during 12 test sessions occurring every 1-2 months over the course of 23 months. We recorded from 708

well-isolated single neurons (432 medial, 276 lateral), with 88±21 neurons identified on a given day (**Figure 13**). As we have previously reported that individual neurons are unlikely to be recorded from after one month (Downey et al., 2018), we assume that data collected from each day represents a unique neural population. We also observed relatively little variability in the signal quality from individual neurons (evaluated as the mean peak-to-peak voltage of neuron spike waveforms; **Figure 13B**) and a gradual decrease in the number of neurons identified from day to day (**Figure 13A**), , consistent with previous observations from the same participants ((Downey et al., 2018)).

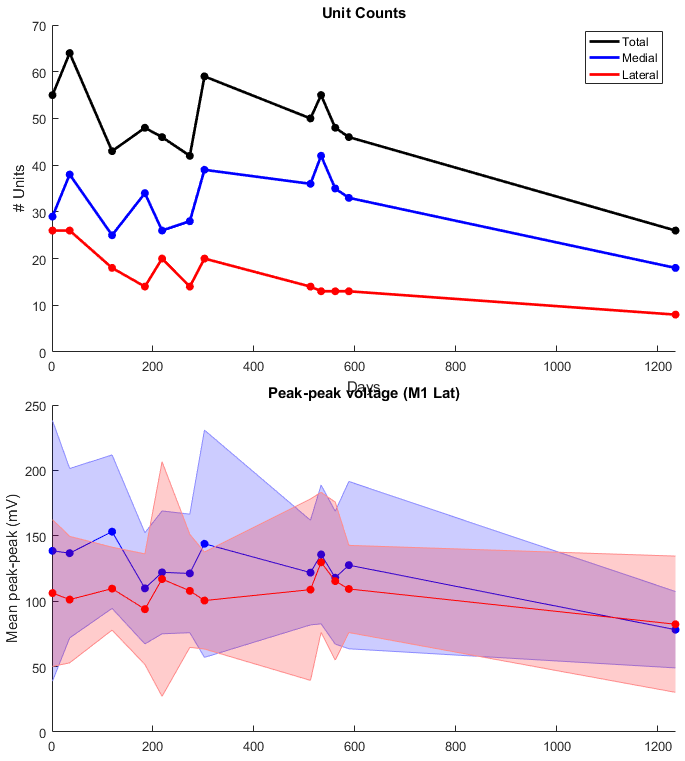

Figure 13: Recording stability from participant 2 over time. (A): number of well-isolated neurons recorded from both arrays during each testing session. (B): peak-peak voltage distribution of well-isolated units recorded from both arrays

Examining the activity of these isolated neurons revealed strong rhythmic activity matching the pacing of the attempted movements. **Figure 14B-G** illustrates the responses of six such neurons, with varied modulation observed during different movement tasks (which are represented by different colors, as shown in **Figure 14A**). In order to assess task-related modulation, we generated peristimulus time-histograms (PSTH) for each neuron by aligning each neuron's spiking activity during movement performance. Since each task was performed as a continuous 10-second period of rhythmic movement, we aligned each neuron's spiking activity to the onset of each individual movement repetition, thereby providing a readout of that neuron's time-series activity during a single performance of each movement. Each panel (Figure 2 B-G) shows a single neuron's PSTH spiking activity (top) and trial-averaged firing rate (bottom) during performance of each movement. By examining how a neuron's spiking activity changes throughout the course of each movement, we aimed to characterize whether it was preferentially modulated (or "tuned") during a certain type of movement, thereby defining a "tuning function" for each neuron (shown inset within bottom firing-rate plots). For example, we identified neurons which displayed more overall modulation during either arm(**Figure 14B/C**), or finger (**Figure 14D/E)** tasks, suggesting that some neurons participate in broadly encoding a general "type" of movement. We also observed neurons which displayed much more activity during a single movement compared to others, indicating the presence of a more "selective" population of neurons.

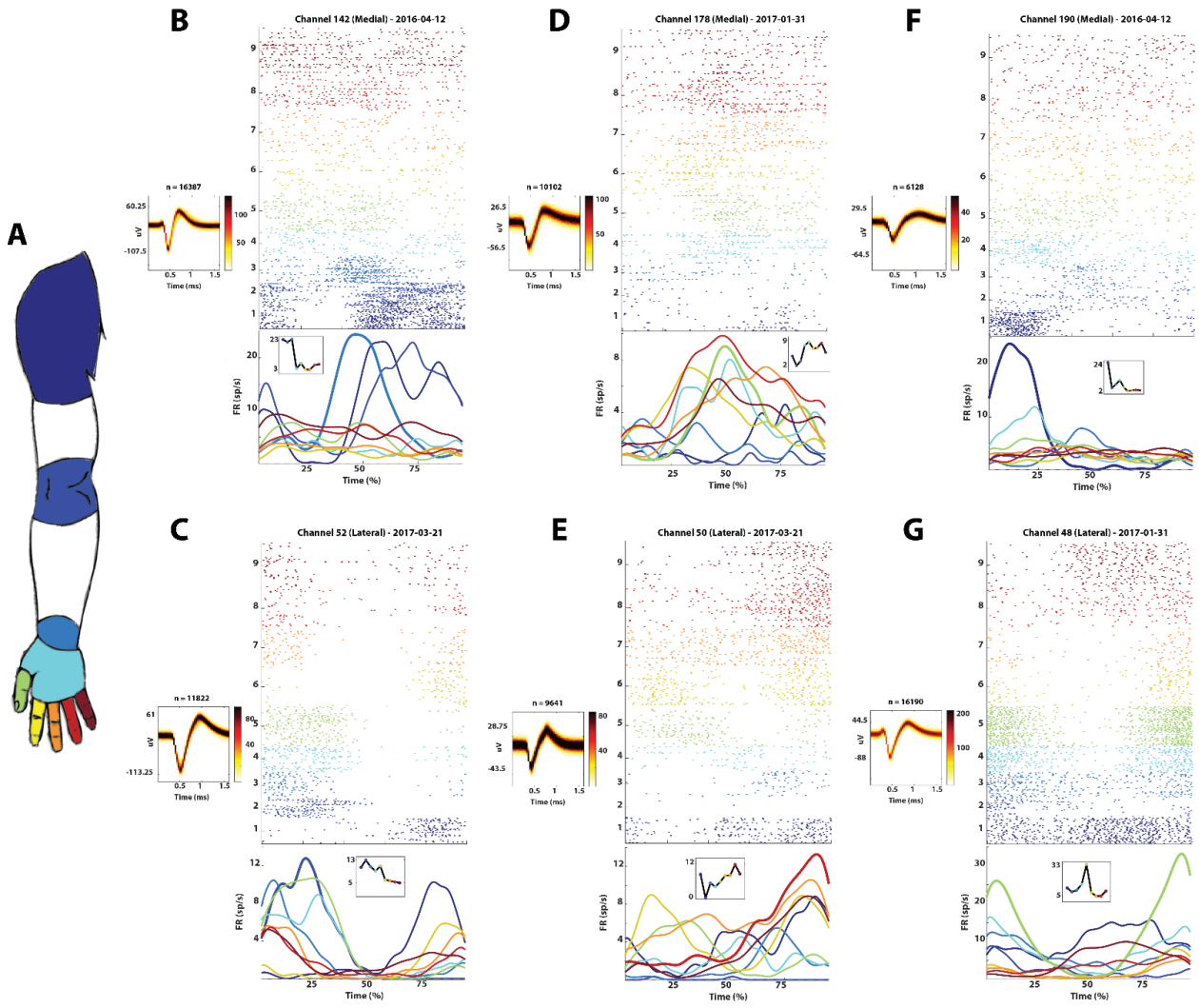

Figure 14: Neural responses during attempted movement. (A) Diagram representing the colors associated with the 9 attempted movement tasks. (B-G) Responses of six example neurons (recorded from participant 2) during attempted movements. Left offset panels shows a density plot of all snippets recorded from each neuron (darker colors = more snippets crossing through a given time-voltage point). Main panels show single-neuron spike rasters across repetitions of each movement Movements are indicated by a number on the y-axis with spikes colored as in A., with averaged instantaneous firing rate below. Inset panels show each neuron's modulation depth (MD) during each task. (B and C): Medial and lateral neurons responding preferentially to proximal movements. (D and E): Medial and lateral neurons responding preferentially to gross movements. (F and G): Medial and lateral neurons responding preferentially to a single movement.

3.3.2 Spatial differences in tuning of broadly-modulated neural populations

We began quantifying these responses by first identifying neurons that displayed significantly different firing rates (FR) during movement compared to rest. When participants attempted to move in time with the stimulus videos, a substantial proportion of identified neurons (43/62 for participant 1, 582/708 for participant 2) displayed significant modulation (i.e. differences in movement-related FR compared to rest) during at least one movement ($p<0.05$, two-tailed Kilmogorov-Smirnoff test), and were thus included for subsequent analysis. **Figure 15C/D** shows histograms representing the number of tasks during which a given neuron displayed significant movement-related modulation. We found that in both participants, neurons were more likely to be "broadly tuned" (significantly modulated during a majority of tasks) than "narrowly tuned" (significantly modulated during a small number of tasks). This effect was especially pronounced in participant 2, where most modulated neurons (300/582) were significantly modulated by all 9 tasks.

Although we found that many neurons display modulation during different movements, we wanted to determine whether those neurons displaying non-global modulation were modulated by specific tasks. **Figure 15A/B** shows the number of neurons significantly modulated by each task. The horizontal line represents the number of globally-modulated neurons, illustrating the number of neurons that display some degree of preferential modulation to specific tasks. For participant 1 we found that each task involved similar numbers of modulated neurons, with a slight bias towards arm movements (particularly wrist on the lateral array). For participant 2, we found little difference in the number of neurons significantly modulated by different tasks, consistent with the dominance of globally-modulated neurons.

These results suggest that there is a large degree of overlap between the populations active in encoding different movements (as opposed to the notion that there would be a separate population of neurons active for different tasks).

Since different movements appear to involve similar numbers of modulated neurons, we sought to determine the degree to which neurons from separate cortical areas participate in generating different movements. We compared the neural modulation depths (MD, see Methods) during each movement, both between arrays (to determine whether one array represents a movement more strongly than the other array)) and within arrays (to determine whether one array represents a movement more strongly than another movement). **Figure 15E/F** shows the distributions of MDs recorded from neurons on each array during each movement.

For participant 1, between-array comparisons revealed no significant differences for any movements, while within-array comparisons revealed slightly higher modulation depths during grasp compared to finger movement ($p=0.0416$, Wilcoxon rank-sum). This lack of differences suggests that neurons within the "hand" area of M1 display similar firing behavior during arm and finger movements. For participant 2, we again observed substantial modulation in both array populations across tasks but found several differences between tasks both within and between arrays. Comparing each task between arrays, we found that shoulder modulation was greater in medial array neurons, while modulation during several tasks (wrist, thumb, ring, and little-finger) was greater on the lateral array neurons (Wilcoxon rank-sum, $p<0.001$). Comparing within arrays, we found that the population recorded from the medial array displayed significantly higher modulation during all arm movements compared to nearly all finger movements, particularly for shoulder movement (Wilcoxon rank-sum, $p<0.001$). Conversely, the population recorded from the lateral array displayed similar modulation across all tasks, with only elbow

and wrist-related modulation higher than that observed during middle and little-finger movements.

Taken together, these results suggest that medial array neurons are biased towards encoding arm movements more strongly than finger movements and modulate more strongly during shoulder movement than lateral array neurons. Lateral array neurons appear to modulate similarly during both arm and finger movements and display stronger modulation during many hand-related movements compared to the medial array neurons.

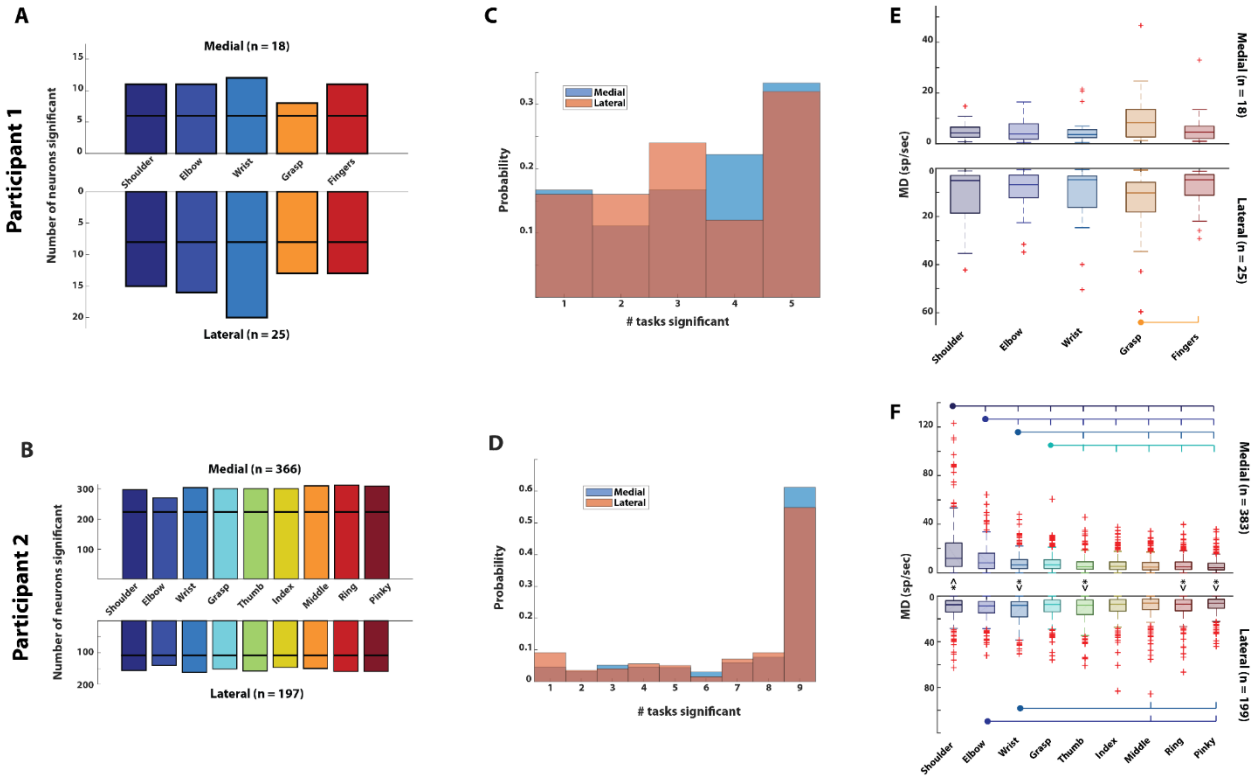

Figure 15: Neural modulation across tasks. Size and magnitude of neural modulation in participant 1 (A,C,E) and participant 2 (B,D,F). (A and B): Number of neurons displaying significant modulation during each movement. Horizontal line depicts number of neurons displaying modulation during all movements. (C and D): Histogram showing the number of tasks during which each neuron displayed significant modulation. (E and F): Distributions of single neuron modulation depths. Boxes depict median, interquartile range, and 5th and 95th percentiles, while crosses depict outlier units. Ticked lines show significant differences between task distributions within each array, while stars show significant differences between array distributions within each task (Wilcoxon rank-sum, $p<0.05$ for E, $p<0.001$ for F).

3.3.3 Arm selectivity is higher in medial neurons

So far, our results have indicated that while neurons from different areas can display a bias towards preferentially encoding one movement type over another, neurons throughout M1 in both participants can be broadly modulated during both arm and finger movements. We then wanted to determine whether these trends are also observed in the tuning preferences of individual neurons. We took advantage of the wider range of movements performed by participant 2 to examine gross-fine preferences within individual neurons in more detail.

To begin comparing the tuning of individual neurons to each movement type, we first grouped each neuron's MD values into gross/fine movements and normalized those values within each group. **Figure 16A/B** shows a heatmap of each neuron's MD during all tasks, with tuning to arm and finger movements normalized separately to that neuron's peak task within a category. Each row represents a single neuron, with the color of each column showing that neuron's modulation depth during each task. To account for differences in each neuron's baseline firing rate, MD values are normalized for each unit to its maximum MD within each movement types separately. Medial array neurons display "darker" colors within arm movements and more uniform "hot" colors within light movements, suggesting that many medial neurons are more "selective" (narrowly tuned) to one arm movement than others. A similar but less pronounced trend is observable in lateral array neurons, suggesting that they may be less selective than medial neurons.

We calculated a "selectivity index" (SI) for each neuron to quantify the degree to which it selectively modulated during one task compared to others ((Lang & Schieber, 2003); see Methods). Using this metric, a neuron's selectivity can range from 0 to 1, where low values

indicate similar modulation during each task and high values indicate strong relative modulation during a single task. We reasoned that while neurons from both arrays appear to be broadly tuned to both movement types, examining the distribution of individual neuron selectivity to movements within each type may provide a more sensitive metric for identifying tuning bias. In other words, to the degree that a neuron displays selective tuning, which movement type (between arm and fine) does that neuron prefer? To that end, each neuron's selectivity was calculated for each movement type separately.

Figure 16C/D shows histograms of the distribution of selectivity on each array for both movement types. Comparing each array's selectivity to the two movement types, we found that the medial population displayed much higher arm selectivity compared to finger (**Figure 16C**; $p=1.3*10^{-20}$, Wilcoxon rank-sum), while the lateral population was only slightly more selective to arm than finger movements (**Figure 16D**; p=0.019). When we directly compared type selectivity between arrays, we found that the medial population displayed significantly higher arm selectivity than the lateral population (**Figure 16E**; p=0.009), while the lateral population displayed significantly higher finger selectivity than the medial population (**Figure 16F**; $p=3.38*10^{-5}$). Together, these findings indicate that medial array neurons display highly selective tuning to individual arm movements (particularly shoulder, as indicated in **Figure 15F**), and that this preference is stronger in medial neurons than lateral neurons. Conversely, lateral array neurons are also slightly selective within arm movements, but to a much smaller degree than medial neurons, and additionally are more selective within finger movements than medial array neurons. In other words, we observed additional evidence of a medial-arm, lateral-fine spatial bias.

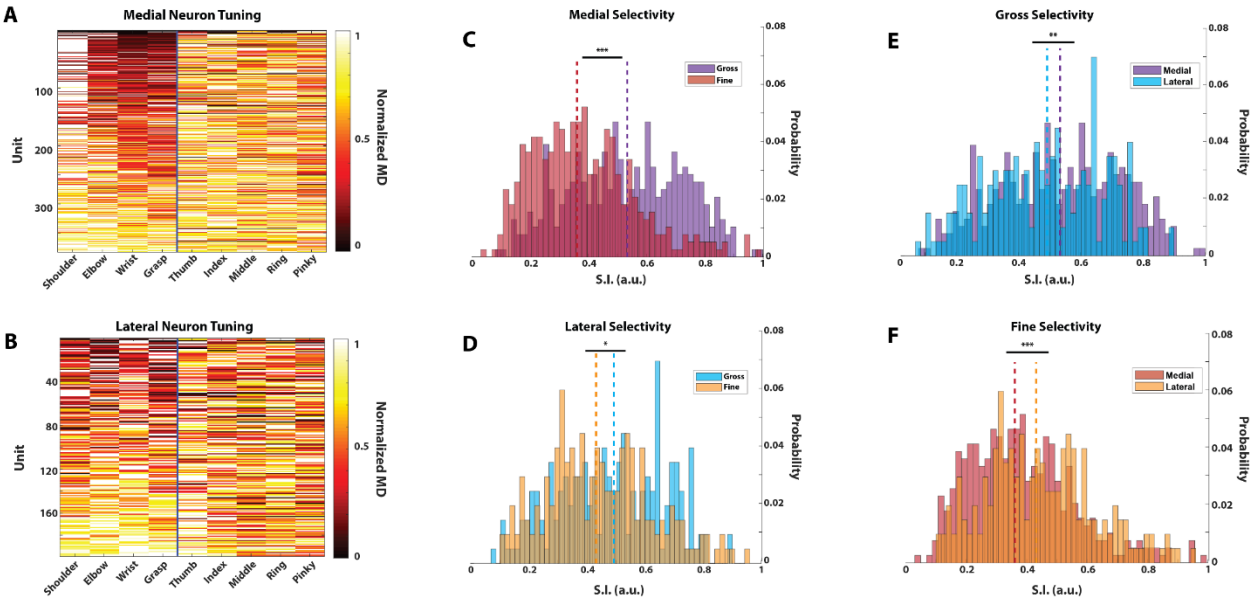

Figure 16: Neural selectivity across movement types in participant 2. Distributions of neural selectivity indexes, calculated from each array population across each movement type. (A and B) heat maps of medial and lateral neuron tuning (MD normalized within each task type) sorted in descending order by selectivity index. (C and D) histograms of medial (C) and lateral (D) neuron selectivity index during gross and fine movements. Vertical dashed lines represent distribution medians. Stars denote significance between distributions (Wilcoxon rank-sum, *=p<0.05, **=p<0.01, ***=p<0.001). (E and F) histograms of gross (E) and fine (F) neuron selectivity index from medial and lateral arrays. Vertical dashed lines represent distribution medians. Stars denote significance between distributions (Wilcoxon rank-sum, *=p<0.05, **=p<0.01, ***=p<0.001)

3.3.4 Individual neurons reflect spatial tuning biases

While these SI values are calculated for each neuron separately, they are still aggregated over many neurons, and thus potentially overlook trends within individual neuron tuning. To further explore the relative representation of each movement type, we directly examined the per-neuron relationship between arm and finger selectivity. **Figure 17A/B** shows each neuron plotted with respect to its arm (x-axis) and finger (y-axis) selectivity. In this space, neurons close to the unity line display equal selectivity to both movement types, while neurons farther off this diagonal are more selective to one type. For example, neurons that selectively fire during a single arm movement, but fire similarly during all finger movements, would be in the lower right quadrant. We quantified the degree to which each neuron displayed a type-selectivity bias by calculating its Euclidean distance from the unity line (**Figure 17C**). A very large proportion of medial array neurons lay below unity, indicating a strong bias towards selectively modulating during arm movements. Lateral array neurons were also slightly more likely to be located below unity, consistent with the slightly higher arm selectivity described above (**Figure 17D**), but were more evenly distributed around the diagonal, indicating more similar selectivity to both movement types. Directly comparing these "bias distances" between arrays revealed significantly more positive values (i.e. further below unity) on the medial array ($p=9.98*10^{-7}$, Wilcoxon rank-sum), meaning that individual medial array neurons tend to be more selective to individual arm movements than to any finger movements.

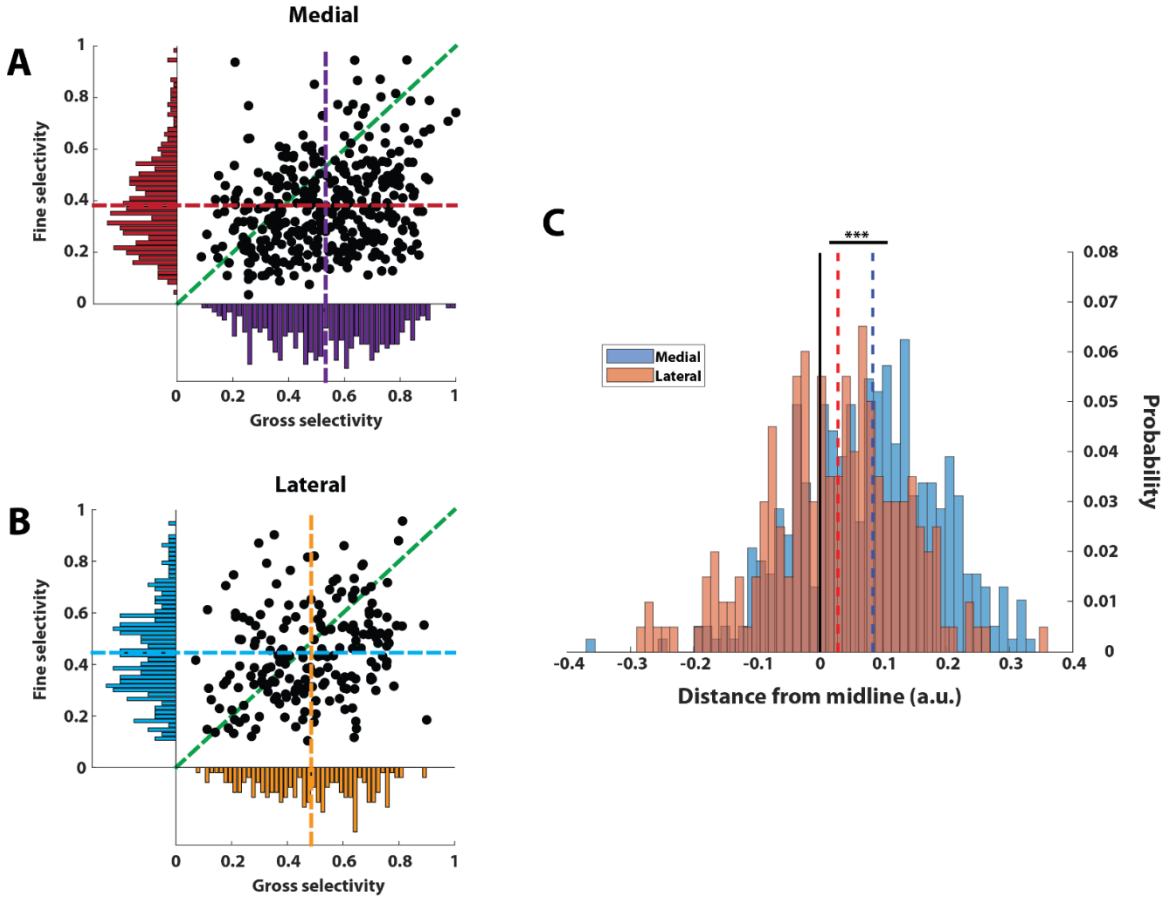

Figure 17: Interaction between neuronal gross/fine selectivity. Selectivity of neural modulation to gross/fine movements. (A and B) interaction between selectivity to gross/fine movements. Each point represents a single neuron. Edge histograms depict distribution of population gross (horizontal) and fine (vertical) selectivity. Green dashed lines represent unity (slope=1). Dashed lines represent distribution medians. (C) histogram of the distance between each neuron and the unity midline for both arrays. Vertical black line represents 0 distance from the midline for reference. Dashed lines represent distribution medians. Stars denote significance between array distributions (Wilcoxon rank-sum, $p<0.001$)

3.3.5 EMG activity shows no arm co-contraction during finger movements

Due to the nature of their spinal cord injury, participant 2 retains some motor and somatosensory function in his upper limb, creating the possibility that neural activity observed during finger movements could relate to co-contraction of arm muscles. To determine whether this occurred, we recorded bipolar EMG activity from 8 upper limb muscles while the participant performed the attempted movement task (**Figure 18**). Movement-related activity was observed in several arm muscles during functionally preserved arm movements (shoulder, elbow, and wrist), but was absent during all finger movements, as well as grasp. These results suggest that while some atypical co-contraction may occur during arm movements, it is unlikely that finger movement activity relates to proximal muscle activation. This provides additional evidence that the neural modulation observed during attempted movements involving paralyzed muscles is related to preserved movement representations, rather than co-contraction of arm muscles.

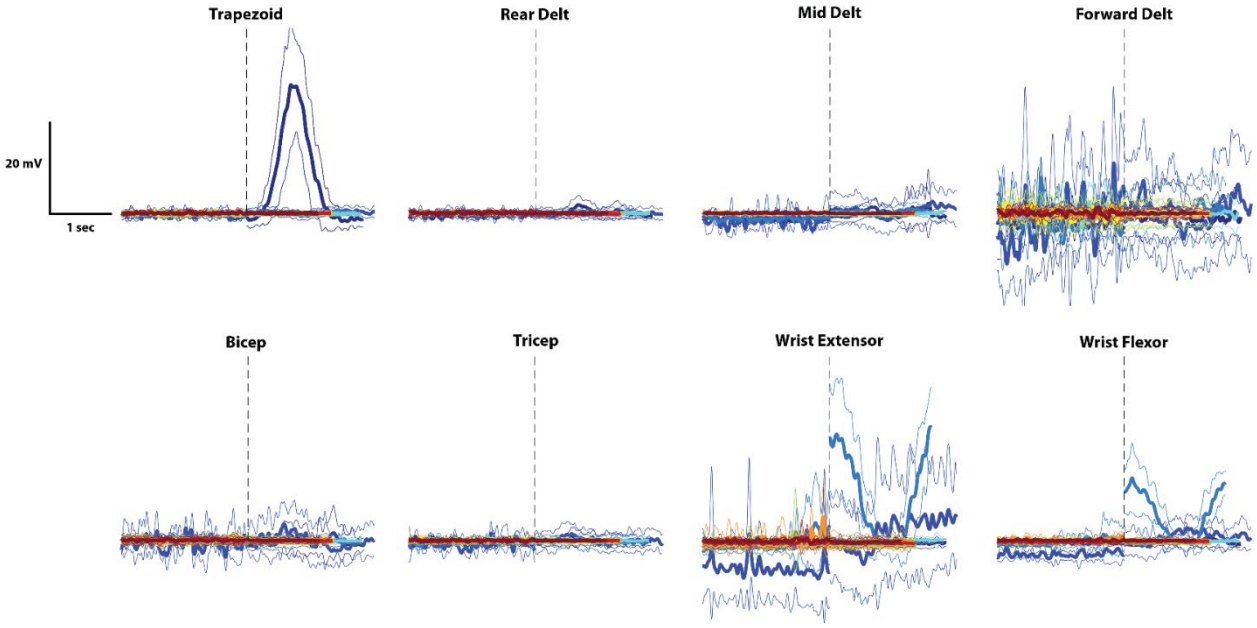

Figure 18: EMG activity from participant 2 during attempted movements. EMG activity recorded from arm muscles during attempted movement tasks. Colored traces represent mean and standard deviation of muscle activity during each task. Vertical dashed line represents movement onset. Movement activity is averaged across individual repetitions throughout each trial (see Methods).

3.3.6 Trends in modulation depth and selectivity are consistent across time

Our analysis was conducted using single unit recordings pooled across 44 months for participant 2. We wanted to determine whether the neural tuning properties of each day's population remained stable over the testing period. **Figure 19** shows the distribution of modulation depths (**A**) and gross/fine selectivity (**B**) on each testing day. While there were significant differences between sessions, we did not observe any systematic trend over the testing period in either task-related modulation or movement type selectivity. Since each test session effectively samples a unique neural population, this consistency suggests that the spatial biases observed here are related to the organization of neural input-output circuits in each area which remain relatively stable over long periods of time.

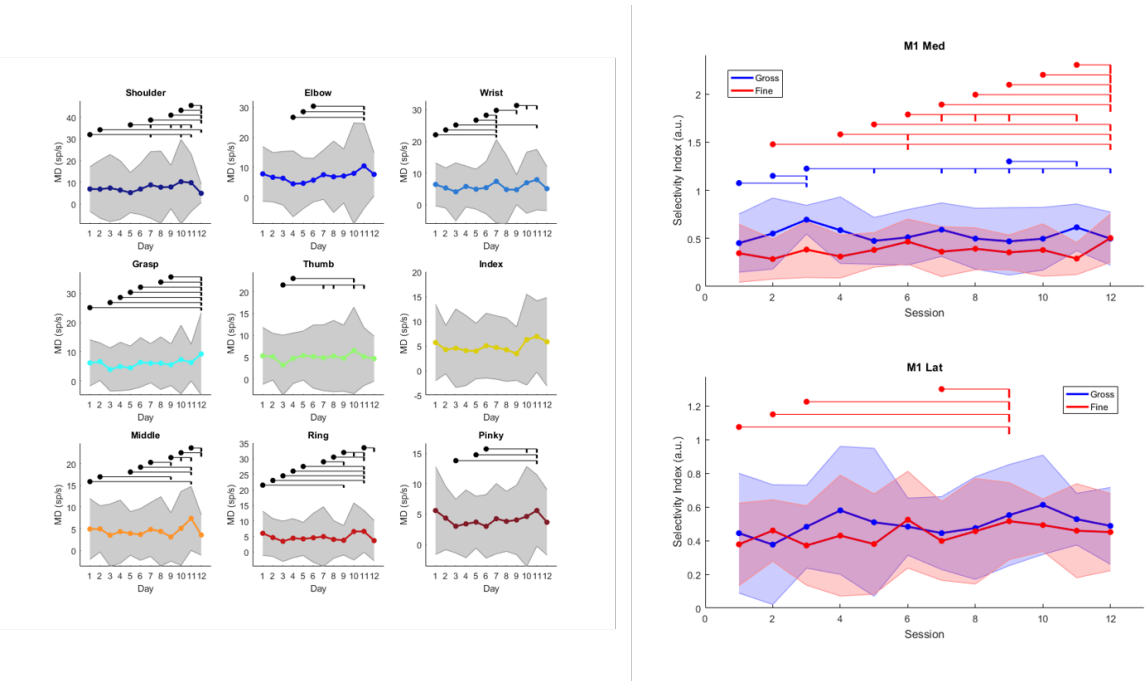

Figure 19: Stability of neural tuning over time for participant 2. (A): distributions of modulation depths from well-isolated neurons on both arrays during each task. Stars represent significant difference between days (Wilcoxon rank-sum, $p<0.05$). (B): distributions of selectivity index from neurons on both arrays across gross (blue) and fine (red) movements. Stars represent significant difference between days (Wilcoxon rank-sum, $p<0.05$).

3.4 Discussion

By simultaneously recording the activity of single neurons from multiple areas of M1 in humans attempting to perform upper limb movements, we have provided evidence that weak somatotopic trends are reflected in the selective modulation of broadly tuned neurons. In both participants, neurons from separate areas were modulated by both arm and finger movements, suggesting that upper limb movements are encoded by a shared population of neurons. In participant 2, neurons recorded from the medial array displayed stronger and more selective modulation during arm movements compared to finger. This was not the case for cells recorded from the lateral array, which displayed similar magnitude and selectivity of activity during both arm and finger movements. These findings provide a basis for relating the large-scale organization observed in human neuroimaging to the behavior of individual neurons and extend results from non-human primates (NHPs) showing an absence of clear somatotopic separation.

We found that neural populations from both lateral and medial areas display significant modulation during both arm and finger movements and observed relatively small differences in the magnitude of spiking activity therein. Our results thus suggest that different movements across the entire upper limb, ranging from shoulder to fingers, are controlled by a shared population of neurons. The fact that spatially separate neurons in M1 produce similar amounts of spiking activity during a given movement suggests that they are involved in a common interconnected neural circuit. This correlation could be the product of shared input from external cortical or subcortical areas, or from direct connections within M1. Anatomical tracer and microsimulation studies have shown that M1 neurons display rich internal connectivity, with connections allowing communication between functionally related somatotopic representations

(Huntley & Jones, 1991). There is also evidence from anatomical results that incoming and outgoing connections from M1 are not uniform but instead heterogeneous and "patchy", providing a possible mechanism for spatially distant neurons to receive similar driving inputs (Dea et al., 2016; Hamadjida et al., 2016). Taken together with our results, these findings indicate that functional circuits underlying upper limb movement may be comprised of large areas of M1.

Beyond the presence of this strong task-related modulation, we also observed that activity recorded from the medial array in participant 2 was significantly more selective within arm movements, meaning that individual neurons were more likely to respond strongly to one arm movement over others. One possible explanation for the lowered selectivity displayed by lateral array neurons could relate to the nature of participant 2's spinal cord injury and the resulting behavioral relevance of the movements preserved above the injury. As participant 2 retains motor and somatosensory function in the muscles that move his shoulder, elbow, and wrist, it is possible that neurons previously involved in finger movement production have undergone plasticity-induced tuning changes to "remap" and better control preserved movements. However, there is substantial evidence suggesting that existing sensorimotor representations are largely preserved even after long periods post-injury ((Kikkert et al., 2016; Urbin et al., 2019; Wesselink et al., 2019)), indicating that the activity we observed during finger movements is evidence of preserved finger movement representation. Rather than the lateral population rewiring to encode arm movements, it is possible that the neurons recorded on the medial array have instead rewired to better encode the range of preserved after the participant's injury. In other words, medial neurons may have become more selective post-injury. Recent models suggest that somatotopy is merely one of many motor parameters encoded in M1, alongside other principles such as

stereotyped actions and peripersonal coordinate space ((Graziano, 2016; Graziano & Aflalo, 2007)). The increased arm selectivity observed in medial population neurons may reflect plasticity-related changes in tuning related to the increased behavioral relevance of arm movements. Future investigations should evaluate the tuning properties of neurons from participants with different sensorimotor impairments in order to determine whether such changes are consistently related to preserved functionality.

If such functionally-relevant plasticity has taken place, it is possible that activity during multi-joint movements, or movements to a wider range of peripersonal space (e.g. object interaction), may reveal more complex changes in neural tuning throughout M1. Our task paradigm was intentionally limited to simple movements in order to restrict the dimensionality of the motor parameters being encoded, and did not represent the full range of neural variability demonstrated by the recorded populations. Future work should examine the magnitude and selectivity of neural activity during a wider range of behavior to determine whether more complex movements alter the spatial trends observed here.

While this study focuses on the activity underlying attempted movements of the participants' native limbs, we have also previously demonstrated that participants are able to use activity from the same electrode arrays to dexterously control robotic limbs and perform tasks of daily living ((Collinger et al., 2012; Wodlinger et al., 2014)). Since the experiments described here were often performed on the same day as these brain-computer interface (BCI) tasks, it is very likely that activity from these same neurons also modulate during BCI control. While directly comparing activity from these different task paradigms is beyond the scope of this study, future work should investigate whether the spatial biases described here are reflected in the decoder weights used to generate robotic limb movement.

In summary, we found that many neurons recorded from spatially separate areas of human M1 appear to participate similarly in encoding many different upper limb movements. While we did observe significant biases in the degree to which neurons from medial and lateral areas preferentially fire during arm and finger movements, the recorded populations overall displayed remarkably broad tuning to all attempted movements. These results suggest that rather than maintaining separate representations of different muscles or movements, neurons throughout M1 operate as a unified system to produce different activity patterns. This view is consistent with recent experimental results (Kaufman, Churchland, Ryu, & Shenoy, 2014; Russo et al., 2018; Sadtler et al., 2014) and theoretical models (Michaels, Dann, & Scherberger, 2016; Shenoy et al., 2013) which interpret M1 as a dynamical system, where each individual neuron contributes to generating high-dimensionality patterns to control ongoing movement. In this framework, our results suggest that this dynamical system consists of neurons throughout M1, with neurons in different areas contributing information depending on their location within the large-scale circuits of input-output connections.

4.0 Movement Representations Across Sensory Context

4.1 Introduction

Classical theories of motor cortex organization describe a large-scale somatotopic organization, where neurons in different areas of M1 selectively modulate their activity to encode the muscle and movement parameters of different movements. Several studies have shown that while such gradients exist, they are broadly distributed and intermixed, resulting in a complex spatial organization (Graziano, 2016; Kakei et al., 1999; M. Schieber & Hibbard, 1993b). These overlapping patterns suggest that the activity of neurons in separate areas may be driven by both shared and private inputs (Dea et al., 2016), allowing them to contribute novel information to the overall pattern of activity projected downstream to generate movement.

In Chapter 2, we demonstrated that the organization of large-scale activity throughout M1 can be affected by multisensory enrichment, suggesting that spatially separate neural populations may receive different information about context-related sensory cues. Additionally, we have shown that neurons recorded from "arm" and "hand" areas of M1 are broadly modulated by both types of movement (Chapter 3). Recent computational theories suggest that this broad modulation and flexible tuning may be evidence of information encoding by a population-level pattern of activity. We sought to determine whether neural population activity recorded from different areas of M1 respond to the multisensory context of attempted movement tasks. We hypothesized that single-neuron and population-level activity recorded from the Lateral array,

located in an area identified as active during hand movements by neuroimaging, would be more strongly affected by multisensory enrichment than Medial array activity.

4.2 Methods

4.2.1 Study participants and surgical procedures

The studies allowing the collection of this data were approved by the institutional review boards at the University of Pittsburgh (Pittsburgh, PA, USA), the Space and Naval Warfare Systems Center Pacific (San Diego, CA, USA), and the Food and Drug Administration (Washington, D.C., USA) under an Investigational Device Exemption. We obtained verbal and written informed consent from the participant before his enrollment in these studies.

Participant 2 was 28 at time of implant, with chronic tetraplegia due to a C5-motor/C6-sensory ASIA-B spinal cord injury (due to automobile accident) approximately 10 years before implantation. Due to the level of injury, this participant retains full use of his shoulder and elbow, partial use (extension) of his wrist, while his hand is completely paralyzed and desensate in the medial part of his hand innervated by the median nerve (see EMG analysis, Chapter 3). Participant 1 was implanted with two 4mm x 4mm x 1.5mm, 88-channel platinum-coated silicon intracortical microelectrode arrays (Blackrock Microsystems, Salt Lake City, UT, USA) in left primary motor cortex. He was also implanted with two 2.4mm x 4 mm x 1.5mm, 60-channel

arrays in primary somatosensory cortex (Flesher et al., 2016), but data from these arrays were not included in this study.

4.2.2 Presurgical neuroimaging

MRI data were collected on a Siemens Technology (Munich, Germany) Trio 3T scanner. The participant received a T1-weighted whole-brain anatomical scan (1 mm^3 isovoxel, 176 slices, 256x256 mm in-plane resolution). Functional scans were collected from dorsal sensorimotor cortex using T2*-weighted echo-planar imaging (EPI) sequence (TR = 2000 ms, TE = 29 ms, voxel size = 2.156 x 2.156 mm, slice thickness = 2 mm, 128x128 mm in-plane resolution, 26 mm field of view).

Functional data were collected while the participant attempted to move his shoulder, elbow, wrist, hand (grasp), and fingers (sequential tapping). This task data was collected using a block design, wherein a 20 second baseline period was followed by 4 alternating 20 second blocks of rest and movement condition. Each run consisted of 4 blocks of rest/move conditions. Rest periods were cued by a gray fixation cross, while movement conditions consisted of a green/red fixation cross changing color at 0.5 Hz, cuing subjects to alternatively grasp and relax with their dominant hand, respectively. During the movement condition, the participant was instructed to "attempt" to physically execute each movement. fMRI data were pre-processed using SPM12 (Ashburner et al., 2013). fMRI images were spatially realigned using a rigid-body transformation, spatially smoothed (6 mm FWHM), and coregistered to the anatomical scan. BOLD responses were determined with a general linear model (GLM) convolved with a

canonical hemodynamic response function. The resulting T-contrast images were then projected onto a cortical surface render (created using Freesurfer (Fischl, 2012)) for visualization(Collinger et al., 2014).

4.2.3 Array placement based on presurgical mapping

In order to record the cortical activity most directly related to upper limb movements, fMRI was used to localize the cortical areas active while the subject attempted to perform various upper limb movements. These functional images served to guide the placement of the microelectrode arrays implanted in the primary motor cortex (see Chapter 3, **Figure 12B/C**). Final positioning was determined intraoperatively based on the cortical surface topography and vasculature. Array position was estimated using post-implantation high-resolution CT and co-registered to the pre-surgical MRI. One array was placed in a lateral area of finger- and grasp-related activity, while the second array was placed in a more medial area thought to be more related to arm movement, although this was not mapped explicitly.

4.2.4 Behavioral task design

The goal of this experiment was to determine how varying levels of multimodal sensory information alter the sensorimotor activity generated during attempted hand movements. To that end, we collected intracortical neural data while the participant performed the covert enrichment task described in Chapter 2. Briefly, this paradigm consisted of 1 Overt attempted movement

task and 3 motor imagery tasks (wrist flex/extend, hand grasp, sequential finger taps), with 4 levels of context-related multisensory enrichment (Simple, Goal, Audio, Stim). Since the participant was generally unable to detect somatosensory stimuli on the hand, we placed these stimulators on the clavicle (where sensation was generally preserved) in order to ensure the detection of timing-related tactile information. Each movement task was presented as a separate block design; a 10-second initial rest period, followed by 4 blocks of movement conditions, followed by a 10-second final rest period. Conditions within each block were intermixed and separated by 8 seconds of rest (cued by fixation cross) and 2 seconds of text cuing the next movement to be performed. Intracortical data were collected while the viewed these stimulus videos of rhythmic movements being performed and was instructed to attempt to perform the movements in time with the videos.

4.2.5 Neural recording

Neural data were recorded from Utah microelectrode arrays implanted in the arm/hand area of M1. Raw voltage signals were sampled at 30KHz with a 250-4500 Hz bandpass filter. Spike snippets were defined as 48-sample (1.6ms) events where the voltage signal crossed a fixed threshold (-4.5*baseline root-mean-square (RMS)) voltage for each channel.

To examine the activity of individual neurons, we sorted spike snippets into ‘neurons’ using the principal component analysis (PCA)-based method described previously ((Downey et al., 2018)). Briefly, we used PCA to visualize each channel’s snippets in the first two components based on waveform shape. Separable clusters were manually identified and used to

initialize a Gaussian mixture model expectation-maximization algorithm, which created the specified number of clusters and assigned each snippet to the most likely unit.

To further isolate activity from individual neurons, neurons primarily containing noise events, i.e. snippets diverging from the stereotyped action potential waveform, were then manually identified and excluded from further analysis. Neurons that displayed any inter-spike intervals (ISI) less than 1ms were also excluded. We then calculated a consistency metric to identify neurons with consistent waveform shapes by taking the dot product of sequential normalized snippets ((Fraser & Schwartz, 2012)). We fit the resulting "consistency" histogram with two normal distributions and identified the threshold separating neurons with low and high consistency, and only included those neurons with waveform consistency above this threshold.

We collected this behavioral neural data on 5 separate days during testing sessions for the BCI study. Due to experimental time constraints during testing sessions, a different combination of the 4 movement tasks were collected on each day. To increase the statistical power of our analysis and to provide a better overall sample of the neural activity observed in each cortical location, we combined neural recordings across days by treating each isolated neuron as an independent observation.

4.2.6 Quantifying neural modulation during single movement repetitions

For this study, as we wanted to examine the neural activity underlying individual movement repetitions, we processed the raw timeseries activity to isolate each individual attempted movement. Stimulus videos were created by filming and looping footage of a single 2-

second repetition to create a continuous 10-second movement period. Neural activity was recorded during this continuous task, then extracted and organized around stimulus onset for each condition. As each task contained 4 "blocks" consisting of 5 repeated 2-second looped individual movement repetitions, this process yielded 2000ms of spike counts (binned at 1ms) for 20 repetitions of each task condition. To calculate a given unit's activity during movement, we calculated a peristimulus time histogram (PSTH) of spike times during all movement repetitions. We then smoothed this trial-averaged spike count with a Gaussian kernel (σ=50ms, width=300ms) to generate smooth instantaneous firing rates for each unit. In order to quantify the degree to which a given neuron was "tuned" to a specific movement, we extracted the firing rate activity from each neuron during these repetitions and calculated the modulation depth (MD) as the mean of the difference between maximum and minimum of the trial-averaged firing rate.

To further determine how neural activity was affected by multisensory enrichment, we wished to identify which condition elicited peak modulation in individual neurons. We compared each neuron's modulation during each condition within each task and quantified the proportion of neurons which displayed peak modulation in a given condition, yielding a "%peak neurons" summary statistic.

4.2.7 Modulated neuron identification

To identify neurons that displayed modulated activity during attempted movement, we compared each neurons' firing rate distributions during movement and rest. To filter out spurious activity, only neurons with mean firing rates >1Hz during both movement and rest were analyzed. For each task, firing rate activity during rest (defined as the 2s prior to movement

onset) and movement (defined as the 2s following movement onset) was concatenated across all trials and compared using a two-tailed Kolmogorov-Smirnov test ($p<0.001$). Any "valid" neuron that was significantly modulated during at least one condition of any task was included for further analysis.

4.2.8 Per-neuron enrichment

To further examine how individual neurons were affected by multisensory enrichment, we sought to determine per-neuron changes in modulation across conditions (similar to the "enrichment effect" discussed in Chapter 2). We defined this "per-neuron enrichment" by calculating the difference between each neuron's modulation depth between each pair of enrichment conditions in a given movement task. These differences were calculated additively, such that positive ΔMD indicates increased activity with increased enrichment (i.e. Goal – Simple, Audio – Goal, etc).

4.2.9 Dynamical state-space analysis

In addition to quantifying the activity of individual neurons, we also wished to examine the structure of shared population activity, i.e. the overall pattern of activity distributed across multiple neurons. We defined a "neural state space" from population-wide activity using principal component analysis (PCA), a dimensionality-reduction technique which isolates the temporal patterns of activity (i.e. principal components, PCs) which explain the most variance

across N-dimensional neural populations. We generated a separate neural space using the activity from all neurons across days. Since a different subset of task data was collected on each day, each of the 4 tasks is generated using a different subset of neural data.

In order to determine how different neural populations respond to multisensory enrichment during covert movement, we generated a neural state space for each movement task using all motor neuron activity (i.e. neurons from both arrays), as well as for each motor array separately. To generate neural state spaces based on "raw" neural activity, we used each neuron's per-repetition spiking data to calculate an instantaneous firing rate for every repetition of each condition and concatenated them into a (time X neurons) matrix, which was used to perform PCA. We then calculated the across-repetition mean of each condition's trajectories and projected these condition-mean trajectories onto the space defined by the first 3 principal components for visualization (i.e. the "neural state space"). To preserve and examine the information of this population activity, we defined the dimensionality of neural trajectory behavior as the number of PCs required to explain 75% of the total variance. To quantify the separability of each condition in this space, we then trained a Naïve Bayes classifier on these N-dimensional neural trajectories. We then wished to examine the spatiotemporal structure of these neural trajectories in more detail. We defined each condition's state-wide temporal activity as the Euclidean distance between the space origin and each timepoint in the trajectories, providing a summary statistic ("trajectory distance") to quantify the overall amount of variance displayed by each condition.

4.3 Results

4.3.1 M1 neurons modulate during enriched covert movements

Across all days, we recorded 281 motor neurons (200 from the medial array, 81 from the lateral array) and identified 256 neurons which displayed significant modulation during at least one movement condition (189 medial, 67 lateral). **Figure 20** shows the spiking activity of an example neuron (recorded from the lateral array) during each condition of the 4 movement tasks.

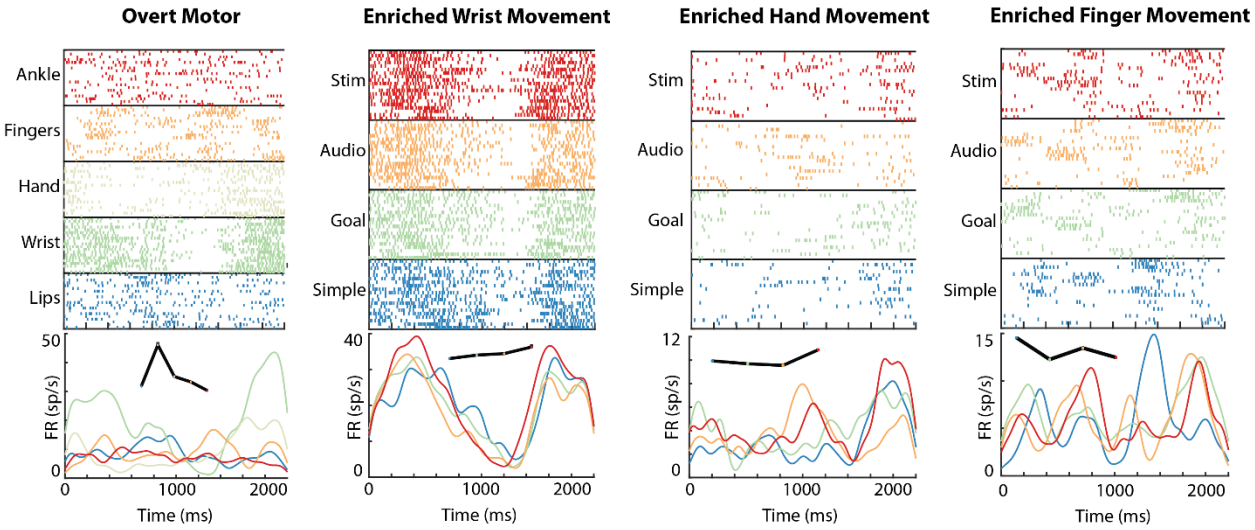

Figure 20: Enriched neural activity. Single-neuron activity recorded from the lateral array during overt and enriched covert movements. Top panels show per-repetition spike times (rows = repetitions). Bottom panels show smoothed trial-averaged firing rates. Inset black lines show relative modulation depth between task conditions.

4.3.2 Broad modulation in M1 neurons during overt movements

In order to determine how the neural population activity underlying different movements is affected by contextual multisensory enrichment, we first wished to determine how those movements are encoded in the absence of said enrichment. Thus we examined the activity of single neurons in M1 during an overt movement task wherein the participant attempted to physically perform the Simple condition of each movement (wrist/hand/fingers), as well as ankle flex/extend and lip purse. **Figure 21A** depicts heatmaps the modulation depth of each neuron during different movements. Each row represents a single neuron, with the color of each column representing that neuron's modulation depth during each movement. Neurons were generally broadly responsive (i.e. displaying significant modulation during multiple movements), consistent with previous results from this participant (see Chapter 3).

We show these neurons grouped vertically by peak condition, illustrating the proportion of neurons from each array which are maximally tuned to each movement. This quantity is shown in **Figure 21B**, revealing that neurons from both arrays displayed preferential tuning (i.e. higher modulation depth) to Wrist movement relative to other movements. However, each movement condition elicited peak modulation from at least 10% of neurons from both arrays, illustrating that neurons throughout M1 participate broadly in encoding different types of movement.

We then compared the modulation depths of neurons from each array during different movement conditions (**Figure 21C**). Lateral array neurons displayed lower modulation in each condition, with significant differences observed between arrays in lip ($p=0.014$), hand ($p=0.096$), and finger ($p=0.012$) movements (Wilcoxon rank-sum). Comparing distributions within arrays

revealed that only Wrist modulation was significantly greater than other movements on both medial and lateral arrays (Medial: Wrist > Lip, p=0.009; Wrist > Fingers, p=0.022. Lateral: Wrist > Lip, p=0.045; Wrist > Ankle, p=0.022, two-tailed t-test).

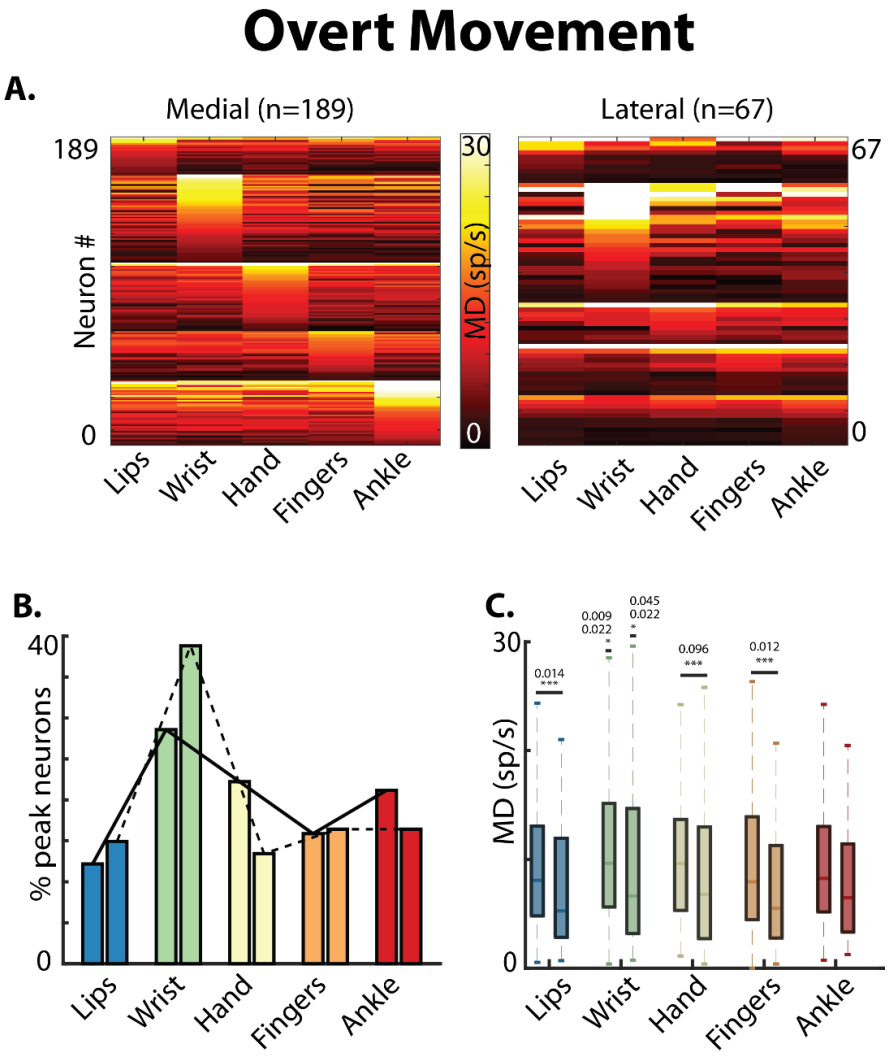

Figure 21: M1 single-neuron modulation during overt movement. (A) Heatmaps showing modulation depth of individual neurons recorded from medial (left) and lateral (right) motor arrays. Neurons are grouped vertically (rows) according to their peak task. (B) Percent of neurons from each array (left = medial, right = lateral) displaying peak modulation during each task. (C) Boxplot showing median, inter-quartile range, and 5/95% of neural modulation depths from each array (left = medial, right = lateral) during each task. *** = significance between arrays in each task ($p<0.05$, Wilcoxon rank-sum). * = significance between conditions in each array ($p<0.05$, two-tailed t-test).

4.3.3 Spatial differences in population encoding of overt movements

Examining single-neuron activity during overt movement demonstrated that individual neurons were broadly tuned, with neurons from both arrays displaying significant modulation during multiple movements. As the overall magnitude of single-neuron activity appears to be similar during different movements, we theorized that enrichment may be more easily observed in the patterns of variance shared between neurons. We then sought to determine whether analyzing the recorded neural activity at the population level could reveal additional insights.

Figure 22A shows the trial-averaged neural trajectories in PC3 space generated from all neurons (n=256) during each movement. Since this projection of the population-wide neural data onto each PC defines the magnitude of a specific aspect of neural variance observed at each time-point, we can interpret the distance traversed by each condition-trajectory as an estimate of the amount of information encoded by the population. In this PC3 space (which accounts for 46% of overall neural variance), we observed that activity during Wrist movement (shown in purple) is highly defined and separable from other condition-trajectories. Lip and Ankle trajectories (orange and red) are more compact and closer to the origin, indicating less overall variance and greater similarity in the population activity during those tasks. The Finger trajectory (blue) is also highly separable, while the Hand trajectory (green) traverses a unique volume of state space but partially overlaps with the Lip and Ankle volumes.

To quantify the separability of these trajectories, we trained a Naïve Bayes classifier using this PC3 activity. **Figure 22B** shows the resulting confusion matrix, revealing that Wrist and Finger trajectories are highly separable (100% accuracy). Hand activity (46%) was partially

mis-classified as Lip (14.5%) or Ankle (37.9%) movement, consistent with their trajectories' proximity in PC3 space.

We then aimed to examine the spatiotemporal structure of these neural trajectories in more detail. We quantified the time-course of each trajectory, defined as its distance from the space origin ([0,0,0]). As the space origin represents the mean population activity, we can interpret a trajectory's distance from this location as the variance (information) encoded at each timepoint. **Figure 22C** shows the origin-distance of each trajectory during the 2000ms movement period. We observed that the three hand-related movements (wrist, grasp, fingers) display a peak distance at ~1500ms, where the Lip and Ankle trajectories deflect towards the origin, supporting the separability between hand and non-hand movements. We also observed a similar outward deflection in Wrist and Finger trajectories at ~500ms which the other trajectories (including Hand) lack, supporting the increased separability of these movements. The overall distributions of trajectory distance were significantly different between all conditions and was generally greater in conditions with higher separability, supporting the relationship between trajectory distance and activity-pattern separability (**Figure 22D**).

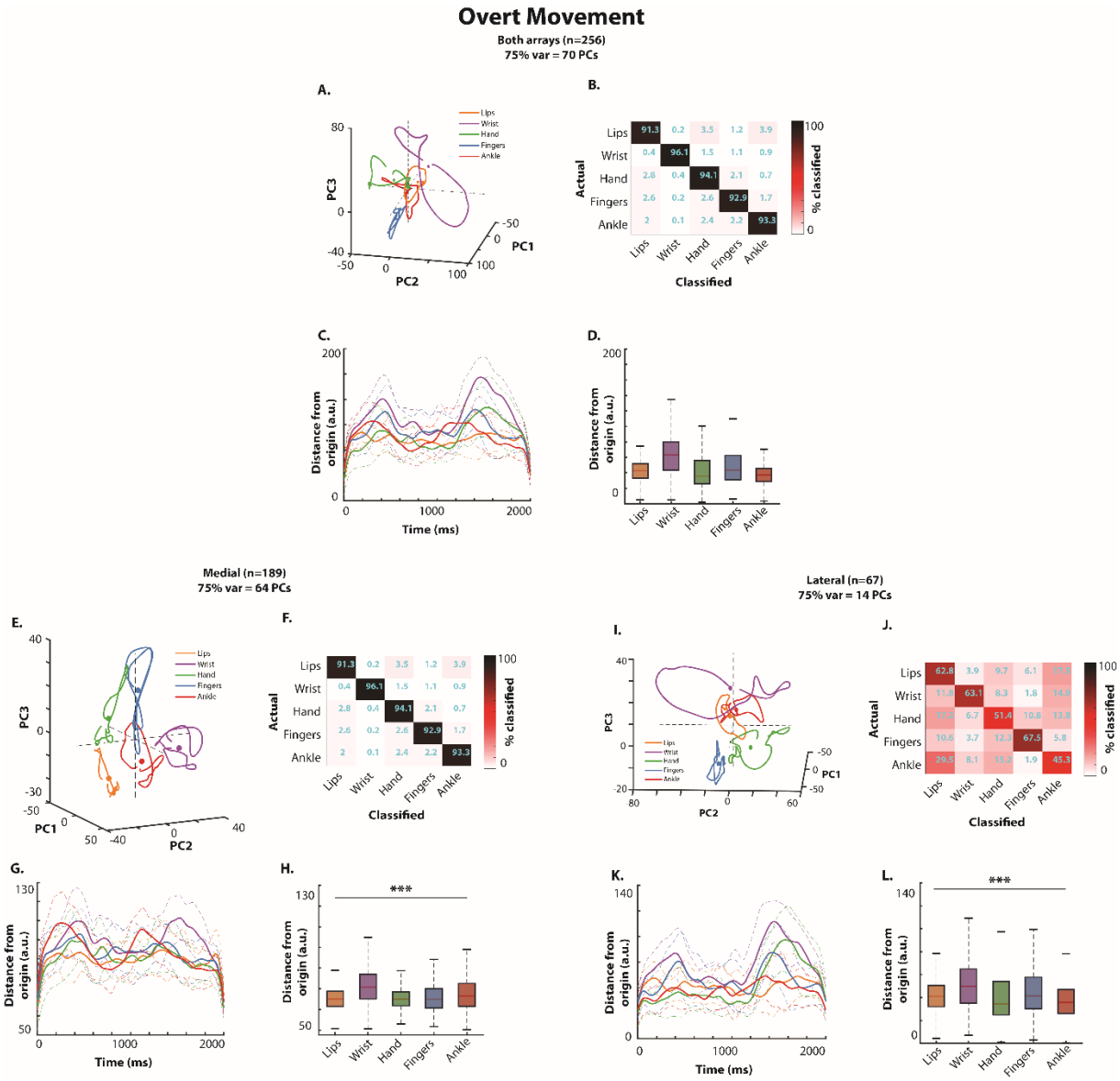

Figure 22: Neural trajectories during overt movement. Neural state spaces were calculated separately using neurons from both arrays (A-D), the medial motor array (E-H), and the lateral motor array (I-J). (A,E,I): Neural trajectories during each task projected into first 3 principal components. Colored points represent trajectory centroid as defined by the Naïve Bayes classifier. (B,F,J): Naïve Bayes classification accuracy based on PC3 neural trajectories. (C,G,K): Time course of neural trajectories (measured as distance from state-space origin during each task. (D,H,L): Distributions (median, inter-quartile range, 5/95%) of origin-trajectory distance during each task.

These results illustrate that population-level analyses reveal informative structure in the shared activity of motor neurons during overt movement. We then examined how spatially separate neural populations contribute to encoding a given movement by generating a separate neural space using activity from each array.

Figure 22 E-H shows the state-space trajectories from the Medial array (n=189 variance). Each movement trajectory is highly separable, occupying a nearly unique volume of space (**E**) and displaying very high classification accuracy (**F**). However, the time-course of each trajectory appears less distinct, lacking the divergent peaks seen in the whole-population space (**G**) and displaying similar ranges of origin-distance (**H**).

Conversely, the trajectories generated from Lateral array activity (**Figure 22 I-L;** n=67) appear to more closely resemble those seen in the whole-population space (**I**). Each movement is less separable compared to the Medial trajectories (**J**), but display separable time-course peaks (**K**) and distance distributions (**L**) similar to the whole-population activity.

Taken together, these results suggest that neural populations throughout M1 modulate to encode overt movements. In this task, the Medial array trajectories displayed very high separability between different movement conditions but did not reflect the specific temporal structure of each movement, while the Lateral array trajectories appeared to define the temporal structure of each movement state at the cost of some separability. Therefore, while neural populations from both areas contribute to the overall pattern of descending motor activity generated to drive each movement, they may preferentially encode different types of information.

4.3.4 Population-level contributions are consistent across enrichment tasks

We then examined single-neuron modulation and population dynamics during enriched Wrist movement. **Figure 23A** shows tuning of single neurons from both arrays during each enrichment condition. The Medial array had similar proportions of peak-tuned neurons during each condition, while the Lateral array displayed a higher number of neurons with peak modulation during the Audio condition (**Figure 23B**). The Lateral array also displayed a higher incidence of strongly modulated neurons compared to the Medial array, these differences were not significant (**Figure 23C**). To further determine how different enrichment condition affected the modulation of individual neurons (rather than the overall array distributions), we calculated the per-neuron difference in modulation depth between each pair of additive conditions (**Figure 23D**). This analysis revealed that while most enrichment conditions did not elicit consistent changes in per-neuron modulation, Lateral array neurons did display significantly greater modulation in the Audio-Simple ($p=0.001$) and Audio-Goal ($p=0.009$, Wilcoxon rank-sum) conditions compared to Medial array neurons.

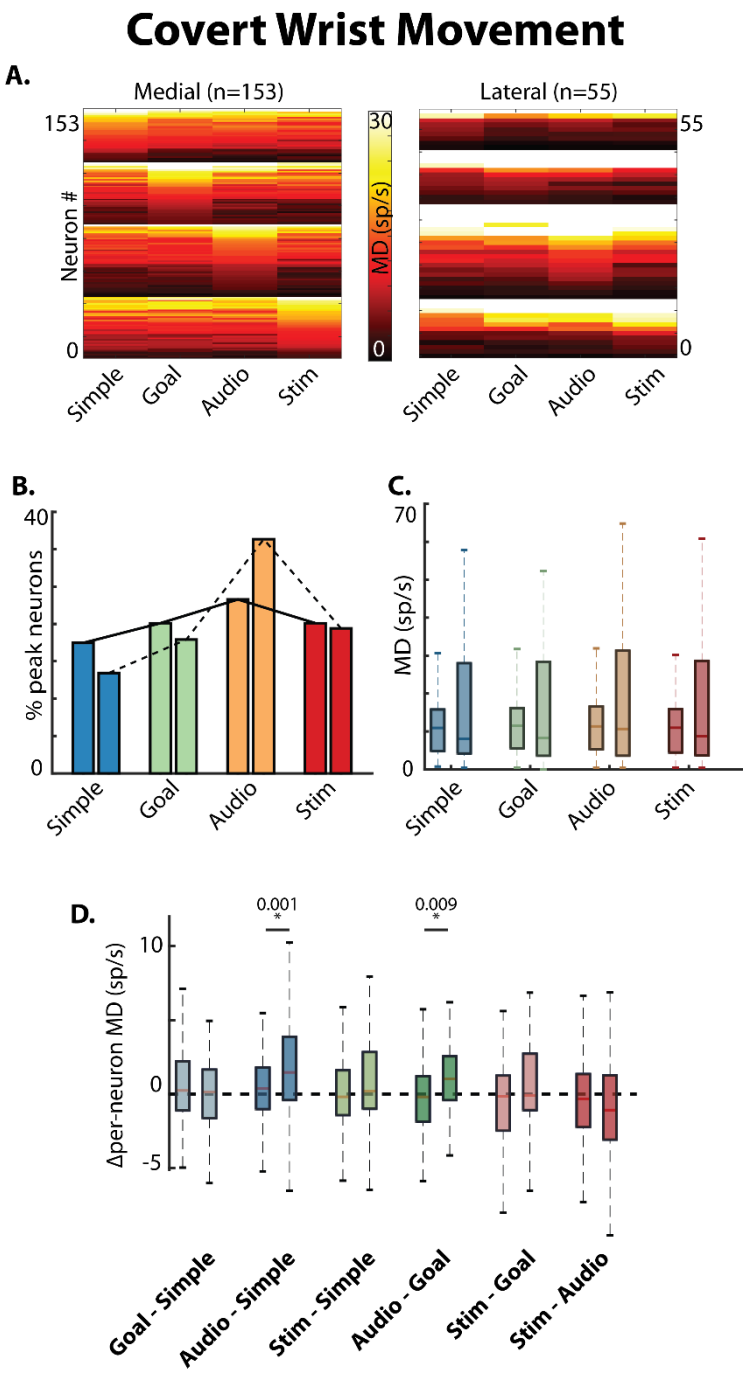

Figure 23: M1 single-neuron modulation during covert wrist movement. (A) Heatmaps showing modulation depth of individual neurons recorded from medial (left) and lateral (right) motor arrays. Neurons are grouped vertically (rows) according to their peak enrichment condition. (B) Percent of neurons from each array (left = medial, right = lateral) displaying peak modulation during each task. (C) Distributions (median, inter-quartile range, and 5/95%) of neural modulation depths from each array (left = medial, right = lateral) during each enrichment condition. (D) Distributions (median, inter-quartile range, and 5/95%) of per-neuron differences in between-condition modulation depth. * = significance between arrays in each task ($p<0.01$, Wilcoxon rank-sum).

We then analyzed the time-varying state trajectories generated from all motor neurons and each motor array separately (**Figure 24**). Examining the whole-population activity (**A-D;** n=208) revealed similar trajectories during each condition (**A**), consistent with the shared kinematics of each enrichment condition. Enrichment condition trajectories appeared to traverse a shared volume of space, with different enrichments inducing greater origin-distance at different time-points (**C**) which generally increased with enrichment (**D**). Trajectories during Simple and Stim conditions displayed the highest separability, although overall accuracy was low, with Goal and Audio trajectories often mis-classified as either Simple or Stim (**B**).

Examining the state-space activity of each array separately revealed substantial differences between arrays. Medial trajectories (**E-H;** n=153) occupied a smaller state volume (**E**) and were less separable (**F**), with each condition trajectory displaying lower and less variable time-courses (**G/H**). Lateral trajectories (**I-L;** n=55) displayed very similar spatial structure (**A**) and time-course (**C**) compared to the whole-population space. Additionally, Lateral trajectory time-courses appeared to increase linearly with additional enrichment (**D**), with each condition following the same temporal pattern while distance increased with enrichment.

Together, these results suggest that while neurons from both Medial and Lateral arrays encode task-related information, the Lateral population is more strongly affected by multisensory enrichment. Since the general spatiotemporal structure of the population activity was preserved across conditions, the increased origin-distance elicited by increased enrichment may illustrate increased robustness in the Lateral population's ability to encode the task.

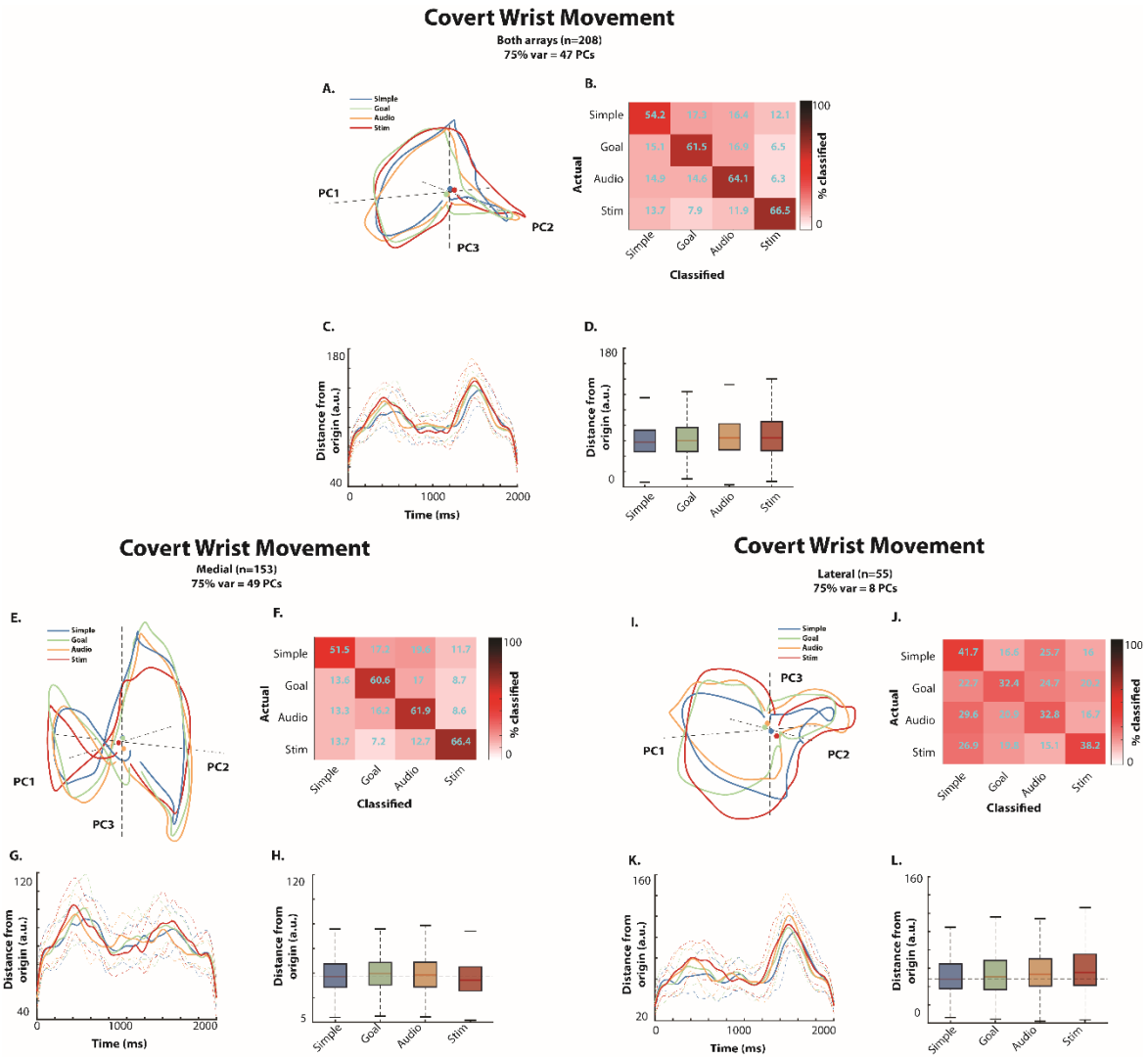

Figure 24: Neural state trajectories during covert wrist movement. Neural state spaces were calculated separately using neurons from both arrays (A-D), the medial motor array (E-H), and the lateral motor array (I-J). (A,E,I): Neural trajectories during each task projected into first 3 principal components. (B,F,J): Naïve Bayes classification accuracy based on PC3 neural trajectories. (C,G,K): Time course of neural trajectories (measured as distance from state-space origin during each task. (D,H,L): Distributions (median, inter-quartile range, 5/95%) of origin-trajectory distance during each task.

We next examined neural activity during enriched covert Hand movement. Analyzing single-neuron modulation (**Figure 25A**) again revealed subpopulations of neurons from both arrays which displayed peak modulation during each enrichment condition. We found that a majority of Medial neurons peaked in the Simple condition, while a majority of Lateral neurons peaked in the Stim condition (**B**). The Medial population also displayed significantly higher firing rates ($p<0.05$, Wilcoxon rank-sum) in each condition compared to the Lateral population (**C**), consistent with the difference observed in the Overt movement case. We did not observe any significant differences between condition MD distributions on either array. Directly calculating per-neuron enrichment revealed no significant differences between arrays or between conditions within each array, as well as a general lack of systematic changes between conditions (**D**). These results indicate that while single neurons from both arrays modulate during enriched hand movement, that enrichment does not appear to significantly affect the activity of individual neurons.

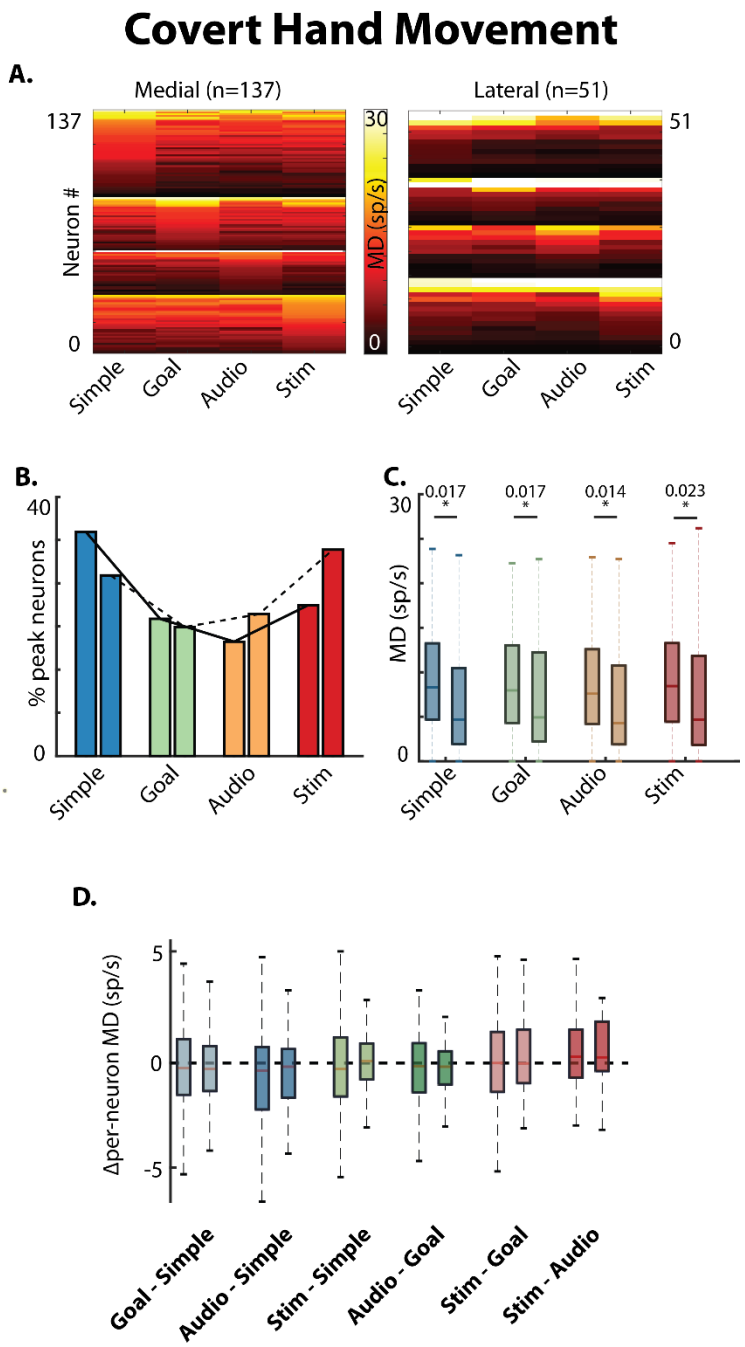

Figure 25: M1 single-neuron modulation during covert hand movement. (A) Heatmaps showing modulation depth of individual neurons recorded from medial (left) and lateral (right) motor arrays. Neurons are grouped vertically (rows) according to their peak enrichment condition. (B) Percent of neurons from each array (left = medial, right = lateral) displaying peak modulation during each task. (C) Distributions (median, inter-quartile range, and 5/95%) of neural modulation depths from each array (left = medial, right = lateral) during each enrichment condition. * = significance between arrays in each task ($p<0.05$, Wilcoxon rank-sum). (D) Distributions (median, inter-quartile range, and 5/95%) of per-neuron differences in between-condition modulation depth.

Conversely, examining population-level activity (**Figure 26**) revealed significant enrichment effects. Whole-population trajectories (n=188) (**A)** behaved similarly to those observed during Wrist movement, with each trajectory traversing a similar path through state space with enrichment-related variance along that path. Audio and Stim trajectories were more separable compared to Simple and Goal (**B**), displayed transient deflections from Simple/Goal trajectories at multiple time-points (most notable at the peak at ~1500ms) (**C**), and displayed the lowest and highest origin-distance time-course distributions respectively (**C/D**).

In the Medial population space (n=137) we again observed more spatially-compact trajectories (**E**), with the Simple condition displaying the greatest separability (**F**), consistent with the higher proportion of Simple-peak single neurons. Medial trajectory time-courses displayed little variance across the movement period (**G**), with similar distance distributions in Simple/Stim conditions and minimal distance in the Audio condition (**H**).

Lateral population trajectories (n=51) again displayed large spatial structures (**I**), as well as increased separability in the Audio and Stim conditions relative to Simple and Goal (**B**). Lateral trajectory time-courses were notably similar to those of the whole population (**K**), and reflect the reduction in Goal/Audio distance and increase in Stim distance (**L**).

These results suggest that during covert Hand movement, Goal and Audio enrichment may decrease the strength of the population-level representation, while Stim enrichment appears to increase it, particularly in the Lateral array population.

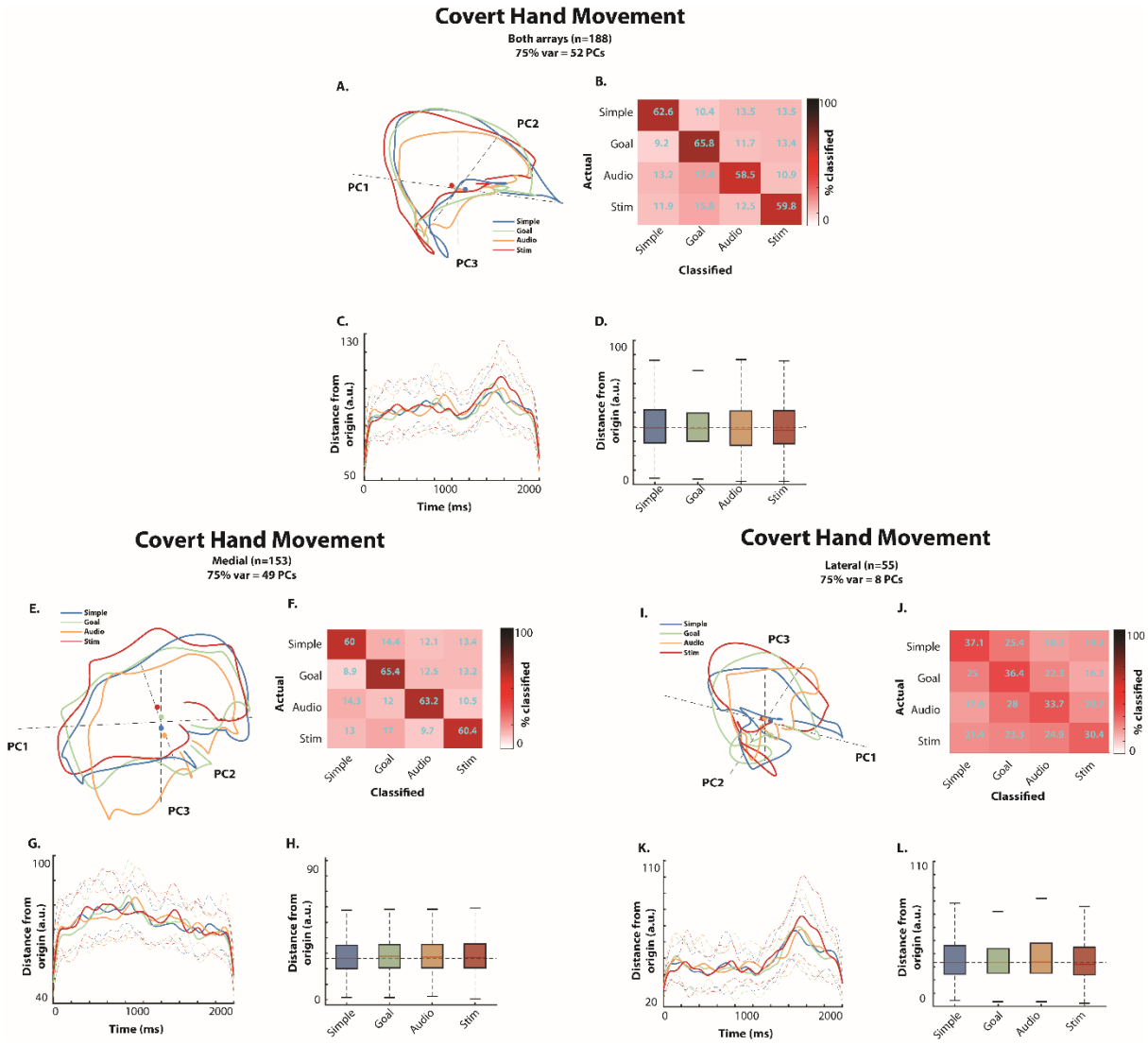

Figure 26: Neural state trajectories during covert hand movement. Neural state spaces were calculated separately using neurons from both arrays (A-D), the medial motor array (E-H), and the lateral motor array (I-J). (A,E,I): Neural trajectories during each task projected into first 3 principal components. (B,F,J): Naïve Bayes classification accuracy based on PC3 neural trajectories. (C,G,K): Time course of neural trajectories (measured as distance from state-space origin during each task. (D,H,L): Distributions (median, inter-quartile range, 5/95%) of origin-trajectory distance during each task.

Finally, we examined neural activity during enriched Finger movement. Analyzing single-neuron modulation (**Figure 27A**) revealed that the Medial population was most likely to show peak modulation during the Stim condition than others, while the Lateral population displayed many more neurons with peak modulation during the Simple condition than others (**B**). However, when we compared the arrays' modulation during each task, we did not observe any significant differences either within or between arrays (**C**), suggesting that single-neuron activity during Finger movement is not significantly altered by multisensory enrichment. Per-neuron modulation differences between pairwise conditions also displayed no significant differences between arrays or conditions within each array, further supporting the lack of interaction between single-neuron activity and multisensory enrichment.

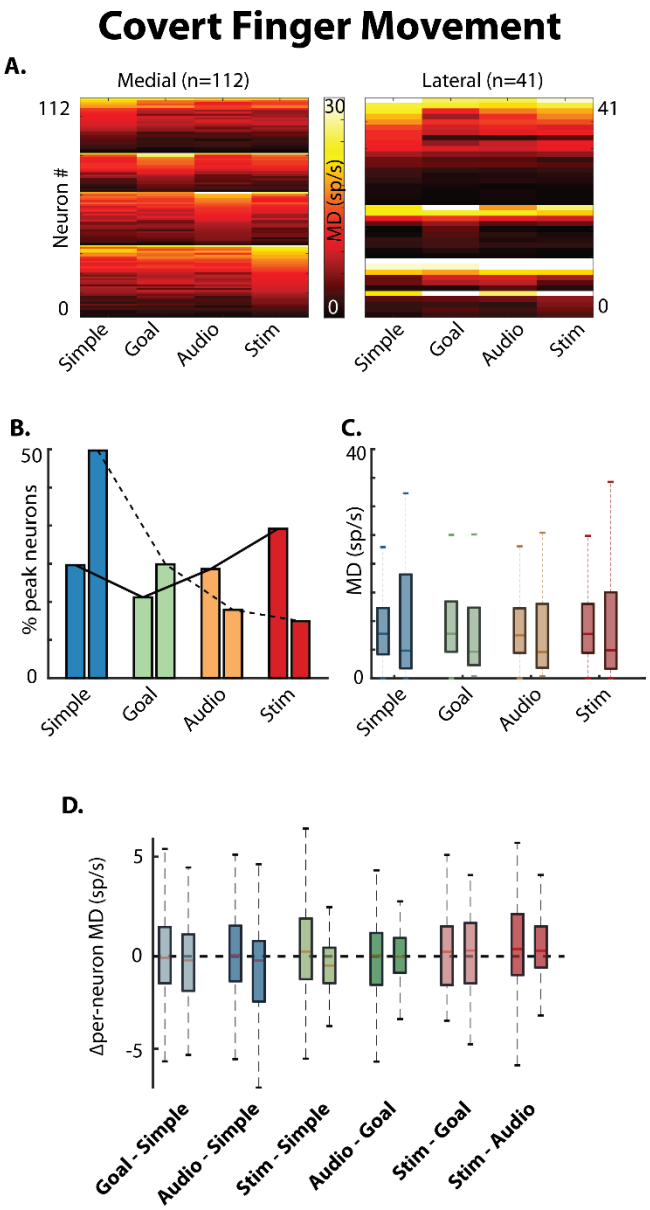

Figure 27: M1 single-neuron modulation during covert finger movement. (A) Heatmaps showing modulation depth of individual neurons recorded from medial (left) and lateral (right) motor arrays. Neurons are grouped vertically (rows) according to their peak enrichment condition. (B) Percent of neurons from each array (left = medial, right = lateral) displaying peak modulation during each task. (C) Distributions (median, inter-quartile range, and 5/95%) of neural modulation depths from each array (left = medial, right = lateral) during each enrichment condition. * = significance between arrays in each task ($p<0.05$, Wilcoxon rank-sum). (D) Distributions (median, inter-quartile range, and 5/95%) of per-neuron differences in between-condition modulation depth.

When we analyzed the neural trajectories generated from the whole population (**Figure 28A**; n=153) we observed dramatic differences in the spatial structure of each condition trajectory. The Simple trajectory was highly separable from all other conditions (**B**), and while the other 3 conditions traversed similar volumes of state space, they appeared to vary more than those observed in the other Covert movement tasks. Additionally, the time-course of the Simple trajectory diverged substantially from those of the other 3 conditions (**C**), each of which displayed greater overall origin-distance (**D**). These findings suggest that the Goal enrichment (a change in the task's visual context, which is shared across the Audio and Stim conditions) had a significant effect on the population-level activity in motor cortex.

Examining trajectories generated from the Medial population (n=112) revealed dramatically different trajectories (**E**), which were highly separable and whose overall spatial structure more closely resembled those generated during the Overt movement task than those observed in the other Covert tasks. The Simple trajectory was highly separable, traversing a small volume of space shared with the Goal and Audio trajectories, which varied around a common plane. The Stim trajectory was completely separate from the other conditions (**F**), and traversed a different time-course (**G**) through a more distant volume of state space (**H**). These findings indicate that the Medial population is significantly affected by enrichment during Finger movement, especially in the Stim condition.

The Lateral population space (n=41) also displayed substantial enrichment effects. Rather than the dramatic spatial separation between conditions observed in the Medial population space, the Lateral trajectories (**I**) appeared to spread out from a common plane, displaying more separability (**J**) than observed in other Covert tasks. The trajectory time-courses (**K**) revealed a stark difference between the Simple condition and the other 3 conditions, which all displayed

similar temporal pattern with distance increasing with enrichment (**L**). These results indicate that the Lateral population, as well as the Medial population, was significantly affected by Goal enrichment and the subsequent additive enrichment conditions.

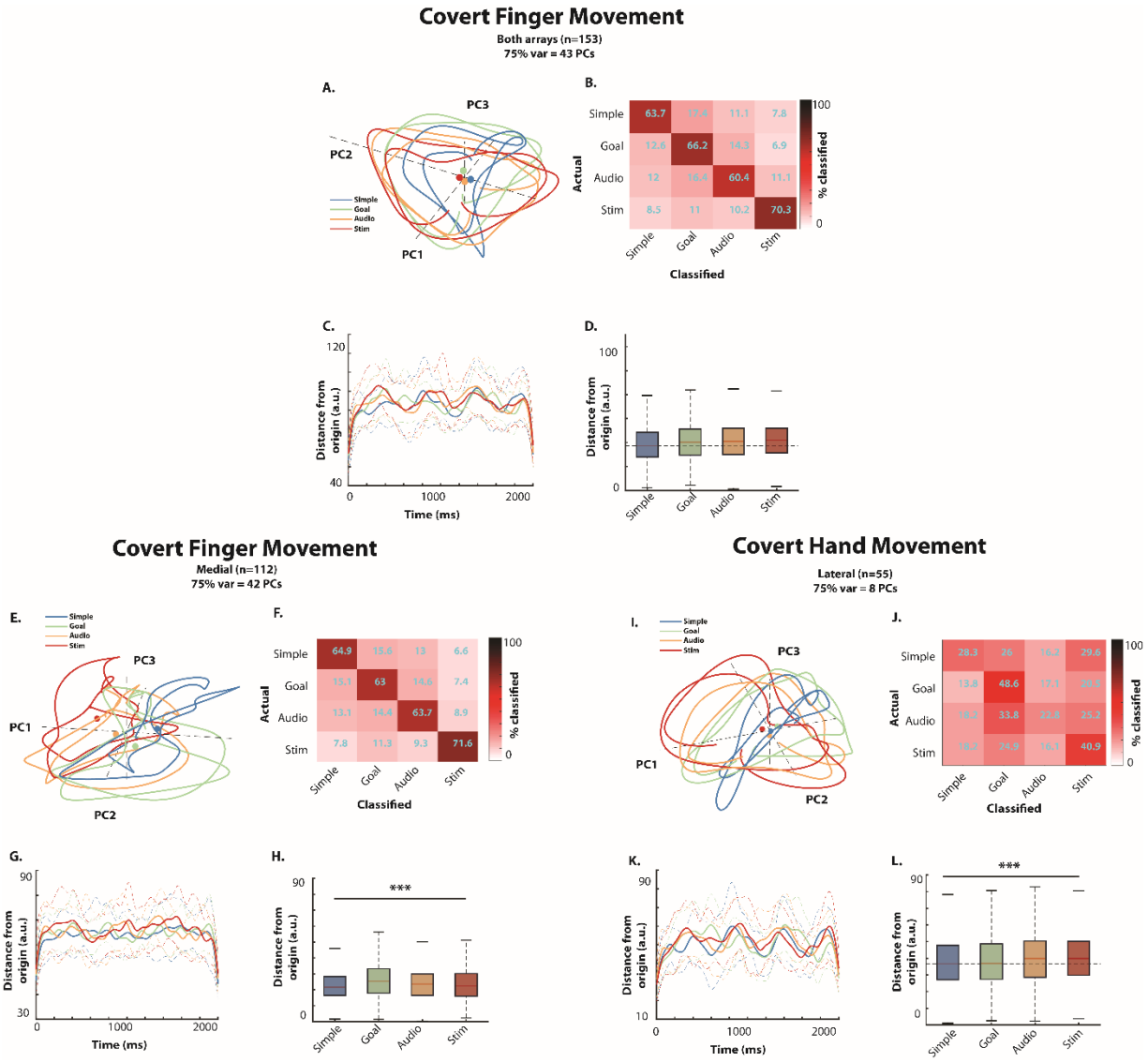

Figure 28: Neural state trajectories during covert finger movement. Neural state spaces were calculated separately using neurons from both arrays (A-D), the medial motor array (E-H), and the lateral motor array (I-J). (A,E,I): Neural trajectories during each task projected into first 3 principal components. (B,F,J): Naïve Bayes classification accuracy based on PC3 neural trajectories. (C,G,K): Time course of neural trajectories (measured as distance from state-space origin during each task. (D,H,L): Distributions (median, inter-quartile range, 5/95%) of origin-trajectory distance during each task.

4.4 Discussion

By simultaneously recording activity from spatially separate neural populations in human M1 during enriched covert movement, we have provided evidence that neural populations in different areas of M1 may receive and process contextual sensory information differently, allowing them each to contribute novel information to a larger population-level activity pattern.

We found that individual neurons from different areas of the upper limb representation were broadly modulated during all movement tasks, consistent with our previous findings of weak single-neuron somatotopy (see Chapter 3). Within each Covert enrichment task, we found only minor differences in neural modulation depth across enrichment conditions, indicating that the overall level of population firing activity remains relatively stable during sensory-variants of a motor task with fixed kinematics. However, when we analyzed the same activity from a population-level perspective, we observed minor changes in the spatiotemporal structure of neural state dynamics during each task's enrichment conditions. Population-level activity from each array contributed different information to the activity of the combined motor population. Whole-population trajectories primarily reflected the temporal structure of Lateral neurons, but traversed greater volumes/distances with more separability in neural state space when combined with Medial neurons.

Examining these population structures during the enriched Covert conditions revealed minor differences in the activity of both populations. In each Covert task, multisensory enrichment increased the distance traversed by the neural state trajectories relative to the unenriched Simple condition. As "distance" in this neural state space corresponds to the degree

of shared variance in population-wide activity, we propose that these enrichment-related increases in trajectory distance relate to increased robustness in the encoding of each movement, possibly due to the additional engagement of premotor and parietal input to integrate the object-related multisensory information (Schaffelhofer & Scherberger, 2016).

We also observed dramatic differences in the structure of neural state trajectories between arrays. The medial array population appeared to encode separation between conditions (i.e. trajectories could be "centered" around distant points rather than space-origin), while the lateral array population appeared to primarily encode the temporal structure of conditions (centered around space-origin, separability by orthogonal rotation). This difference could indicate that the lateral array, which is located in a cortical area shown to be "hand-related' by large-scale neuroimaging, samples a neural population that has access to a greater proportion of hand-related sensory input from higher-order cortical areas, and therefore corresponds closely to the temporal profile of the movement task. Conversely, as the medial array is located outside of this "hand-related" area, it samples neurons which participate less directly in generating the exact temporal pattern of activity, but which are involved broadly in coordinating ongoing movement.

We also observed that neural state trajectories during many tasks/conditions tended to display circular structure and dynamics. These rotational dynamics can be partly explained by the nature of PCA, which is to define space that maximally separates the data (i.e. identify patterns of greatest variance between conditions), and are also consistent with current models of population activity (Russo et al., 2018).

Ideally, to determine whether multisensory enrichment increases the "effective somatotopy" (i.e. increases the separability of neural activity representing different

movements/conditions), we would compare the population activity of different movements (Wrist/Hand/Fingers) during each enrichment condition. Due to limitations on experimental testing time, we were only able to collect partial data sets on each testing session. While we were able to collect Overt task data each day, incomplete data sets collected for Covert tasks means that we are analyzing a slightly different (partially overlapping) neural population. Future experiments should utilize intermixed designs in order to generate continuous activity from a common population.

In summary, our work demonstrates that activity from throughout M1 coordinates to represent not only the detailed kinematics of ongoing movement, but also to a lesser degree the multisensory context in which it is performed. These results provide insight into the nature of neural computation and multisensory integration, and can be used to inform the development of intracortical neuroprosthetics.

5.0 Conclusions

One of the core challenges in neuroscience is the hierarchical nature of neural computation. Individual neurons connect together to create neural circuits, which convey information within and between brain areas, as well as to and from the spinal cord and the rest of the body. As a result of this organization, neural activity can be interpreted and studied across spatial scales, ranging from the activity of individual neurons to the aggregate signals of millions of neurons together. Extensive research has been done to identify relationships between neural activity measured at different spatial scales, but such links remain elusive. In recent years, the development of intracortical brain-computer interfaces has offered a unique opportunity to investigate the activity of human neural populations in sensorimotor cortex. We sought to determine how the organization of large-scale activity in M1 was reflected in the activity of spatially separate individual neurons, and how activity at both of these spatial scales is affected by task context. While this work has implications for a wide range of neuroscientific studies, it was performed specifically in the context of intracortical BCIs for the purpose of controlling prosthetic arms and hands. In this context, our work focused on evaluating the validity and ideal strategy for using neuroimaging for presurgical planning of intracortical microelectrode arrays.

Typically, implant location is planned based on identifying the generally somatotopic location of fMRI activity during a specific movement task (Collinger et al., 2014, 2012). We have shown that the spatial distribution of the large-scale activity in M1 representing different hand movements is widely distributed and overlapping (Chapter 2). We observed peaks of activity during each overt movement in a spatially consistent area (the “hand knob”), indicating that some cortical areas are more likely to be involved in processing activity directly related to

overtly performed hand movements. However, we also found that this activity is also present throughout M1, suggesting that this common "core" area is merely the peak of a widespread representation involving neurons from many different areas. This finding is supported by our analysis of single neurons recorded from multiple sites in M1 (Chapter 3). The fMRI activity collected for presurgical planning in this subject suggested that the lateral array would sample neurons more likely to be modulated by hand and finger movements. Based on conventional large-scale somatotopy, the medial array was predicted to sample neurons more likely to be modulated by arm movements. We observed that neurons from both medial and lateral areas of this "hand knob" were broadly modulated by both arm and hand movements, although medial array neurons displayed stronger and more selective modulation during arm movements compared to finger movements. Together with the large-scale overt activity described in Chapter 2, these results support the idea that upper limb movements are controlled by widespread populations of neurons in M1, where the location of peak large-scale activity may reveal neurons that are preferentially driven by different types of movement.

However, the distribution of this large-scale activity during movements under different multisensory contexts reveals that these representations are even more complex. We found that the activity underlying various hand movements was significantly affected by the presence of multisensory enrichment, even when the basic kinematics of each movement was unchanged (Chapter 2). Although this enriched activity partially overlapped with the areas seen to be active during unenriched movements, goal-directed enrichments elicited activity in more ventral areas of M1 compared to simple movement. This increased spatial variance suggests that goal-directed movements, which may require additional processing of hand-posture shaping and anticipated sensory consequences, may recruit additional areas of M1 beyond those involved in simple

movement production. Additionally, the distribution and magnitude of this enrichment effect varied between different movements, suggesting that the sensorimotor system may integrate such multisensory cues differently based on the type of movement and the behavioral relevance or congruence of the sensory information. When we examined intracortical activity from separate areas of M1 during the same behavioral task (Chapter 4), we found that single neurons in the "hand knob" were generally unaffected by this multisensory enrichment. This finding is in line with our results from Chapter 2, where enrichment-related activity was often seen in more ventral areas relative to these array locations. Together, these results suggest that this multisensory enrichment can be used to increase the amplitude and volume of large-scale activity elicited by covert movement tasks, improving the utility of presurgical neuroimaging. However, they also reveal that such representations are even more complex and widespread than previously thought.

While the majority of our intracortical analysis was focused on the activity of individual neurons, we also explored whether population-level analysis approaches could reveal additional insights. When we examined the structure of population-level neural activity during different movements and conditions (Chapter 4), we found that activity from the medial and lateral arrays contributed very different information to the overall pattern of activity generated from both arrays combined. Lateral array activity consistently appeared to preferentially represent the temporal structure of different movements, while medial array activity appeared to preferentially separate different movements and multisensory conditions from one another. These findings are in line with the large-scale organization observed in the presurgical neuroimaging, which suggested that the lateral array sampled neurons which receive more hand-related activity. This increased input may drive these neurons to participate in defining the temporal structure of hand-

related movements, while neurons recorded from the medial array, which is removed from this peak input area, may encode more general information related to which movement is being performed. Combined with the widespread representations observed at both meso- and micro-scales (Chapters 2 and 3 respectively), these results suggest that neural populations in different areas of M1 may contribute different types of information to the overall descending motor command based on their location in this large-scale organization.

To broadly summarize, our results demonstrate that the large-scale organization of cortical activity can be used to broadly predict the behavior of neurons in different areas of M1. We have shown that populations of neurons throughout M1 participate in encoding a wide range of intended movements, and that the overall "preferences" of those neurons aligns with their location relative to large-scale patterns of activity. However, the broad participation of these populations, and the widespread changes resulting from contextual sensory information, demonstrate that these representations reflect the high-dimensional nature of the various movement parameters which may be encoded. Rather than an orderly modular structure where different movements are represented by activity in different areas, the organization of activity in M1 may instead be a necessary by-product of the brain's computational requirement to represent multiple dimensions of movement-related information in the low-dimensional space of the neurons within the cortical sheet (Aflalo & Graziano, 2006; Graziano & Aflalo, 2007). Such organization would suggest that different types of information may be encoded in the activity of different cortical areas based on their anatomical inputs and outputs as well as local connectivity (Dea et al., 2016; Hamadjida et al., 2016). Moreover, this organization would suggest that the relative similarity between patterns of activity underlying different movements would reflect the similarity between those movements. This idea is supported by recent studies showing that M1

activity during individual finger movements reflects the natural statistics of finger use (Ejaz et al., 2015; Kikkert et al., 2016). Our results suggest that this type of high-dimensional encoding is also implemented in the activity of neural populations, consistent with other studies showing that neural activity from multiple areas of the brain reflect the complex movement and sensory-related information of object interaction tasks (Menz et al., 2015; Schaffelhofer et al., 2015; Schaffelhofer & Scherberger, 2016).

Taken together, this work demonstrates that although neuroimaging can be used to predict the behavior of neural populations in M1 and thus to inform the location of implanted microelectrode arrays, it will be important to incorporate more complex representational models into these efforts. Rather than targeting areas which display stronger activity during a desired task, it may be more advantageous to employ multivariate decoding strategies to identify areas which provide the greatest separation and temporal definition between different tasks. For example, based on the distribution of both meso- and micro-scale activity in the BCI participant described here, we can hypothesize that another array placed more ventrally may sample neurons which are more involved in processing contextual sensory information, allowing us to account for goal-related information. This approach can be applied to multiple different movement parameters (i.e. arm vs hand, object context, movements towards different regions of space) to identify cortical areas which provide the most separation between different conditions, thus allowing us to record from neurons encoding a wider array of complex information and improving our ability to decode different movements with high precision across contexts.

This work focused primarily on examining spiking activity, which relates to motor output and is thus thought to be more directly related to intended movement production. However, fMRI activity relates more closely to LFPs than to spikes (N K Logothetis et al., 2001; Nikos K.

Logothetis & Wandell, 2004), and spikes and LFPs in motor cortex may encode partially distinct information (Perel et al., 2015). Analyzing LFPs may provide an additional mechanism for defining relationships between representations at different spatial scales. Additionally, fMRI activity appears to closely resemble cortical surface activity measured with ECoG (Siero et al., 2014), which corresponds closely to LFP signals (Buzsáki, Anastassiou, & Koch, 2012).

Concurrent with the intracortical data presented here, the intracortical participant was enrolled in an ongoing BCI trial, where he was able to use neural activity recorded from the same arrays to control a wide range of neuroprosthetic effectors, including robotic arms. It is currently not known how the somatotopic organization we observed (i.e., arm-related activity predominant on the medial array, hand-related activity predominant on the lateral array) relates to the structure of decoders built to enable neuroprosthetic arm control. If the spatial trends in neural population activity observed here are consistent when that activity is applied to BCI control, further investigations could leverage such differences to inform the design of BCI decoders to preferentially drive specific movements, potentially improving their performance.

Bibliography

Aflalo, T. N., & Graziano, M. S. A. (2006). Possible Origins of the Complex Topographic Organization of Motor Cortex: Reduction of a Multidimensional Space onto a Two-Dimensional Array. *Journal of Neuroscience*, *26*(23), 6288–6297. https://doi.org/10.1523/JNEUROSCI.0768-06.2006

Ajiboye, A. B., Willett, F. R., Young, D. R., Memberg, W. D., Murphy, B. A., Miller, J. P., … Kirsch, R. F. (2017). Restoration of reaching and grasping movements through brain-controlled muscle stimulation in a person with tetraplegia: a proof-of-concept demonstration. *The Lancet*, *389*(10081), 1821–1830. https://doi.org/10.1016/S0140-6736(17)30601-3

Alkadhi, H., Crelier, G. R., Boendermaker, S. H., Golay, X., Hepp-Reymond, M. C., & Kollias, S. S. (2002). Reproducibility of primary motor cortex somatotopy under controlled conditions. *American Journal of Neuroradiology*, *23*(9), 1524–1532.

Anumanchipalli, G. K., Chartier, J., & Chang, E. F. (2019). Speech synthesis from neural decoding of spoken sentences. *Nature*, *568*(7753), 493–498. https://doi.org/10.1038/s41586-019-1119-1

Ashburner, J., Barnes, G., Chen, C., Daunizeau, J., Moran, R., Henson, R., … Phillips, C. (2013). SPM12. *Functional Imaging Laboratory*, 475–1. https://doi.org/10.1111/j.1365-294X.2006.02813.x

Beisteiner, R., Windischberger, C., Lanzenberger, R., Edward, V., Cunnington, R., Erdler, M., … Deecke, L. (2001). Finger somatotopy in human motor cortex. *NeuroImage*, *13*(6 Pt 1), 1016–1026. https://doi.org/10.1006/nimg.2000.0737

Buzsáki, G., Anastassiou, C. A., & Koch, C. (2012). The origin of extracellular fields and currents-EEG, ECoG, LFP and spikes. *Nature Reviews Neuroscience*, *13*(6), 407–420. https://doi.org/10.1038/nrn3241

Caspers, S., Zilles, K., Laird, A. R., & Eickhoff, S. B. (2010). ALE meta-analysis of action observation and imitation in the human brain. *NeuroImage*, *50*(3), 1148–1167. https://doi.org/10.1016/j.neuroimage.2009.12.112

Choe, A. S., Jones, C. K., Joel, S. E., Muschelli, J., Belegu, V., Caffo, B. S., … Pekar, J. J. (2015). Reproducibility and Temporal Structure in Weekly Resting-State fMRI over a Period of 3.5 Years. *Plos One*, *10*(10), e0140134. https://doi.org/10.1371/journal.pone.0140134

Collinger, J. L., Kryger, M. a, Barbara, R., Betler, T., Bowsher, K., Brown, E. H. P., … Boninger, M. L. (2014). Collaborative approach in the development of high-performance brain-computer interfaces for a neuroprosthetic arm: translation from animal models to human control. *Clinical and Translational Science*, *7*(1), 52–59. https://doi.org/10.1111/cts.12086

Collinger, J. L., Wodlinger, B., Downey, J. E., Wang, W., Tyler-kabara, E. C., Weber, D. J., … Schwartz, A. B. (2012). High-performance neuroprosthetic control by an individual with tetraplegia. *The Lancet*, *6736*(12).

Cunningham, D. a., Machado, A., Yue, G. H., Carey, J. R., & Plow, E. B. (2013). Functional somatotopy revealed across multiple cortical regions using a model of complex motor task. *Brain Research*, *1531*, 25–36. https://doi.org/10.1016/j.brainres.2013.07.050

Dea, M., Hamadjida, A., Elgbeili, G., Quessy, S., & Dancause, N. (2016). Different Patterns of Cortical Inputs to Subregions of the Primary Motor Cortex Hand Representation in Cebus apella. *Cerebral Cortex*, *26*(4), 1747–1761. https://doi.org/10.1093/cercor/bhv324

Dechent, P., & Frahm, J. (2003). Functional somatotopy of finger representations in human primary motor cortex. *Human Brain Mapping*, *18*(4), 272–283. https://doi.org/10.1002/hbm.10084

Degenhart, A. D., Hiremath, S. V, Yang, Y., Foldes, S. T., Collinger, J. L., Boninger, M. L., … Wang, W. (2017). Remapping cortical modulation for electrocorticographic brain-computer interfaces: a somatotopy-based approach in individuals with upper-limb paralysis. *Journal of Neural Engineering*. https://doi.org/10.1088/1741-2552/aa9bfb

Desikan, R. S., Ségonne, F., Fischl, B., Quinn, B. T., Dickerson, B. C., Blacker, D., … Killiany, R. J. (2006). An automated labeling system for subdividing the human cerebral cortex on MRI scans into gyral based regions of interest. *NeuroImage*, *31*, 968–980. https://doi.org/10.1016/j.neuroimage.2006.01.021

Devor, A., Ulbert, I., Dunn, A. K., Narayanan, S. N., Jones, S. R., Andermann, M. L., … Dale, A. M. (2005). Coupling of the cortical hemodynamic response to cortical and thalamic neuronal activity. *Proceedings of the National Academy of Sciences of the United States of America*, *102*(10), 3822–3827. https://doi.org/10.1073/pnas.0407789102

Downey, J. E., Brane, L., Gaunt, R. A., Tyler-kabara, E. C., Boninger, M. L., & Collinger, J. L. (2017). Motor cortical activity changes during neuroprosthetic- controlled object interaction. *Scientific Reports*, (October), 1–16. https://doi.org/10.1038/s41598-017-17222-3

Downey, J. E., Schwed, N., Chase, S. M., Schwartz, A. B., & Collinger, J. L. (2018). Intracortical recording stability in human brain-computer interface users. *Journal of Neural Engineering*. https://doi.org/10.1088/1741-2552/aab7a0

Dum, R. P., & Strick, P. L. (1991). The origin of corticospinal projections from the premotor areas in the frontal lobe. *The Journal of Neuroscience : The Official Journal of the Society for Neuroscience*, *11*(March), 667–689. https://doi.org/S0022510X0200268X [pii]

Ejaz, N., Hamada, M., & Diedrichsen, J. (2015). Hand use predicts the structure of representations in sensorimotor cortex. *Nature Neuroscience*, *103*(June). https://doi.org/10.1038/nn.4038

Fabbri, S., Stubbs, K. M., Cusack, R., & Culham, J. C. (2016). Disentangling Representations of Object and Grasp Properties in the Human Brain. *Journal of Neuroscience*, *36*(29), 7648–7662. https://doi.org/10.1523/JNEUROSCI.0313-16.2016

Fischl, B. (2012). FreeSurfer. *NeuroImage*, *62*(2), 774–781. https://doi.org/10.1016/j.neuroimage.2012.01.021

Flesher, S. N., Collinger, J. L., Foldes, S. T., Weiss, J. M., Downey, J. E., Tyler-Kabara, E. C., … Gaunt, R. A. (2016). Intracortical microstimulation of human somatosensory cortex. *Science Translational Medicine*, *8*(361), 361ra141-361ra141. https://doi.org/10.1126/scitranslmed.aaf8083

Flesher, S. N., Downey, J. E., Weiss, J. M., Hughes, C. L., Herrera, A. J., Tyler-Kabara, E. C., … Gaunt, R. A. (2019). Restored tactile sensation improves neuroprosthetic arm control. *BioRxiv*, 653428. https://doi.org/10.1101/653428

Foldes, S. T., Weber, D. J., & Collinger, J. L. (2017). Altered modulation of sensorimotor rhythms with chronic paralysis. *Journal of Neurophysiology*, jn.00878.2016. https://doi.org/10.1152/jn.00878.2016

Fraser, G. W., & Schwartz, A. B. (2012). Recording from the same neurons chronically in motor cortex. *Journal of Neurophysiology*, *107*(7), 1970–1978. https://doi.org/10.1152/jn.01012.2010

Gentile, G., Guterstam, A., Brozzoli, C., & Ehrsson, H. H. (2013). Disintegration of multisensory signals from the real hand reduces default limb self-attribution: an fMRI study. *The Journal of Neuroscience : The Official Journal of the Society for Neuroscience*, *33*(33), 13350–13366. https://doi.org/10.1523/JNEUROSCI.1363-13.2013

Georgopoulos, A. P., Kalaska, J. F., Caminiti, R., & Massey, J. T. (1982). On the relations between the direction of two-dimensional arm movements and cell discharge in primate motor cortex. *Journal of Neuroscience*, *2(11)*(11), 1527–1537. https://doi.org/citeulike-article-id:444841

Georgopoulos, A. P., Schwartz, A. B., & Kettner, R. E. (2009). Neuronal population coding of movement direction. *Science*, *233*(4771), 1416–1419. Retrieved from http://dx.doi.org/10.1126/science.3749885

Ghez, C., Gordon, J., & Ghilardi, M. (1995). Impairments of reaching movements in patients without proprioception. II. Effects of visual information on accuracy. *Journal of Neurophysiology*, *73*(1), 361–372. https://doi.org/10.1152/jn.1995.73.1.361

Gordon, J., Ghilardi, M. F., & Ghez, C. (1995). Impairments of reaching movements in patients without proprioception. I. Spatial errors. *Journal of Neurophysiology*, *73*(1), 347–360. https://doi.org/10.1152/jn.1995.73.1.347

Graziano, M. S. A. (2016). Ethological Action Maps: A Paradigm Shift for the Motor Cortex. *Trends in Cognitive Sciences*, *20*(2), 121–132. https://doi.org/10.1016/j.tics.2015.10.008

Graziano, M. S. A., & Aflalo, T. N. (2007). Mapping behavioral repertoire onto the cortex. *Neuron*, *56*(2), 239–251. https://doi.org/10.1016/j.neuron.2007.09.013

Graziano, M. S. A., Taylor, C. S. R., & Moore, T. (2002). Complex movements evoked by microstimulation of precentral cortex. *Neuron*, *34*(5), 841–851. https://doi.org/10.1016/S0896-6273(02)00698-0

Griffin, D. M., Hoffman, D. S., & Strick, P. L. (2015). Corticomotoneuronal cells are "functionally tuned." *Science*, *350*(6261), 667–670. https://doi.org/10.1126/science.aaa8035

Hamadjida, A., Dea, M., Deffeyes, J., Quessy, S., & Dancause, N. (2016). Parallel Cortical Networks Formed by Modular Organization of Primary Motor Cortex Outputs. *Current Biology*, *26*(13), 1737–1743. https://doi.org/10.1016/j.cub.2016.04.068

Henderson, L. a, Gustin, S. M., Macey, P. M., Wrigley, P. J., & Siddall, P. J. (2011). Functional reorganization of the brain in humans following spinal cord injury: evidence for underlying changes in cortical anatomy. *The Journal of Neuroscience : The Official Journal of the Society for Neuroscience*, *31*(7), 2630–2637. https://doi.org/10.1523/JNEUROSCI.2717-10.2011

Hlustik, P. (2001). Somatotopy in Human Primary Motor and Somatosensory Hand Representations Revisited. *Cerebral Cortex*, *11*(4), 312–321. https://doi.org/10.1093/cercor/11.4.312

Hochberg, L. R., Serruya, M. D., Friehs, G. M., Mukand, J. A., Saleh, M., Caplan, A. H., … Donoghue, J. P. (2006). Neuronal ensemble control of prosthetic devices by a human with tetraplegia. *Nature*, *442*(7099), 164–171. https://doi.org/10.1038/nature04970

Hotz-Boendermaker, S., Funk, M., Summers, P., Brugger, P., Hepp-Reymond, M. C., Curt, A., & Kollias, S. S. (2008). Preservation of motor programs in paraplegics as demonstrated by attempted and imagined foot movements. *NeuroImage*, *39*, 383–394. https://doi.org/10.1016/j.neuroimage.2007.07.065

Huntley, G. W., & Jones, E. G. (1991). Relationship of intrinsic connections to forelimb movement representations in monkey motor cortex: a correlative anatomic and physiological study. *Journal of Neurophysiology*, *66*(2), 390–413.

Intveld, R. W., Dann, B., Michaels, J. A., & Scherberger, H. (2018). Neural coding of intended and executed grasp force in macaque areas AIP, F5, and M1. *Scientific Reports*, *8*(1), 17985. https://doi.org/10.1038/s41598-018-35488-z

Irwin, Z. T., Schroeder, K. E., Vu, P. P., Bullard, A. J., Tat, D. M., Nu, C. S., … Chestek, C. A. (2017). Neural control of finger movement via intracortical brain–machine interface. *Journal of Neural Engineering*, *14*(6), 066004. https://doi.org/10.1088/1741-2552/aa80bd

Jarosiewicz, B., Bacher, D., Sarma, A. A., Masse, N. Y., Simeral, J. D., Sorice, B., … Hochberg, L. R. (2014). Virtual typing by people with tetraplegia using a stabilized, self-calibrating intracortical brain-computer interface. *IEEE BRAIN Grand Challenges Conference, Washington, DC*, *7*(313), 1–11. https://doi.org/10.1126/scitranslmed.aac7328

Jones, E. G., & Pons, T. P. (1998). Thalamic and brainstem contributions to large-scale plasticity of primate somatosensory cortex. *Science (New York, N.Y.)*, *282*(5391), 1121–1125. https://doi.org/10.1126/science.282.5391.1121

Kakei, S., Hoffman, D. S., & Strick, P. L. (1999). Muscle and movement representations in the primary motor cortex. *Science*, *285*(5436), 2136–2139. https://doi.org/10.1126/science.285.5436.2136

Kaufman, M. T., Churchland, M. M., Ryu, S. I., & Shenoy, K. V. (2014). Cortical activity in the null space: permitting preparation without movement. *Nature Neuroscience*, *17*(3), 440–448. https://doi.org/10.1038/nn.3643

Kikkert, S., Kolasinski, J., Jbabdi, S., Tracey, I., Beckmann, C. F., Johansen-Berg, H., & Makin, T. R. (2016). Revealing the neural fingerprints of a missing hand. *ELife*, *5*, e15292. https://doi.org/10.7554/eLife.15292

Kim, S.-P., Simeral, J. D., Hochberg, L. R., Donoghue, J. P., & Black, M. J. (2008). Neural control of computer cursor velocity by decoding motor cortical spiking activity in humans with tetraplegia. *Journal of Neural Engineering*, *5*(4), 455–476. https://doi.org/10.1088/1741-2560/5/4/010

Kirsch, E., Rivlis, G., & Schieber, M. H. (2014). Primary motor cortex neurons during individuated finger and wrist movements: Correlation of spike firing rates with the motion of individual digits versus their principal components. *Frontiers in Neurology*, *5 MAY*(May), 1–11. https://doi.org/10.3389/fneur.2014.00070

Kokotilo, K., Eng, J., & Curt, A. (2009). Reorganization and preservation of motor control of the brain in spinal cord injury: a systematic review. *Journal of Neurotrauma*, *26*(11), 2113–2126. https://doi.org/10.1089/neu.2008.0688.Reorganization

Kokotilo, K. J., Eng, J. J., Curt, A., & Boyd, L. A. (2009). Reorganization and preservation of motor control of the brain in spinal cord injury: a systematic review. *Journal of Neurotrauma*, *26*(11), 2113–2126. https://doi.org/10.1089/neu.2008.0688

Kriegeskorte, N. (2008). Representational similarity analysis – connecting the branches of systems neuroscience. *Frontiers in Systems Neuroscience*, *2*(November), 1–28. https://doi.org/10.3389/neuro.06.004.2008

Kuehn, E., Haggard, P., Villringer, A., Pleger, B., & Sereno, M. I. (2018). Visually-driven maps in area 3b. *Journal of Neuroscience*, *38*(5), 1295–1310. https://doi.org/10.1523/JNEUROSCI.0491-17.2017

Lang, C. E., & Schieber, M. H. (2003). Differential Impairment of Individuated Finger Movements in Humans After Damage to the Motor Cortex or the Corticospinal Tract. *Journal of Neurophysiology*, *90*(2), 1160–1170. https://doi.org/10.1152/jn.00130.2003

Lang, C. E., & Schieber, M. H. (2004). Reduced Muscle Selectivity During Individuated Finger Movements in Humans After Damage to the Motor Cortex or Corticospinal Tract. *Journal of Neurophysiology*, *91*(4), 1722–1733. https://doi.org/10.1152/jn.00805.2003

Logothetis, N K, Pauls, J., Augath, M., Trinath, T., & Oeltermann, a. (2001). Neurophysiological investigation of the basis of the fMRI signal. *Nature*, *412*(6843), 150–157. https://doi.org/10.1038/35084005

Logothetis, Nikos K. (2012). Intracortical recordings and fMRI: An attempt to study operational modules and networks simultaneously. *NeuroImage*, *62*(2), 962–969. https://doi.org/10.1016/j.neuroimage.2012.01.033

Logothetis, Nikos K., & Wandell, B. A. (2004). Interpreting the BOLD Signal. *Annual Review of Physiology*, *66*(1), 735–769. https://doi.org/10.1146/annurev.physiol.66.082602.092845

Lotze, M., Erb, M., Flor, H., Huelsmann, E., Godde, B., & Grodd, W. (2000). fMRI evaluation of somatotopic representation in human primary motor cortex. *NeuroImage*, *11*, 473–481. https://doi.org/10.1006/nimg.2000.0556

Mahan, M. Y., & Georgopoulos, A. P. (2013). Motor directional tuning across brain areas: directional resonance and the role of inhibition for directional accuracy. *Frontiers in Neural Circuits*, *7*(May), 92. https://doi.org/10.3389/fncir.2013.00092

Makin, T. R., & Bensmaia, S. J. (2017). Stability of Sensory Topographies in Adult Cortex. *Trends in Cognitive Sciences*, *21*(3), 195–204. https://doi.org/10.1016/j.tics.2017.01.002

Maynard, E. M., Nordhausen, C. T., & Normann, R. A. (1997). The Utah Intracortical Electrode Array: A recording structure for potential brain-computer interfaces. *Electroencephalography and Clinical Neurophysiology*, *102*(3), 228–239. https://doi.org/10.1016/S0013-4694(96)95176-0

Meier, J. D., Aflalo, T. N., Kastner, S., & Graziano, M. S. A. (2008). Complex Organization of Human Primary Motor Cortex: A High-Resolution fMRI Study. *Journal of Neurophysiology*, *100*(4), 1800–1812. https://doi.org/10.1152/jn.90531.2008

Menz, V. K., Schaffelhofer, S., & Scherberger, H. (2015). Representation of continuous hand and arm movements in macaque areas M1, F5, and AIP: a comparative decoding study. *Journal of Neural Engineering*, *12*(5), 056016. https://doi.org/10.1088/1741-2560/12/5/056016

Michaels, J. A., Dann, B., & Scherberger, H. (2016). Neural Population Dynamics during Reaching Are Better Explained by a Dynamical System than Representational Tuning. *PLOS Computational Biology*, *12*(11), e1005175. https://doi.org/10.1371/journal.pcbi.1005175

Oosterhof, N. N., Wiestler, T., Downing, P. E., & Diedrichsen, J. (2011). A comparison of volume-based and surface-based multi-voxel pattern analysis. *NeuroImage*, *56*(2), 593–600. https://doi.org/10.1016/j.neuroimage.2010.04.270

Penfield, W, & Rasmussen, T. (1950). *The cerebral cortex of man*. *New York* (Vol. 221).

Penfield, Wilder, & Boldrey, E. (1937). Somatic motor and sensory representation in the cerebral cortex of man as studied by electrical stimulation. *Brain*, *60*(4), 389–443. https://doi.org/10.1093/brain/60.4.389

Perel, S., Sadtler, P. T., Oby, E. R., Ryu, S. I., Tyler-Kabara, E. C., Batista, A. P., & Chase, S. (2015). Single-Unit Activity, Threshold Crossings, and Local Field Potentials in Motor Cortex Differentially Encode Reach Kinematics. *Journal of Neurophysiology*, jn.00293.2014. https://doi.org/10.1152/jn.00293.2014

Picard, N., & Strick, P. L. (1996). Motor areas of the median wall: a review of their location and functional activation. *Cerebral Cortex*, *6*, 342–353. https://doi.org/10.1093/cercor/6.3.342

Plow, E. B., Arora, P., Pline, M. A., Binenstock, M. T., & Carey, J. R. (2010). Within-limb somatotopy in primary motor cortex – revealed using fMRI. *Cortex*, *46*(3), 310–321. https://doi.org/10.1016/j.cortex.2009.02.024

Ratcliffe, N., & Newport, R. (2017). The Effect of Visual, Spatial and Temporal Manipulations on Embodiment and Action. *Frontiers in Human Neuroscience*, *11*(May), 1–11. https://doi.org/10.3389/fnhum.2017.00227

Rathelot, J.-A., & Strick, P. L. (2006). Muscle representation in the macaque motor cortex: An anatomical perspective. *Proceedings of the National Academy of Sciences*, *103*(21), 8257–8262. https://doi.org/10.1073/pnas.0602933103

Rathelot, J.-A., & Strick, P. L. (2009). Subdivisions of primary motor cortex based on cortico-motoneuronal cells. *Proceedings of the National Academy of Sciences*, *106*(3), 918–923. https://doi.org/10.1073/pnas.0808362106

Rathelot, Jean-Alban, Dum, R. P., & Strick, P. L. (2017). Posterior parietal cortex contains a command apparatus for hand movements. *Proceedings of the National Academy of Sciences*, 201608132. https://doi.org/10.1073/pnas.1608132114

Russo, A. A., Bittner, S. R., Perkins, S. M., Seely, J. S., London, B. M., Lara, A. H., … Churchland, M. M. (2018). Motor Cortex Embeds Muscle-like Commands in an Untangled Population Response. *Neuron*, *97*(4), 953-966.e8. https://doi.org/10.1016/j.neuron.2018.01.004

Sadtler, P. T., Quick, K. M., Golub, M. D., Chase, S. M., Ryu, S. I., Tyler-Kabara, E. C., … Batista, A. P. (2014). Neural constraints on learning. *Nature*, *512*(7515), 423–426. https://doi.org/10.1038/nature13665

Sanders, Z.-B., Wesselink, D. B., Dempsey-Jones, H., & Makin, T. R. (2019). Similar somatotopy for active and passive digit representation in primary somatosensory cortex, 1–36. https://doi.org/10.1101/754648

Sanes, J. N., Donoghue, J. P., Thangaraj, V., Edelman, R. R., & Warach, S. (1995). Shared neural substrates controlling hand movements in human motor cortex. *Science*. https://doi.org/10.1126/science.7792606

Schaffelhofer, S., Agudelo-Toro, A., & Scherberger, H. (2015). Decoding a wide range of hand configurations from macaque motor, premotor, and parietal cortices. *The Journal of Neuroscience : The Official Journal of the Society for Neuroscience*, *35*(3), 1068–1081. https://doi.org/10.1523/JNEUROSCI.3594-14.2015

Schaffelhofer, S., & Scherberger, H. (2016). Object vision to hand action in macaque parietal, premotor, and motor cortices. *ELife*, *5*, 1–24. https://doi.org/10.7554/eLife.15278

Schieber, M. H. H. M. H. (2001). Constraints on Somatotopic Organization in the Primary Motor Cortex. *Journal of Neurophysiology*, *86*(5), 2125–2143. Retrieved from http://www.ncbi.nlm.nih.gov/pubmed/11698506%5Cnhttp://jn.physiology.org/content/86/5/2125.short%5CnPM:11698506%5Cnfile:///C:/Users/v&msrg/Eigene Databases/Mendeley/2001/Schieber - 2001 - Constraints on somatotopic organization in the primary motor cortex

Schieber, M., & Hibbard, L. (1993a). How somatotopic is the motor cortex hand area? *Science*, *261*(5120), 489–492. https://doi.org/10.1126/science.8332915

Schieber, M., & Hibbard, L. (1993b). How somatotopic is the motor cortex hand area? *Science*, *261*(5120), 489–492. https://doi.org/10.1126/science.8332915

Shenoy, K. V, Sahani, M., & Churchland, M. M. (2013). Cortical Control of Arm Movements: A Dynamical Systems Perspective. *Annual Review of Neuroscience*, *36*(1), 337–359. https://doi.org/10.1146/annurev-neuro-062111-150509

Siero, J. C. W., Hermes, D., Hoogduin, H., Luijten, P. R., Ramsey, N. F., & Petridou, N. (2014). BOLD matches neuronal activity at the mm scale: A combined 7T fMRI and ECoG study in human sensorimotor cortex. *NeuroImage*, *101*, 177–184. https://doi.org/10.1016/j.neuroimage.2014.07.002

Stippich, C., Ochmann, H., & Sartor, K. (2002). Somatotopic mapping of the human primary sensorimotor cortex during motor imagery and motor execution by functional magnetic resonance imaging. *Neuroscience Letters*, *331*(1), 50–54. https://doi.org/10.1016/S0304-3940(02)00826-1

Szameitat, A. J., Shen, S., Conforto, A., & Sterr, A. (2012). Cortical activation during executed, imagined, observed, and passive wrist movements in healthy volunteers and stroke patients. *NeuroImage*, *62*(1), 266–280. https://doi.org/10.1016/j.neuroimage.2012.05.009

Todorova, S., Sadtler, P., Batista, A., Chase, S., & Ventura, V. (2014). To sort or not to sort: the impact of spike-sorting on neural decoding performance. *Journal of Neural Engineering*, *11*(5), 056005. https://doi.org/10.1088/1741-2560/11/5/056005

Tzourio-Mazoyer, N., Landeau, B., Papathanassiou, D., Crivello, F., Etard, O., Delcroix, N., … Joliot, M. (2002). Automated anatomical labeling of activations in SPM using a macroscopic anatomical parcellation of the MNI MRI single-subject brain. *NeuroImage*, *15*(1), 273–289. https://doi.org/10.1006/nimg.2001.0978

Urbin, M. A., Royston, D. A., Weber, D. J., Boninger, M. L., & Collinger, J. L. (2019). What is the functional relevance of reorganization in primary motor cortex after spinal cord injury? *Neurobiology of Disease*, *121*, 286–295. https://doi.org/10.1016/j.nbd.2018.09.009

Wesselink, D. B., van den Heiligenberg, F. M., Ejaz, N., Dempsey-Jones, H., Cardinali, L., Tarall-Jozwiak, A., … Makin, T. R. (2019). Obtaining and maintaining cortical hand representation as evidenced from acquired and congenital handlessness. *ELife*, *8*, 1–19. https://doi.org/10.7554/eLife.37227

Wodlinger, B., Downey, J. E., Tyler-Kabara, E. C., Schwartz, a B., Boninger, M. L., & Collinger, J. L. (2014). Ten-dimensional anthropomorphic arm control in a human brain-machine interface: difficulties, solutions, and limitations. *Journal of Neural Engineering*, *12*(1), 016011. https://doi.org/10.1088/1741-2560/12/1/016011

Yoo, P. E., Oxley, T. J., John, S. E., Opie, N. L., Ordidge, R. J., O'Brien, T. J., … Moffat, B. A. (2018). Feasibility of identifying the ideal locations for motor intention decoding using unimodal and multimodal classification at 7T-fMRI. *Scientific Reports*, *8*(1), 1–15. https://doi.org/10.1038/s41598-018-33839-4